MANCHESTER
1824
The University of Manchester

Modelling of multiphase and multicomponent flows at high-density and high-viscosity contrasts by Lattice Boltzmann methods

A thesis submitted to the University of Manchester for the degree of
Master of Philosophy
in the Faculty of Science and Engineering

2022

Enatri Enan
Department of Mechanical, Aerospace and Civil Engineering

Contents

Word Count:17404

List of figures

List of tables

List of publications

The work presented in this thesis has contributed to the following research outputs:

1] A De Rosis*, E Enan, ”A three-dimensional phase-field lattice Boltzmann method for incompressible two components flows”, Physics of Fluids 33,043315(2021); doi.org/10.1063/5.0046875

2] E Enan, A De Rosis, ”Numerical modelling of the multi-mode turbulent Rayleigh-Taylor instability by a central-moments-based lattice Boltzmann method” (Ready to be submitted)

Nomenclature

2D	Two dimension
3D	Three dimension
F_{ν}	Viscous force
$\bullet\rangle$	Row vector
$\langle\bullet$	Column vector
μ	Dynamic viscosity
μ_{ϕ}	Chemical potential
∇	Spatial derivative operator
∇^2	Laplacian operator
ν	kinematic viscosity
ϕ	Order parameter-related quantity
ρ	Density
σ	surface tension
τ	Relaxation time
τ_H	Relaxation time of Heavy fluid
τ_L	Relaxation time of Light fluid
ξ	Interface thickness
c_i	Lattice direction
$\tilde{c_i}$	Lattice directions shifted by the local fluid velocity
c_s	Lattice sound speed
F	Force vector
F_b	External body force
f_i	Distributions for the velocity field
F_s	Surface tension force
g_i	Distributions for the order parameter

H Heavy fluid

i Index number

k_i Central moments

L Light fluid

M Mobility coefficient

p Pressure

$\tilde{p}$ Normalized pressure

r_i Raw moments

t Time

w_i Chemical potential

$\overline{c}_i$ Discrete velocity

A-C Allen-Cahn

At Atwood number

BGK Bhatnagar-Gross-Krook

C-H Cahn-Hilliard

Ca Capillarity number

CFD Computational fluid dynamics

CFL Courant–Friedrichs–Lewy

Ch Cahn number

CLBM Central moment based lattice Boltzmann method

CM Central moment

CM_s Central moments

CPU Central processing unit

FD Finite differences

FDM Finite difference methods

FEM Finite ellements

FFIB Flexible forcing immersed boundary

FVM Finite volume methods

GMR General multiple relaxation time

GPU Graphics processing unit

HSLBM Higher simplified LBM

I Unit tensor

IB-LBM Immeresed boundary lattice Boltzmann method

LBE Lattice Boltzmann equation

LBM Lattice Boltzmann method

MLBFS Multiphase lattice Boltzmann flux solver

MPI Massege passing interface

MRT Multiple relaxation time

N-S Navier-Stokes

Palabos Parallel lattice Boltzmann solver

Re Reynolds number

RLB Regularized lattice Boltzmann

RM Raw Moment

RSLBM Revised lattice Boltzmann method

RTI Rayleigh-Taylor instability

SLBM Simplified lattice Boltzmann method

SRT Single relaxation method

TRT Two relaxation time

Abstract

Numerical modelling of multiphase flows remains a challenging subject in fluid mechanics. Multiphase and multicomponent flows are predominant in nature. Such applications are like melting ice and freezing water into ice cubes. And boiling and the formation of snow into the clouds are popular examples routinely experienced in daily life. Interestingly, phase transitions play an important role in several industrial areas. Common applications involve cooling devices, ranging from medicine/vaccine storage to fresh product transportation and the design of battery thermal management systems for electric vehicles. Especially, the design of battery thermal management systems for electric vehicles is a challenging problem involving phase change materials. To develop and validate Computational Fluid Dynamics(CFD) model for studying such problems in the industry is needed. A deep understanding of the laws governing phase transitions may significantly improve the design process of such industrial systems.

The main goals are to understand the physics of multiphase and multicomponent fluids. The physical domain is a container filled by two fluids; namely heavy fluid and light fluid, such as air and liquid. computational domain is meshed by an uniform fine grid. The computational domain is defined by an equidistant fine grid. This can be attained without a significant loss of computational performance since Lattice Boltzmann Methods (LBM) require much less memory and CPU time than conventional finite volume, finite difference methods.

The purpose of this present research project is to investigate the multiphase and multicomponent fluids flow at high density and high viscosity ratios. The numerical simulation used by the phase-field-based Lattice Boltzmann model(LBM). Heavy fluid and lighter fluid are considered such are water and air. Interface tracking methods for multi-component fluids are analysed by the Central moments (CMs) method. Analysis of the evolution at the interface with various time instants has been observed through several test cases.

Two sets of equations are considered which are the Navier-Stokes equations and Allen–Cahn equation [1][2] . Allan-Chan equation(conservative form) is used to track the interface of the two fluids. Finally, phase-field-based LBM is discussed in the result section. Rayleigh Taylor instability is the phenomena of instability analysis between two different density fluids that occur at the interface of the two fluids. Examples of Rayleigh Taylor instability are the behaviour of oil suspended above water in the gravity of Earth. Rayleigh-Taylor instability analysis shows that the Allen-Cahn equation can be correctly recovered by this model successfully with second-order accuracy [3].

The result shows a broad range of behaviours of the interface, that depends on the Reynolds number, and Atwood number. In particular, the emergence of saddle point or fluid tip, droplet and later mixing part in which Kelvin Helmholtz(KH) instability takes place. Kelvin Helmholtz instability is used in the fluid dynamics field to understand turbulent phenomena of the two different fluid's behaviour. Where turbulent phenomena is the chaotic mixing of the two fluids. Furthermore, this behaviour is associated with the Rayleigh Taylor instability with lower and higher Reynolds number fluid flow interface at the initial stage to intermediate stage of the simulation.

Lay abstract

Multiphase and multicomponent flows are of importance in both nature and industrial processes. For many years scientists and researchers used the Lattice Boltzmann method (LBM) as a powerful tool to solve the real engineering problem in several applications such as energy science-fuel cell (proton exchange membrane fuel cell) (PEMFC)[4], Earth science field (Soil filtration) [5], bioengineering flows(human cardiovascular system)[6] and porous media flows[7].

The purpose of the thesis is to investigate and analyse the multiphase and multicomponent flows using a new variant of the existing LBM model. The case study is based on two incompressible fluids which are heavy and light fluids with high and low density respectively. In the numerical setup, a rectangular box is considered which heavy fluid on the top and lighter fluid on the bottom. These multiphase fluids are simulated by LBM to observe the interface behaviour at various time instances.

For that, we have investigated several test cases with high Reynolds numbers and high Atwood numbers to check the Rayleigh-Taylor instability phenomena in terms of flow behaviour at the interface zone at various stages such as are initial stage, intermediate stage and final stage. Flow convergence analysis is done by considering various lattice or grid sizes. Many applications in real-world engineering that have been considered as the fall of droplet [8], the recovery of crude oil [9] and the design of microfluidic chip [10][11] which are the key problems in the fields of the energy, environment and chemical engineering. It is necessary to develop an efficient method to capture the fluid interface behaviour accurately. Phase field interface tracking method model[12] is one of the widely used methods for multiphase fluid flow at various time instances.

To analyse and understand the interface behaviour of the multiphase fluid flow, the novel method coupled Allan-Cahn- Navier-stokes equations have been considered and solved by LBM. In the present model, two sets of equations are considered one is the Navier-Stokes equation for two immiscible fluids and the evolution of the interface between the two fluids is tracked by the conservative form of Allen–Cahn equation [1][2].

Declaration of originality

I hereby confirm that no portion of the work referred to in the thesis has been submitted in support of an application for another degree or qualification of this or any other university or other institute of learning.

Copyright statement

i The author of this thesis (including any appendices and/or schedules to this thesis) owns certain copyright or related rights in it (the "Copyright") and s/he has given The University of Manchester certain rights to use such Copyright, including for administrative purposes.

ii Copies of this thesis, either in full or in extracts and whether in hard or electronic copy, may be made *only* in accordance with the Copyright, Designs and Patents Act 1988 (as amended) and regulations issued under it or, where appropriate, in accordance with licensing agreements which the University has from time to time. This page must form part of any such copies made.

iii The ownership of certain Copyright, patents, designs, trademarks and other intellectual property (the "Intellectual Property") and any reproductions of copyright works in the thesis, for example graphs and tables ("Reproductions"), which may be described in this thesis, may not be owned by the author and may be owned by third parties. Such Intellectual Property and Reproductions cannot and must not be made available for use without the prior written permission of the owner(s) of the relevant Intellectual Property and/or Reproductions.

iv Further information on the conditions under which disclosure, publication and commercialisation of this thesis, the Copyright and any Intellectual Property and/or Reproductions described in it may take place is available in the University IP Policy (see `http://documents.manchester.ac.uk/DocuInfo.aspx?DocID=24420`), in any relevant Thesis restriction declarations deposited in the University Library, The University Library's regulations (`http://www.library.manchester.ac.uk/about/regulations/`) and in The University's policy on Presentation of Theses.

Acknowledgements

The knowledge I have gained and experienced from the core of my research for past twenty one months when the whole world was in pandemic and shuttered, which has given me a new direction of thinking and explore the unknowns in the real world.

“The power of imagination makes us infinite.”
— John Muir

My profound gratitude to Dr. Alessandro and Prof. Alistair. Especially, Dr. Alessandro, your enormous support is incredible. Thank you so much Alessandro. I deeply appreciate your valuable guidance throughout my research. Your enormous guidance kept me to learn and achieve my goal. Learnt a huge amount of knowledge that I could ask for. Apart from, whenever I needed assistance in coding, doubts in how to proceed further in project work even its not weekly meeting, text you in slack and emails, you were always available to clarify my doubts. You are a great mentor and supervisor and a kind human being.

Alistair, You have been a great support for my whole educational life. Your valuable feedback is always enlighten me to think more scientifically and do extra ordinary things makes me thoughtful person in my research field especially CFD. You have been navigated me wisely and kept me in track. I have become more optimistic and dedicated, hard worker at my present life. Which directs me towards the great future. Thank you for your prodigious support throughout the time. I am grateful to you.

To CFDemons, How can I thank you so much, you were my small family in Manchester. This group has been given me so much joy and happiness through out my research. Small activities like outing, Christmas party, Halloween party, weekend lunch what not, the list goes on. I deeply thank to all of my friends and colleagues.

Especially, Mary, You are an amazing person who I call as another sister, my friend, my colleague, my neighbour and all that uncounted fun we had together for past two years. And the evening walk, chit-chat with Xutong and mary about CFD , LBM, Aerodynamics. Its memorable. I never felt that I am away from home. Thank you so much both of you.

And Yang, Jie, Andrew, Marta, Rui, you all are incredible fun loving human beings. And I would like to include my other friend Fate, Thank you for arranging small fun activities in PGR MACE indoor and outdoor, lunch etc. I have a lots of memories with you all which I will cherish every moment further in my life. And little Matilda, my little sweet human being and little dearest friend who's unconditional love and smile always will be their in my heart. Thank you Matilda.

Emilia, My dearest friend. You are an amazing person. The time we have been spent in Manchester together, weekend shopping, lunch, dinner etc. its speechless. Without you I would have been lost. And you have been tolerating me for 5 years. This time I will make up to you. Good plans are coming way.

At last, to my loving family- Jo-my dearest sister, Nick-dearest brother, dearest mom, Akhil-dearest friend, Thank you all for your huge support and encouraging me throughout past couple of years when I decided to dive in the research world and refused to do job. Thank you for your incredible support through out my life and fulfill my one step of my dream. I can't thank much. Love you all.

Chapter 1

Introduction

Modelling multiphase flows is a challenging subject in fluid mechanics. Despite significant advances in computational fluid dynamics (CFD), analysis of multiphase and multicomponent fluids with high density and high viscosity ratios remains intractable. The transport processes of the multiphase flows are very complicated due to the topological changes of the interface among multiphase under the migration, breakup, deformation, and merging of the fluid phase-interface [13][14]. A coupling problem in the multiphase and multicomponent fluid flow, it is hard to find out the exact solution via analytical method [15][16][17]

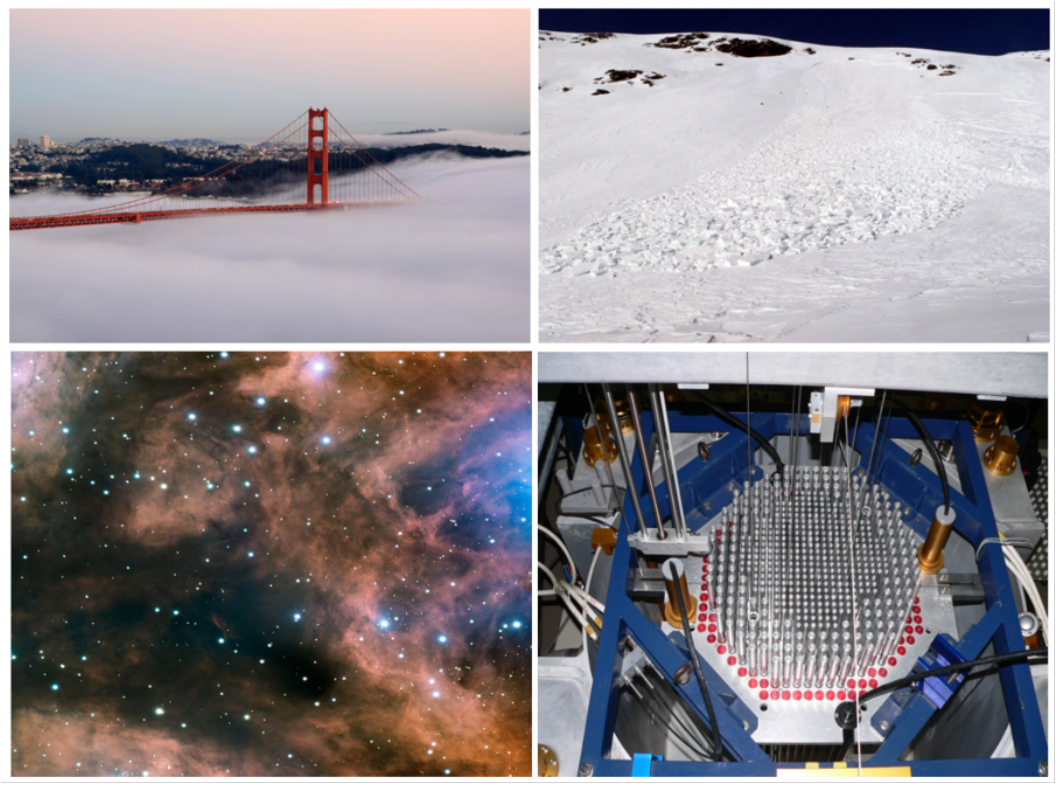

Figure 1.1. Multiphase flow in nature and industry:(a) From top-left-fog engulfing the Golden Gate Bridge[18] (b)top right-Avalanche on the Alps[19] (c) bottom left-interstellar cloud[20] (d) bottom right-Nuclear reactor[21]

In the past decades, the experimental method has been widely used to study multiphase flow problems, and can also capture the macroscopic dynamic behaviour of interface [22][23][24] while it is difficult to accurately describe the details of the fluid flows [25].

Analysis of multicomponent fluids with multiphase via the Lattice Boltzmann Method is quite challenging though it is a popular method for the researcher, scientist and engineers. Modelling of such complex fluids is challenging due to their interfacial dynamics between the two-phase flows. For example, liquid-gas, liquid-liquid, gas-solid, liquid-gas, liquid-solid etc are examples in many applications such as bubbly flow in nuclear reactors, and fibre suspension flows within the pulp and paper industry [26]. Figure 1.1 represents a few examples of the application for multiphase flows.

1.1 Aim and Objectives

The aim of this project is to investigate the lattice Boltzmann (LB) model to solve the coupled Allen-Cahn-Navier-Stokes equations for immiscible incompressible multiphase fluids. It is the new combination of the recent existing models such as the central moment-based Lattice Boltzmann model. The methodology combines solving the two LB equations and the collision stage is performed in the central moment's space. Both equations are calculated mathematically in a multiple-relaxation-time framework. The main motivation is to understand the simplicity of the model allows us to understand the salient behaviour of multiphase fluids or complex fluids. The main research aims are,

- To explore the 2D and 3D numerical analysis of single-mode and multi-mode Rayleigh-Taylor instability
- Mainly focused on the interface evolution behaviour between the two fluids at the simulation process
- To examine several test cases based on Reynolds number and Atwood number
- To analyse the fluid flow behaviour under the lower to higher Reynolds number and Atwood number
- To study and analyze the various size of the lattice grid

1.2 Overview

Chapter 1 gives the introduction, aim and objectives, overview

Chapter 2 enlighten the Literature Review of the present work and describes the solution methodology in which two equations are coupling scheme with relevant physics and model technique

Chapter 3 describes the results of the present work with the test case analysis of the single-mode Rayleigh-Taylor instability(RTI)

Chapter 4 describes the final results presents about the multi-mode Rayleigh-Taylor instability(RTI) analysis

Chapter 5 summarises the main findings and concludes the limitations and future work

Chapter 2

Background research and methodology

In this chapter, we will review the background of multiphase and multicomponent fluid flows with the Lattice Boltzmann model and discuss the LBM model with various techniques. To begin with, the Introduction of LBM, defining multiphase and multicomponent fluid, introducing collision operator and relaxation time, background study of phase field interface tracking method, and background study of Rayleigh Taylor instability analysis. And the Methodology section Allan-Cahn-Navier-Stokes equation, Bhatnagar-Gross-krook equation and Lattice Boltzmann equation with governing equations are introduced. The Time step process is discussed with the collision and streaming operator.

2.1 Introduction of LBM

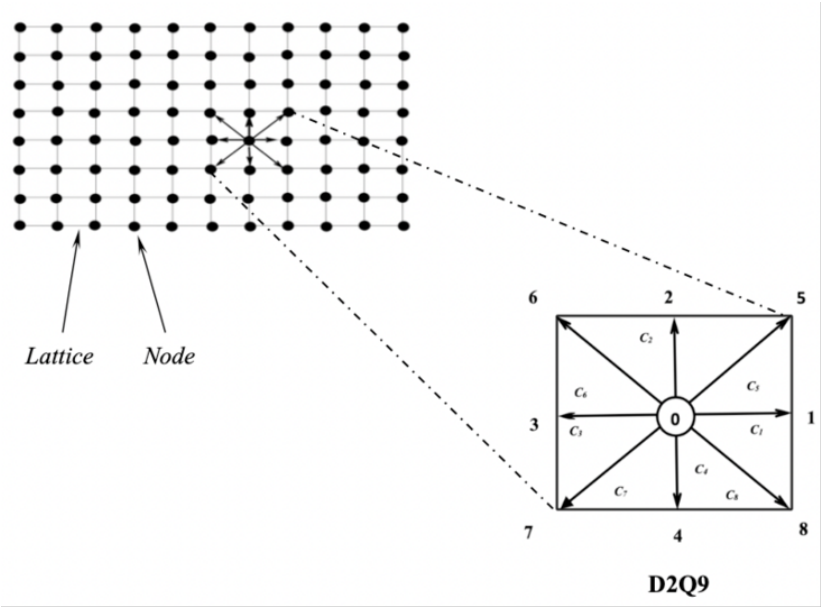

Figure 2.1. LBM lattice with D2Q9 model

Lattice Boltzmann method (LBM) is a popular method known as the mesoscopic method for numerical modelling of the multiphase and multicomponent fluid flows. Hardy, Pomeau, and de Pazzis [27] introduced the lattice gas model. In their LBM model, they have considered macroscopic (molecule/particles) an infinite structure of square lattice with four neighbour lattice points where each lattice streams forward and collides with each time step. And where each node conserves mass and momentum when the particle collides with the node[28]. Figure 2.1 is the example of Lattice Boltzmann D2Q9 model for the lattice and nodes. Which two-dimensional model and 9 is the set's number of velocities. At the fixed Cartesian, the LBM represents a fluid that gives an idea of a ghost or an imaginary particle distribution in the fluid. That can move along with the links at the Cartesian. Hence, these mesoscopic quantities carry with them information about the macroscopic variables such are density and momentum. In these streaming and collide states, the nodes are in a solid body known as ghost nodes which represents the extrapolation of fluid properties. For complex flow simulation, the LBM model is considered for its simplicity to track the distribution of the particles than the conventional methods such are FVM, FDM and FEM. Especially, in the case of complex structure(geometry) fluids that are characterised as breaking the interface of two different density fluids (e.g., water, air or water, oil) and in the scenario of interface behaviour. The interface behaviour is delineated as bubble growth, bubble motion and chaotic mixing. Such real problems are kept in mind and focused on numerical analysis issues with the accuracy, stability, computational cost and computation time (for multiphase and multicomponent fluids).

2.2 Dimensionless Parameters of LBM

LBM simulations require a good knowledge of lattice unit conversion. Due to inherent restrictions of the LBM algorithm, it is necessary to balance the physical units/parameters to achieve stability, accuracy, and efficiency for the simulation. [28]

Such physical parameters are,

- The lattice constant Δx = the distance between neighbouring lattice nodes
- Physical units of Δx = meter(m)
- length of a time step denoted by Δt; where Δt = second (s)
- τ is a physical relaxation time, where τ = second (s)
- $\tau^{\star}$ is the the dimensionless relaxation parameter
- The dimensionless fluid density is $\rho^{\star}$ set as an unity.
- The velocity length over time, $U^{\star}$ (m/s)
- The lattice speed of sound , $c_{\mathrm{s}}^{\star}$ = $\sqrt{1/3} \approx 0.577$
- Lattice Mach number, Ma $= U^{\star}/c_{\mathrm{s}}^{\star}$

By the conversion factors for length, time and density which are equal to the dimensional values for the lattice constant, time step and density. Where the units defined as

- $\Delta x^{\star} = 1$ and $\Delta t^{\star} = 1$ are known as lattice units.
- $\Delta x = L/N_x$ which applied each lattice direction

2.3 Defining multiphase and multicomponent flow

Lattice Boltzmann method has been used for so many years to investigate the Multiphase and multicomponent flow field. Multiphase flows are well known in various engineering and scientific applications, and are challenging due to their complexity in dynamic interfacial between different phases [29]. Four types of approaches are used to analyse multiphase and multicomponent flows. They are Color-gradient model [30], the Free energy model [31], the Pseudopotential model [32] and mean-field model [31]. The other new model is the conservative Phase-field model [33] used for tracking the interface of two fluids.

2.3.1 Color-gradient model

Color gradient model is for immiscible multiphase flows based on the cellular automata model which reported by Rothman [34], gunstensen [35] and Latva-Koko-Rothmans [36]. The color fluid model is known as R-K or color gradient model. The color-fluid type model and issues are solved by a recolouring algorithm. The color-gradient model is able to track multiphase and multicomponent flows for fluid mass conservation and interfacial tension adjustment by flexibility and stability for a higher number of viscosity ratios. The Rothman-Keller model is used to capture the interface between a red and a blue fluid. Later, the introduction of density and viscosity ratios were modified to form of distribution functions for the gas particles [37]. The particles were red or blue and the collision stage was modified to obtain surface tension between the two immiscible fluids. However, lattice-gas models are not free of problems in terms of multiphase fluids. Two of the most serious disadvantages are the difficulty of extending the model, particularly for the multiphase model.

2.3.2 Free energy model

The free energy model is basically used for two types of models which are the liquid gas model and the binary model. The free-energy model is commonly used for single-component multiphase LBM flows. In the particle-based models, the energy depends on the position and orientation of the particles which includes three functions name as bulk free energy, gradient term and interaction between the fluid and solid. Free-energy LB model is thermodynamically consistent [31][37][38]. However, this model is eligible to capture the bubble bouncing, adhesive between immiscible droplets but lacks the Galilean invariance and spurious velocity, and limited density ratio in the fluid.

2.3.3 Pseudopotential model

The Pseudopotential model is known as the Shan-Chen model which leads to end up with force and finally induced to phase separation process [28]. The model is a particle/molecular-based model which describes the particle distribution function for various spices. This model falls under two categories one is a single distribution function for lower and higher density and the other another one is for multicomponent flows (complex geometries flows) for more distribution function which tends to achieve phase separation (for eg; porous media). However, the pseudopotential model is not suitable for density and viscosity ratio contrast fluid flows in terms of accuracy and stability due to its higher interfacial tension which the multiphase interface is too thin [39].

2.3.4 Phase-field model

Phase-field model is defined as an interface tracking method. This method has been used to track the interface for multiphase and multicomponent fluids for high density and high viscosity ratios. The naiver-Stokes-Allen-Cahn equation can be used to track the interface of two or multiphase fluids. Basically, this method is going to be considered for this present work. It has been discussed in detail in a further section.

2.4 Introducing Rayleigh Taylor instability

The Rayleigh-Taylor [40]–[42] instability is described as an instability for two different fluids with different densities. It is represented as the heavy fluid is in the top and the lighter fluid is in the bottom and shows the phenomena of the interface of two fluids. The main focus of this thesis is to explore the Rayleigh-Taylor instability phenomena quantitatively with regard to fluid with high density and high viscosity ratio. In the present work, RTI was examined numerically for single-mode RTI and multi-mode RTI by several test cases for lower to high Reynolds number fluids. Basically, computation analysis considered two sets of LBM equation and BGK collision operator and coupled Alan-Cahn-Navier-Stokes equation. The Bhatnagar–Gross–Krook operator (abbreviated BGK operator) term refers to a collision operator used in the Boltzmann equation and in the lattice Boltzmann method, a computational fluid dynamics technique. The computation process has been investigated to check the interface behaviour, flow accuracy, grid convergence and flow instability. These kinds of flow properties can be resolved by using the lattice Boltzmann method, in which the phase field model has been used to capture the interface of two fluids and resolved by coupled Alan-Cahn-Navier-Stokes equation. Further, more insights have been reviewed in the background research of Rayleigh-Taylor instability for the multiphase fluid section.

2.5 Introducing collision operator and Relaxation time

In the LBM, the collision operators used BGK collision operator[28][43] due to binary (two) fluids collisions between molecules or particles. And it is known as lattice Boltzmann equation with BGK collision operator (LBGK). Because of the first order approximation of the collision operator convert to integral form and provides LBGK equation. However, due to high density of the fluid, liquid particles shows complexity when it interacts with more particles. The property of collision operator is described as mass and momentum conservation.The relaxation leads us to equilibrium, and the relaxation time. SRT is defined as single relaxation time which is known as Bhatnagar- Gross-Krook (BGK) approximation of the lattice Boltzmann collision integral of classical kinetic theory. The resulting method is known as the LBGK model[44]. This model is limited for flow stability domain at the minimum grid size and time step (fourier space). In general, multiple-relaxation-time (MRT) formulation, advanced techniques to calculate the gradients and used to achieve complex geometry fluids phase separation in immiscible/incompressible fluid flows. MRT is known as an advanced relaxation method that has the largest number of free parameters to recover accuracy and stability. And MRT model confronts for having great flexibility in terms of recovering relaxation of individual moments[28]. However, It is not always best to advise using the MRT relaxation parameter for an average LBM user.

2.6 Background study of phase-field interface tracking method

The interface is a challenging task when the flow involves the behaviour of interface changes including mixing, splashing and capturing one fluid above another. Interface schemes such are volume of fluid, front tracking and level set schemes discussed by Dinesh et al [45]. Figure 2.2 shows the interface of two fluids which top and bottom part is with heavy fluid and light fluid respectively. In the multiphase flow model, interface tracking is extensively used technique [29][46][47]. Their observation reported that the different fluids are separated by a sharp interface and the density and viscosity of the fluid are discontinued at the interface. The diffuse interface method for the multiphase flow field was proposed by Anderson et al and Jacqmin et al[48] and [49]. Their study shows the advantages over the sharp interface phase method in the multiphase flows in which the interface goes a higher deformation and breaks up [29].

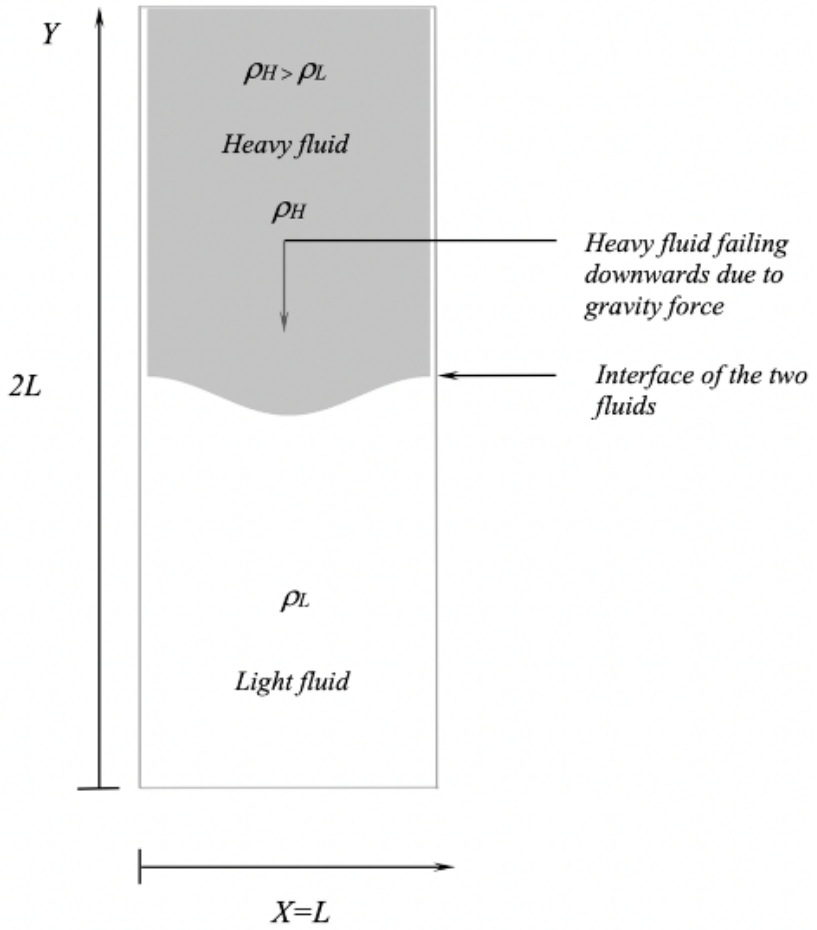

Figure 2.2. Two incompressible fluids of infinite depth, having densities ρH, ρL, meet at an interface. For times t> 0, where the interface fluid develop a perturbed shape.

A popular incompressible multiphase model was proposed by He et al [50]. The new lattice Boltzmann multiphase model is derived by discretising the continuous kinematic equation. Kinetic theory base formulation has been considered a natural way to assimilate the microscopic molecular interaction which is known as interfacial dynamics. Phase-field multiple-relaxation-time lattice Boltzmann model (LBM) for incompressible multiphase flow systems is suggested by Liang et al[29]. One distribution function has been used to solve the Chan-Hilliard equation and the other one is adopted to solve the Navier-Stokes equations. Their investigation suggests that the model can successfully reduce the spurious velocity and fluctuation of the kinematic energy than the single relaxation time method. Two sets of distribution which are velocity and pressure distribution have been used in their method. One is for the function to track the velocity and the pressure. And another one is for the density field. Their work proposed the numerical simulation which has been reported for the Rayleigh-Taylor instability for single-mode and multi-mode initial perturbations of the fluids. However, their work needed more attention towards the Rayleigh Taylor instability analysis.

Likewise, another study is considered by Liang et al[51] that has been reported for numerical two-dimensional (2D) analysis of the multiphase fluids. Especially, concentrated on the multi-mode immiscible and incompressible fluids to check Rayleigh-Taylor instability with a lower Atwood number. An advanced phase-field lattice Boltzmann method has been used for numerical analysis than the conventional LB method. Such conventional methods are the Finite Volume and Finite Difference methods. In terms of capturing the interface of two fluids smoothly, an advanced phase-field lattice Boltzmann method was used by them. Basically, from their[51] observation was to capture the interface behaviour of two fluids with high density and viscosity. Velocity growth, linear growth and chaotic mixing growth of fluid flow have been studied by them. They reported an analysis on flow instability with a higher Reynolds number (Re = 30 000) and the result suggests the interfacial breakup, turbulent or chaotic mixing that leads to flow instability. Mainly higher Reynolds number affects the initial state and provides an instability growth at the initial perturbation wavelength and amplitude.

Analysis of the stability and accuracy of the Turbulent flows has been studied by Nathen et al [52]. Reported turbulent flow has been simulated by the Lattice Boltzmann method. Especially, investigated in the case of SRT, MRT and RLB (Regularized lattice Boltzmann methods). Their investigation was reported for the numerical analysis of 3D Taylor-Green vortices of homogeneous isotropic turbulent flows with different Reynolds numbers and grid resolutions. Their review shows that the BGK method requires higher grid resolution for a stable and accurate simulation. In their case study, MRT has achieved accuracy and stability without failing the turbulence model.

And from the investigation, RLB shows the breakup nature of the flow. Similarly, the break-up nature appears at the higher Reynolds number flow which gives more insight into the flow resolution and meshes convergence. Their RLB test case results show the numerical dissipation at the flow with lower accuracy. LBM method has become a suitable scheme for turbulence models in case of stability and accuracy. Their report suggests that when there is a resolution higher, there is grid convergence and the accuracy of the flows is obtained. Their work agreed with the study of Imamura et al[53].

The local time step method on a non-uniform grid is considered by Imamura et al[53] that assists to accelerate the solution to get the converged steady state on a non-uniform grid by various Reynolds numbers. They have conducted test cases simulation on the steady flow. Their study shows that the CPU time is reduced effectively for lower Reynolds number that depends on the flow condition and grid arrangement. In contrast, when the Reynolds number increases then there is a size of grid change or increase between maximum and minimum grid size. And a reduction in CPU time which becomes less while the number of grids is less.

2.7 Background study of Rayleigh-Taylor instability (RTI) for multiphase fluid

Two-dimensional (2D) simulation has been investigated for immiscible fluids with high density and viscosity to analysis the RTI by Yuana [54]. Mainly, their investigation was focused on interfacial behaviour such are positions of bubbles, spikes and average density in horizontal orientation with the various time difference.

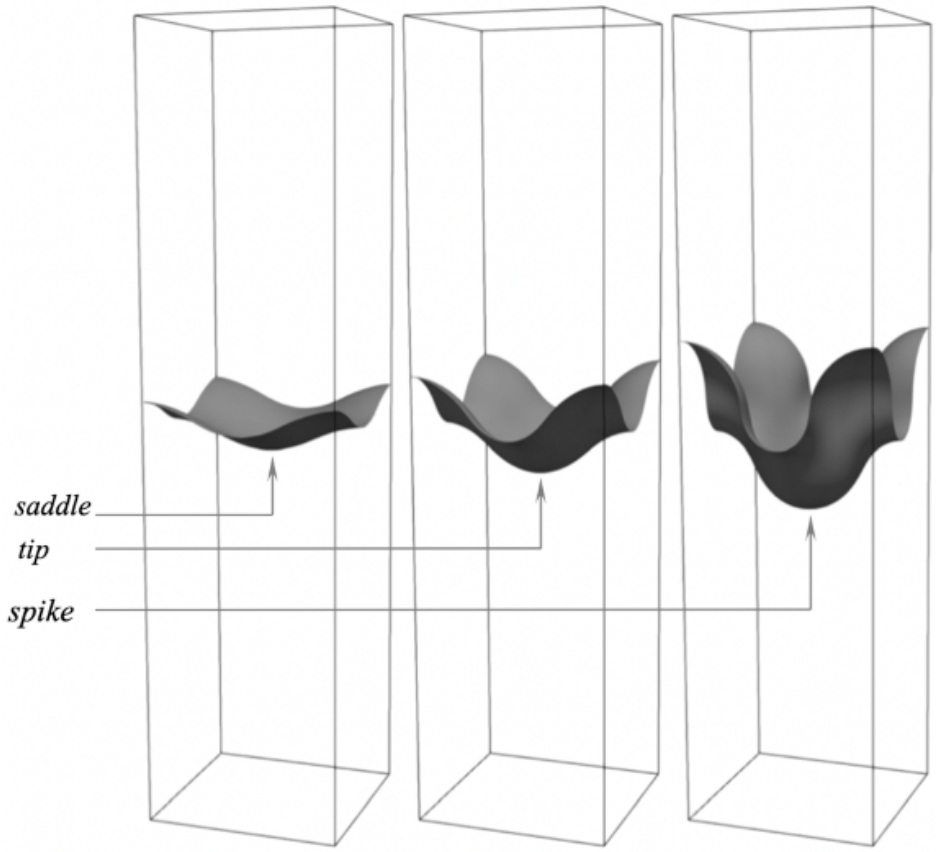

Figure 2.3. Snapshots of 3D Rayleigh-Taylor instability[2]

Such interfacial pattern or behaviors bubbles position, bubbles tip, bubbles spikes are highlighted Figure 2.3 as perturbation continuation, head and neck shape, Kelvin Helmholtz Instability (KHI) and turbulence flow. In their investigation, higher Reynolds number has been used to investigate the RTI stages that effects the fluid interfacial behavior by the rapid chaotic mixing of fluids at various time instance. And the investigation of the RTI process were done by considering Atwood number 0.1 to 0.5. Their simulation results were verified with bubbles travel distance gap at each time step. The examined result shows that the mixing process was faster in RTI at higher Reynolds and Atwood numbers. That means their simulation results substantiate that the Atwood number has more dominant than the Reynolds number in the

case of the RTI mixing process. The position of the bubbles and spike's behaviour was changed with a higher Atwood number than the Reynolds number. Their study suggests that the interfacial behavior tremendously changes when there is an increase of Atwood number.

Rayleigh Taylor instability (RTI) for Three-dimensional anlysis by lattice Boltzmann model for multiphase incompressible flow has been studied by He et al[55]. Single-mode Rayleigh-Taylor instability was considered in their study. The investigation was focused on the 3D advancement of the interface structure. They visualize the behaviour of a saddle point, bubble and spike fronts in the simulation. Their results show the interface behaviour such are saddle point, bubble front, and spike tip and compared with different time stages with Atwood numbers At= 0.5 and 0.9. Their study suggests that Raleigh-Taylor instability depends on the density ratio.

The MRT lattice Boltzmann model based on phase field theory is used to simulate the incompressible flow[29]. The MRT collision model is used for simulating the low viscosity and an average density ratio for two-phase flows. Their observation was interfacial behavior from the linear stage to the chaotic mixing stage. Which the process of reacceleration and chaotic development of the flow discussed. Their simulation result achieves a good agreement with the experiment result. The reported result shows that their model is more stable and accurate to capture the interface perfectly. Hence, their study indicates that their model can play an important role in the complex interfacial flow further.

Phase-field-based lattice Boltzmann method to track the interface of binary fluid flows is examined by Ren et al[56]. Their work reported on the Rayleigh Taylor instability analysis for high-density and high-viscosity fluids. Their model was ineffective to simulate the water-air system. Dimensionless numbers such as the high-density ratio of 800(dimensionless number) and high viscosity ratio are 58(dimensionless number) are considered. To take this into account, our present work will cover the mean flow with higher density and viscosity ratio for the multiphase fluid.

Liang et al[29] reported the numerical simulation for incompressible fluids flow system by phase-field lattice Boltzmann model. MRT collision operator used to perform in moment space. Their method is used to track the interface evolution and analyse the RT instabilities with high Reynolds numbers. Mainly their observation was to analyse the interface linear growth to chaotic mixing process at lower to higher Reynolds numbers. Their simulation results suggest that the model was able to reduce the spurious velocity and capture the interface with lower viscosity.

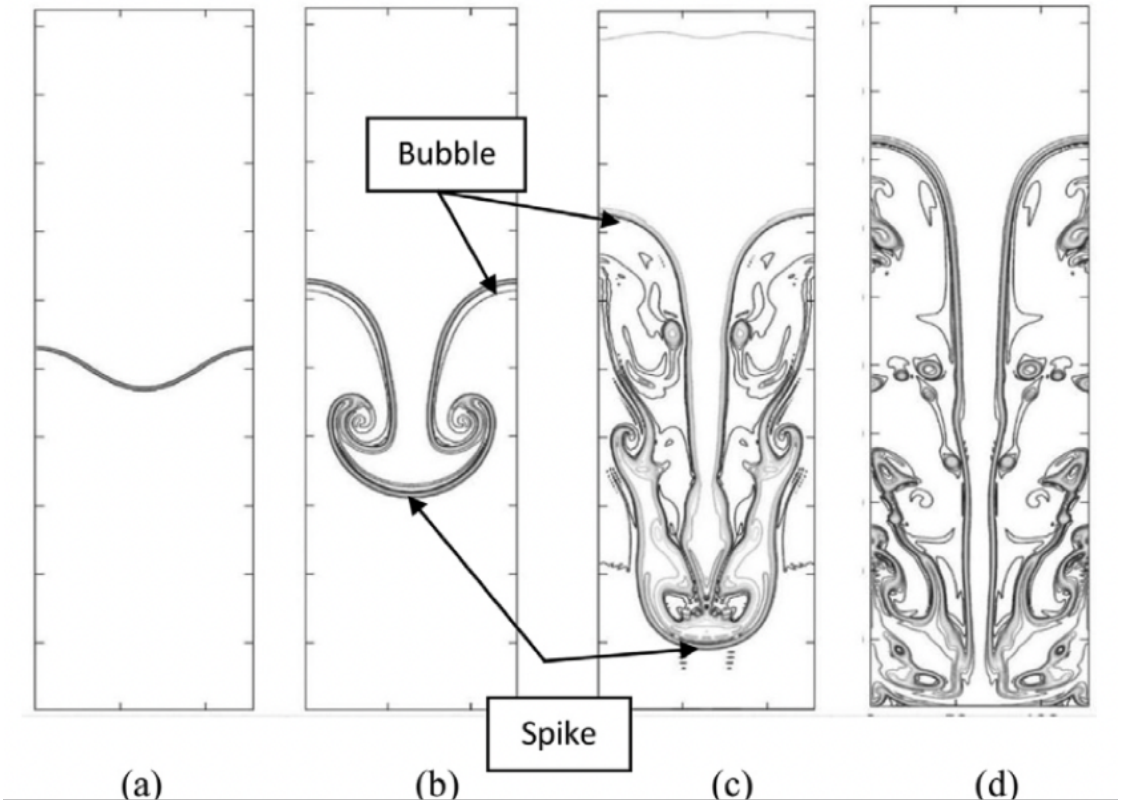

Figure 2.4. The growth of RTI phenomena: (a) first stage, (b) second stage, (c) third stage, and (d) fourth stage. [57]

In spite of outstanding development in computational fluid dynamics (CFD), flow with high-density ratios and high Reynolds number remains challenging to work which is not investigated properly so far[33][58]. Their study suggests that perturbing of the interface in the flow causes an RTI instability. The layered Poiseuille flow in a rectangular channel and the rise of a Taylor bubble in a duct, single mode Rayleigh Taylor instability reported by Fakhari et al[33]. Mainly, their work was focused on multiphase lattice Boltzmann simulation for immiscible fluids at high-density ratios. They focused on analyze the stability and accuracy of model in terms of capturing the interface behavior such as linear stage, bubble growth with the spike and deformation at the chaotic mixing stage. One can observe these various stage from the Figure 2.4. The distribution function has been used for tracking the interface and recovering the properties of hydrodynamics. Especially, in the case of numerical modelling of two-phase flows air and water constitute challenges due to the large density difference between them. The sharp interface and the different time and length scales are involved in the different physical processes like water wave propagation. The reported simulations result is a good match with available experimental[59][60] and numerical data[56][61].

Inamuro et al[62] has been reported as two-phase immiscible fluids with large density difference fluid which is simulated by a lattice Boltzmann method. In their work, the high density is treated by the projection method where the continuity equation in the interface region is satisfied at every time step. The investigation has been reported on the numerical simulation for the capillary waves, bubble flows and binary droplets collision. Which their result is agreed with their theoretical ones.

High-density ratios between two phases like air-water and different space-time scales were involved in the flow regimes for the deep water wave(capillary wave) proposed by Dinesh et al[45]. Their work involved the simulation of a deep water wave breaking with high density and high Reynolds number and their result exhibit the excellent property of mass conservation. The investigation was for complex test cases like the rising of an air bubble, the splash of a water droplet on a thin wet bed and Raleigh-Taylor instability. The Rayleigh-Taylor instability(RTI) with higher density flow was simulated and showed a similar result to the work of Ren et al and Fakhari et al[56][33]. The simulation results has shows that the model can control the high density and high viscosity of the fluid flow.

Other cases such as two-dimensional problems, where a rigid body interacts with the interface between two fluids which was reviewed by Rosis et al[63]. Their investigation reported the hydrodynamic instability problem. In their work, they develop a different lattice Boltzmann model which is central moment-based LBM and BGK for the numerical analysis. The investigation was successful in terms of capturing the instability in the simulation. Another study reported for the experimental and numerical analysis of the free-falling cylinder by using a different LBM model. Their results were demonstrated between CMs (central moments) based on LBM and BGK LBM. The results shows that the CMs based (experimental) method was able to simulate the entire time span, which BGK breaks out at a particular point and the central moment is involved to perform a stable simulation for the water exit problem.

Likewise, three Dimensional numerical simulations for water exit of a sphere with different vertical velocities by lattice Boltzmann model demonstrated by Haohao et al[64]. The case study was considered on simplified liquid-gas two-phase flow as a single free surface flow. And their simulation result for the experimental data confirm that their study was well matched with the flow accuracy and ability. The experimental study reported on the smooth particle hydrodynamics for water exit problems and it highlighted the results for the non-uniform distribution of velocity. Consequently, the free surface breaks after the sphere in which water exits completely.The hydrodynamics and wake dynamics are acting on the sphere and sphere moves underneath the water surface affects at higher Reynolds number.

Numerical simulations for the water entry problem of hydrophobic objects have been presented by Shentu et al[65]. Mainly they focused on the behavior of cross-line motion and the cavity shape decay in the process of water entry. Their method is based on the Boundary data immersion method and the volume of fluid method. They analyzed the water crown, the cavity shape, and the flow pattern by the sphere with rotation. Their numerical results suggest that the velocity decay depends on the sphere's density ratio.

Which sphere's density ratio is smaller than the water, the sphere rises inversely. And there are no significant changes in sphere decay with the higher density ratio. And cavity shape inversion behavior is shortened by increasing of entry velocity for the cylinder.

Gunstensen et al[30] proposed the three-dimensional (3D) simulation of two immiscible fluids which was simulated by a lattice Boltzmann model. Their model has been reported as the three-dimensional numerical analysis of the microscopic model(microscopic collision rules) for the two-phase flow in a porous medium. They have verified the theoretical value and numerical data for immiscible fluid with the surface tension in the microscopic collision rule. In contrast, their result was well matched with the theoretical value with the numerical simulation.

Resis et al[66]reviewed the three-dimensional analysis (3D) channel for the Poiseuille flow which is a two- or three-layer combination of immiscible binary fluids flow. In their work, decomposition of the same density and viscosity for the binary (two) fluids have been reported. Their simulation is revealed by comparing the numerical and theoretical results predictions of surface tension which is a function of density. A good agreement with the analytical test solutions. Their result shows the mass flux for a pressure gradient in the configuration of three-layer that occurrence of a large velocity with the same magnitude of body force as the two layers of configuration. Finally, their simulation results have revealed that their model can predict the higher density ratio than the R-K(Rothman-Killer) type lattice Boltzmann method, in which they have reported the Rothman-Killer[34] lattice Boltzmann model that is simulated for the immiscible binary (two) fluids for D2Q9 lattice.

Similarly, Lui et al[67] examined on the three-dimensional (3D) immiscible binary fluids which simulated by lattice Boltzmann color fluid model using by D3Q19 lattice. Their investigation reveals the droplet deformation and break-up in shear flow. Recoloring step and interfacial tension are created by the perturbation step for promoting phase segregation that reduces the spurious velocities. perturbation step has been used to maintain the surface. Their numerical results were a good agreement with the theoretical predictions and experiment results. In their model, the phase field function is used to distinguish the different fluids by using the perturbation operator of MRT to understand the effect of interfacial tension. Recoloring operator has been used to ensure the immiscibility of both fluids that they have been adapted from the previous work of Latva-Kokko et al[68]. Their results were verified with the present color gradient model and the original color gradient model. Their present color-gradient model's result has disclosed the satisfaction prediction of a velocity profile for the layered channel flow simulation. And original color-gradient has shown the huge deviation due to unwanted errors from the analytical solution. There is a quantitative agreement for the prediction of bubble and spike interface position result for the present model that provides a satisfying result when it verifies with the previous work result of He and Chiappini et al [50][69].

2.8 Review of different LBM schemes

3D multiphase flows with high Reynolds number and high-density ratio numerical simulation by lattice Boltzmann method is proposed by Banari et al[70]. They focused on tracking the interface and studying the interface evolution process of rising bubbles, splashing water, and a breaking ocean wave. And to achieve higher computational efficiency, they used the algorithm parallel general-purpose graphics-processing-Unit (GPGPU) co-processor for the entire model. They reported benchmark problems such as higher computational efficiency than other authors' work [62]. Inamuro et al was confident that GPUs implementation with an acceleration of the pressure Poisson equation would be the best way to make the model a powerful tool for complex 3D fluids simulation, in order to study new physics and solve complex engineering problems which deal with high Reynolds numbers and high density of the fluid. The suitability of using parallel GPU on distributed-memory machines was discussed by Fakhari et al [33]. This suggests that limiting nonlocal variables' data improves the parallel performance on GPU. And it makes the model adequate for high-performance computing. That means it reduces computational cost for the lattice Boltzmann method for multiphase flow at high density and high viscosity ratio.

To reduce the inconsistency, accuracy in space, two collision operators are used such as MRT(multiple-relaxation time) and Generalmultiple-relaxation-time (GMRT) which used in the collision process to perform in the moment space[44][71][72]. Different moments in space were observed at different time relaxation rates. The study of Fei et al[71] suggests the relation between MRT and CLBM under a general form. And the numerical simulation executed by the cascade lattice Boltzmann method (CLBM). GMRT collision operator used in CLBM to reduce the inconsistency, and achieve the accuracy in space.

Similarly, immiscible multiphase flows to developing the incompressible, velocity-based cascaded lattice Boltzmann model is proposed by Gruszczyński et al[73] to find the relation between the planar Taylor bubble rising velocity for the flowing fluid and stagnant and their work is extended work from Fakhari et al [33]. Lattice Boltzmann equation for incompressible hydrodynamic and the interface tracking. The relaxation functioning in the central moment space that admits the work of Fei et al[71]. And to find the relation between the planar Taylor bubble rising velocity for the flowing fluid and stagnant.

LBM method is known as a mesoscopic computational fluid dynamic method. The kinetic-based development equations for the distribution functions discussed by Ba et al[74]. Their proposed method is based on the color-gradient lattice Boltzmann model for two-phase flow.

And numerical simulation executed for the two immiscible fluids with the high Reynolds number and high-density ratio. To develop the simulation, they the stability, and the multiple relaxation time (MRT). Their test results were verified with the simulation of steady and unsteady cases like a static droplet in a steady flow and the layered channel flow in which the density ratio is maximum up to 1000 (dimensionless number). And test cases have been examined on the Rayleigh-Taylor instability and splashing droplets on a thin liquid layer for unsteady flow respectively. Their results shows the spurious velocities with lower values and errors in the interfacial tension are exhibited in the static droplet. To solve this problem, they used their present model (color-gradient) that well matched with the work of Reis and Liu et al[66][67].

Three-dimensional (3D) color fluid lattice Boltzmann model for immiscible two-phase flow is discussed by Saito et al [36]. The reported model has been considered to develop the three-dimensional analysis for the 27 velocity lattice (D3Q27). Their suggested model was to enhance the equilibrium distribution function (equilibrium moments) and the Galilean invariance(spurious velocity). The numerical test were focused specifically a static droplet, Rayleigh Taylor instability and an oscillation of droplet. The sinus break up and flow with poor circulation and atomization regimes has been reported in this study and successfully they were able to produce the breakup predicted regimes.

Lattice Boltzmann model for immiscible two-phase flow simulation with the central moments discussed by Satio et al[75]. Their work was a combination work for the earlier model as 3D nonorthogonal central moment based lattice Boltzmann method that has been reported by Satio et al and De Rosis et al [75][76]. Previous work was for the 3D color-gradient lattice Boltzmann method by Saito et al[36]. Numerical simulation has taken place for the hydrodynamic jet break up and flow simulation with high Reynolds number. MRT Collision operator used for the numerical model. And the simulation has proceeded for the melt-jet breakup to observe the typical jet breakup regimes in liquid-liquid systems such as dripping, varicose and sinus with and without entertainment. Including atomization and a map of breakup regimes. Especially, they have concentrated on the breakup of the liquid jet in the terms of Reynolds number, density ratio, viscosity ratio, weber number and froude number.

To improve the multicomponent and multiphase fluid flows, the wetting properties with the lattice Boltzmann method especially with the color-gradient method extending its various usefulness in applications such as porous media is reported by Leclaire et al [77]. Their proposed model has been investigated for the 3D numerical analysis for D3Q15, D3Q19 and D3Q27 lattice which is an extension of two-dimensional (2D) color-gradient simulation analysis. They have been revealed that the color-gradient method is capable of modelling 3D capillary waves (for liquid-liquid) with density and viscosity ratios.

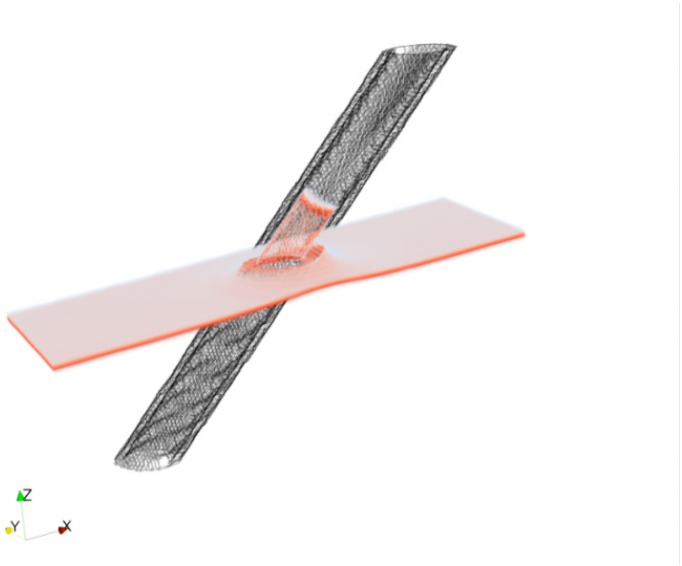

Figure 2.5. Graphical representation of the rotated tube geometry with the bottom fluid highlight. As predicted by Jurin's law, the capillary rise is clearly visible. Note that the lattice resolution $s = 2$, the viscosity ratio $\nu_B/\nu_T = 20$, the Laplace number $La = 10$, the contact angle $\theta_c = 45°$, and the geometry rotations $(\theta_x, \theta_y, \theta_z) = (30°, 30°, 30°)$ [77]

They have have considered three-dimensional (3D) imbibition and drainage experiment in digitalized Berea sandstones and recreate the fluid regimes to capture it shown in Figure 2.5. And they have regularized the inlet and outlet velocity and density boundary conditions to find a better observation from numerical analysis 2D color-gradient method to observe the viscous fingering, capillary fingering, and stable displacement. Their test result was for simulating imbibition in porous media wetting boundary conditions.

On the other hand, Leclaire et al[78] has reviewed the external force in the color-gradient-based Lattice Boltzmann model. Real immiscible fluids like water, mercury and hexane were studied numerically for hydrostatic pressure and Poiseuille flow. The quantitative study of bubble dynamics suggests that model for a gravity or pressure gradient (external force) is shown to be successful with the involvement of variant density ratios. Particularly, their test results were compared with the quantitative test result of bubble dynamic in two-dimensional (2D) model and the three-dimensional standard FE methods (finite elements) and coupled with the interface tracking algorithm. Although the color-gradient model shows great improvement. This type of model still requires a thorough validation and study which large errors may arise for example discontinuity problem that affects the use of the lattice Boltzmann method.

Li et al[79] proposed a new method to simplify and reduce the amount of calculation of mutliphase LBM at a higher density ratio. The model has been named the simplified LBM as simplified lattice Boltzmann model and their numerical result was verified with the experimental one. Numerical results have been reviewed on an impact of a single droplet onto

a stationary liquid film. Another side, multiphase (two-phase) flow numerically analyzed by lattice Boltzmann method for double droplets that time travel and horizontal distance onto a liquid film has been considered. A central difference scheme has been used in this numerical process. The simplified methods simulation result shows excellent stability with the extremely lower parasitic current.

The highly accurate simplified lattice Boltzmann method (HSLBM) combined with the local second-order simplified and highly stable lattice Boltzmann method (SHSLBM) reported by Chen et al[80]. Their target was to achieve the correlation between the grid spacing and streaming distance by a high-order interpolation algorithm. Their investigation was for various test cases such are various applications like Two-dimensional (2D) lid-driven flow, plane Poiseuille flow, polar cavity flow, three-dimensional (3D) lid-driven cavity flow and flow past a stationary circular cylinder. Overall, they examined the flexibility and robustness of the higher simplified lattice Boltzmann method (HSLBM). HSLBM and SHSLBM results were verified, and it shows that HSLBM provides more accurate results than SHLBM for the same size of the grid. HSLBM reduced the computational time and virtual memory more than SHSLBM. Additionally, SHSLBM shows good numerical stability in HSLBM.

Chan and Shu et al reporetd the simplified lattice Boltzmann method (SLBM)[80] based on the non-Newtonian power-law fluid flows. Their study has adopted a new method named predictor-corrector. And constructed the solutions for the macroscopic equations that are recovered from the lattice Boltzmann method by expanding the Chapmann-Enskog analysis. The truncated power law is included in this method to locally improve the physical viscosity and incorporated relaxation parameters to recover the behaviour of the non-Newtonian fluid. D2Q9 lattice model simulated for plane Poiseuille flow, lid-driven cavity flow, and 3D lid-driven flow by SLBM. Their results were verified with the conventional lattice Boltzmann and SLBM. Their proposed result shows that the new method of SLBM eliminates the drawbacks that are the high cost of virtual memory and inconvenient execution of physical boundary conditions than the conventional LBM method.

Chen et al[81] reported numerical analysis based on diffusion of simplified lattice Boltzmann method. Their study suggests phenomena of numerical diffusion in the simplified lattice Boltzmann method (SLBM) with the non-equilibrium distribution function at the time of evaluation. That makes the numerical flow unstable and less accurate. Their study suggests that their model was able to achieve better accuracy by recovering the flow structures for the complex flow by reducing numerical diffusion. Moreover, to correct the flow properties in the non-equilibrium distribution function and improve the numerical acerbity, they introduced a revised simplified lattice Boltzmann method (RSLBM). In the RSLBM predictor-corrector scheme used for the unsteady flows. RSLBM carried out 2D Lid-driven cavity flow scheme

used for the unsteady flows. RSLBM carried out 2D Lid-driven cavity flow, 3D lid-driven cavity flow, and decaying vortex are reported for the numerical simulation for SLBM and RSLBM. Their results were verified with the numerical results and the SLBM and RSLBM. The results show that SLBM is better for high Reynolds numbers and numerical stability scenarios. RSLBM improve the ground structure for the SLBM. The accuracy of the test result shows for the decaying vortex flow that RSLBM is having more accuracy than the SLBM on the same size of the mesh. For the case of two dimensional (2D) lid-driven test, RSLBM executes the better performance to recover the flow structure because of lower numerical diffusion. RSLBM take over better numerical stability of SLBM in the case of coarse grid size. In three-dimensional (3D) simulation for lid-driven cavity flow, RSLBM showed better accuracy than SLBM for the nonuniform grids.

Simplified lattice Boltzmann flux solver (LBFS) for multiphase fluid with higher computational efficiency is studied by Yang et al[82] in detail. Multiphase lattice Boltzmann flux solver (MLBFS) which is based on the FVM method (finite volume). Their model improved a model name the simplified multiphase LBFS with higher computational efficiency than the original conventional model. MLBFS is free from limitations like a uniform grid, grid spacing, coupled time step and high virtual memories. Their investigation considered for MLBFS simulation for the bubble rising under buoyance, Laplace law, Raleigh-Taylor instability and droplet splashing on a film to verify the computational efficiency and accuracy. Their study suggests that the flow simulation could deal with high-density ratios and complex interface interaction. The proposed results shows that their method predicts the same results as the original lattice Boltzmann flux solver (LBFS) in terms of accuracy and stability. The reliability and accuracy of the original model maintained in the present model. Moreover, their method reduces computational time. Their results suggests that the simplified method is a good recommendation for computational efficiency and especially on occasions with a large number of grids.

Peng et al[83] reported a simplified thermal energy distribution model. A new distribution function that was able to simulate the temperature field. And the bounce-back rule is applied for the non-equilibrium distribution function for this work. For the test case, an application as a porous plate is taken into account to investigate the accuracy in space. From the analytical solution, the velocity field in a steady state has been reviewed. Later, they concentrated on the numerical analysis versus lattice spacing error numerical simulation. In the original thermal energy distribution model, the velocity and macroscopic density fields were simulated by the density distribution function. The simplified thermal energy distribution model has the subsequent great features as verified with the original thermal energy distribution model. They examined numerical simulation for the natural convection in a 2D square cavity at various

ranges of Rayleigh numbers (relationship between the buoyancy and viscosity within a fluid). They suggest high Rayleigh number is better for the model improvement (e.g., the Rayleigh number is 10^4). Their simulation results were able to attain the accuracy in the flow more successfully than the original thermal model. Regarding the computational efficiency for the same size of grid size, the simplified thermal model shows the thermal model consumes less computation time than the original method. The uniform grid taken into account for all the test case simulation.

An Immersed boundary-simplified lattice Boltzmann (IB-SLBM) developed by Chen et al[84] considering the 2D numerical analysis of incompressible viscous flows with immersed objects. Simplified lattice Boltzmann method (SLBM) that is combined with the boundary condition-enforced immersed boundary method. The combined solver named as immersed boundary simplified lattice Boltzmann method. They verified the results of SLBM and IB-SLBM with various case studies. Such test cases are involved with flow past a stationary circular cylinder, flow past a transversely oscillating cylinder, uniformly accelerated flat plate and flow around a flapping foil. The governing equations resolved by using the predictor-corrector scheme. SLBM used in the predictor step to analyse intermediate flow variables. And IBM uses to impose the velocity correction on the intermediate quantities at the stage of the corrector. The simulations result successfully investigated for flow stability and convergence. That apparently demonstrates the flexibility and accuracy of IB-SLBM in the case of modelling the moving boundary problems.

Similarly, Dash et al[85] reported a work on flexible forcing immersed boundary-simplified lattice Boltzmann method (FFIB-SLBM). Two-dimensional (2D) and three-dimensional (3D) numerical simulation executed for interaction of fluid-solid. Mainly they were focused on various applications such are Taylor-green decaying vortex, flow over a stationary circular cylinder, single circular particle sedimentation, inclined lid-driven cavity, two circular particle sedimentation, flow over a stationary sphere, and single sphere sedimentation. They studied the FFIB-SLBM algorithm which is advantageous over the conventional immersed boundary lattice Boltzmann method (IB-LBM). The results were suggest to reduce the mathematical formulation and avoiding the requirement of memory. And memory to store the functions of density distribution in the standard LBM. FFIB-SLBM notably reduces the effort in the new computational code evolution.

Droplet deformation and breakup in shear flow have been studied by Komrakova et al[86]. Lattice Boltzmann methods used for simulating the 3D numerical analysis of binary systems to observe the conditions of droplet deformation and breakup in a simple shear flow. Diffuse interface used for the numerical analysis. They investigated the droplet behaviour in shear

flow by numerically and experimentally. For the stokes flow simulations, a single drop is considered. In this simulation, convergence has been used for increasing the resolution to an asymptotic value. To attain the drop's moderate resolution, they the droplet radius of less than 30 lattice units and there is an insignificant thickness of the interface. For the large droplet (32-64 lattice point), they used GPU (Graphics processing units) to attain smooth grid convergence. Grid convergence was performed by the thickness of the interface (Peclet and Cahn numbers) to check the accuracy and stability.

Xi et al[87] discussed the 3D numerical simulation for the Taylor experiment on droplet deformation in a shear flow. The investigation was for the single droplet deformation and breakup under simple shear flow was achieved by the Lattice Boltzmann method. In The Galilean-invariant, the 3D model was considered for the D3Q19 lattice. The mixing process in a shear flow is divided into three stages stretching and deformation of liquid droplets, the break up of the droplets and the coalescence of the resulting droplets over collision. They have been considered 3D two-fluid systems with the same kinematic viscosity and density. Simulation has been considered for small deformation limit of droplet shear and larger deformation to break up. They successfully achieve the accuracy for the flow.

2.9 Background study of computational grid analysis

Analysis of the stability and accuracy of different lattice Boltzmann methods has been reported for direct numerical simulations of turbulent flows[52] by SRT, MRT and RLB(regularized lattice Boltzmann methods. They have investigated the numerical analysis of 3D Taylor-Green vortices for homogeneous isotropic turbulent flows with different Reynolds numbers and grid resolutions. Their review shows, that the method requires a higher grid resolution for achieving stability and accuracy for the flow simulation. MRT was able to achieve accuracy and stability without failing the turbulence model and RLB shows the breakup nature of the flow. Similarly, the break-up nature appears at the higher Reynolds number flow which provides more insight into the flow resolution and grid convergence. Their RLB test case results show the numerical dissipation at the flow with lower accuracy. LBM method becomes a suitable method for turbulence models in terms of stability and accuracy of the flow. Their report indicates that flow accuracy was obtained due to the higher grid resolution. This agrees with other work with the local time step of Inamura et al[53]. Imamura et al reported the local time step method on the non-uniform grid. That assists to accelerate the solution to achieve the convergence of the flow in the steady state on a non-uniform grid at various Reynolds numbers. CPU depended on flow conditions and grid arrangement. CPU was

reduced significantly for lower Reynolds number and lower grid arrangement. As Reynolds number increases, grid resolution increases and CPU increases.

Three dimensional(3D) and two dimensional (2D) orthogonal central moment that significantly reduced the computational cost that reported by De Rosis et al[76][88]. In their recent paper, the D3Q27 lattice is considered for further simulation with the multi-relaxation color gradient model. Multi-relaxation time (MRT) uses for the simulation. Their discussion was on the single-phase collision operator with nonorthogonal central moments on account of the directness of its correlation to multi-relaxation time (MRT) and single relaxation time (SRT). Their test result shows the prediction of the interfacial tension for various density ratio up to 1000 (dimensionless number) with less error (0.40 $\%$) which was able to reduce the spurious velocity to a great extent. And numerical simulation for the corresponding to an actual reactor, reveals model stability that was more. Jet breakup length and median fragment diameter have been discussed in the UT simulation and experiments for the jet in the FT simulation to achieve the regime of atomization.

Chan and Shu et al[80] reported two-dimensional (2D) and three-dimensional (3D) simulations for incompressible viscous flows to accomplish the third order of accuracy in space. From the grid spacing, streaming distance was eliminated by the virtual streaming nodes. Various drawbacks are discussed for the lattice Boltzmann method that includes numerical instability at higher Reynolds numbers, the higher cost in virtual memory, implementation execution of physical boundary conditions, link-up of the streaming distance and time step. Computational cost and memory consumption for D3Q19-CM-LBM rather than D3Q27-CM-LBM. Memory usage is involved by the D3Q19-CM-LBM and D3Q27-CM-LBM within a generic LB run. The most complete discretization involves an additional cost of 30% [89][90].

2.10 Navier-Stokes equation

Let us consider a 2D Cartesian space x= [x; y] where x, y are the coordinates. The macroscopic behavior of a system composed of two immiscible fluids is governed by the Navier–Stokes equations [2][91]

$$\nabla.u = 0 \tag{2.1}$$

Where velocity vector $\mathbf{u} = \left[u_x, u_y\right]$ and $F = \left[F_x, F_y\right]$

$$\rho[\delta_t u + (u.\nabla)u] = \nabla_p + \mu\nabla^2 u + F \tag{2.2}$$

2.11 Allen-Cahn Equation

The evolution of the interface between the two fluids is tracked by the conservative form of the Allen-Cahn equation [1], that reads as follows

$$\delta\phi + \nabla.\phi u = \nabla.M\left[\nabla\phi - \frac{\nabla\phi}{|\nabla\phi|}\frac{1-4(\phi-\phi_0)^2}{\epsilon}\right] \tag{2.3}$$

Where M is mobility coefficient, ϵ is the interface thickness, ϕ is the order parameter that varies between ϕ_H = 1 for the heavier fluid and ϕ_L = 0 for lighter fluid one and ϕ_0 can be written as

$$\phi_0 = \left(\phi_H + \phi_L\right)/2 = 1/2$$

The Allen–Cahn equation is written by assuming that the interface velocity is split into a normal interface speed and an interface velocity due to external advection. Moreover, the normal interface speed is only proportional to the interface curvature. In addition, the equilibrium phase-field profile for an interface located [1] at $x = x_0$ is

$$\phi(x) = \frac{1}{2}\left[1 - \tanh\left(\frac{2\left|x - x_0\right|}{\xi}\right)\right] \tag{2.4}$$

Dimensionless parameters are considered as [92]: the Reynolds number, the Peclet number and the Cahn number, defined as

$$Re = \frac{U_0 L_0}{\nu}$$

$$Pe = \frac{U_0 L_0}{M}$$

$$Ch = \frac{\epsilon}{L_0} \tag{2.5}$$

2.12 Bhatnagar-Gross-Krook LBM Equation

Let us consider the 3D nineteen-velocity D3Q19 lattice discretization. Two sets of populations are involved in the computations. Controls the velocity field, The former, $|f_i\rangle = [f_0, ..., f_8]^T$, monitors the evolution of the order parameter $|.\rangle$ denotes a row vector and the superscript $^\top$ indicates the transpose operator. Distributions move on a fixed Cartesian cubic lattice along the links i = 0 . . . 8 with velocity $c_i = [|cx_i\rangle, |cy_i\rangle]$ defined as [28]

$$\begin{aligned} |c_{xi}\rangle &= [0, 1, -1, 0, 0, 0, 0, 1, -1, 1, -1, 1, -1, 1, -1, 0, 0, 0, 0]^\top \\ |c_{yi}\rangle &= [0, 0, 0, 1, -1, 0, 0, 1, -1, -1, 1, 0, 0, 0, 0, 1, -1, 1, -1]^\top \\ |c_{zi}\rangle &= [0, 0, 0, 0, 0, 1, -1, 0, 0, 0, 0, 1, -1, -1, 1, 1, -1, -1, 1]^\top \end{aligned} \tag{2.6}$$

The fluid density ρ is computed by a linear interpolation[73] that is,

$$\rho = \rho_L + \frac{\phi - \phi_L}{\phi_H - \phi_L} (\rho_H - \rho_L) \tag{2.7}$$

2.13 Lattice Boltzmann Equation

The governing lattice Boltzmann equations (LBEs) reads as follows [28] :

$$\begin{aligned} |f_i\left(x+c_i, t+1\right)\rangle &= |f_i^\star(x,t)\rangle \\ |g_i\left(x+c_i, t+1\right)\rangle &= |g_i^\star(x,t)\rangle \end{aligned} \tag{2.8}$$

where the superscript $\star$ represents the post-collision state. To lighten the notation, the dependence on space x and time t will be implicitly assumed in the rest of this section. Within the BGK approximation, post-collision [93] populations can be computed as

$$\begin{aligned} f_i^\star &= f_i + \frac{1}{\tau + 1/2}\left(f_i^{eq} - f_i\right) + F_i \\ g_i^\star &= g_i + \frac{1}{\tau_\phi + 1/2}\left(g_i^{eq} - g_i\right) + G_i \end{aligned} \tag{2.9}$$

where the equilibrium states are [73]

$$\begin{aligned} f_i^{eq} &= w_i\left[\tilde{p} + \frac{\mathbf{c}_i\cdot\mathbf{u}}{c_s^2} + \frac{\left(\mathbf{c}_i\cdot\mathbf{u}\right)^2}{2c_s^4} - \frac{\mathbf{u}^2}{2c_s^2}\right] \\ g_i^{eq} &= w_i\phi\left[1 + \frac{\mathbf{c}_i\cdot\mathbf{u}}{c_s^2} + \frac{\left(\mathbf{c}_i\cdot\mathbf{u}\right)^2}{2c_s^4} - \frac{\mathbf{u}^2}{2c_s^2}\right] \end{aligned} \tag{2.10}$$

$\tilde{p} = p/\left(\rho c_s^2\right)$ being the normalized pressure. Weighting factors are $w_0 = 1/3, w_{1,6} = 1/18$ and $w_{7\ldots18} = 1/36$ The lattice sound speed is $c_s = 1/\sqrt{3}$ [28].

2.14 Relaxation time

The relaxation times are evaluated as

$$\begin{aligned} \tau &= \tau_L + \frac{\varphi - \phi_L}{\phi_H - \phi_L}\left(\tau_H - \tau_L\right) \\ \tau_\phi &= \frac{M}{c_s^2} \end{aligned} \tag{2.11}$$

Where $\tau_L = \mu_L / (\rho c_s^2)$ and $\tau_H = \mu_H / (\rho c_s^L)$ are the relaxation times associated with the dynamic viscosities of the light and heavy fluids, respectively [73] The two forcing terms are [33]

$$\begin{aligned} F_i &= w_i \frac{\mathbf{c}_i \cdot F}{\rho c_s^2} \\ G_i &= w_i \frac{\mathbf{c}_i \cdot F_\phi}{c_s^2} \end{aligned} \tag{2.12}$$

where

$$F_\phi = \left[F_{x,\phi}, F_{y,\phi}, F_{z,\phi}\right] = c_s^2 \frac{1 - 4\left(\phi - \phi_0\right)^2}{\xi} \cdot \frac{\nabla \phi}{|\nabla \phi|} \tag{2.13}$$

The force F gathers four contributions [33]

$$F = F_s + F_p + F_\nu + F_b \tag{2.14}$$

F_s accounts for the surface tension r as

$$F_s = \mu_\phi \nabla \phi \tag{2.15}$$

with the chemical potential

$$\mu_\phi = 4\beta\left(\phi - \phi_L\right)\left(\phi - \phi_H\right)\left(\phi - \phi_0\right) - \kappa \nabla^2 \phi \tag{2.16}$$

where $\beta = 12\sigma/\xi$ and $\kappa = 3\sigma\xi/2$ [33]

Gradient and Laplacian of / can be computed by isotropic finite differences (FD)[94]

$$\nabla\phi = \frac{1}{c_s^2}\sum_i w_i \mathbf{c}_i \phi\left(x + \mathbf{c}_i\right) \tag{2.17}$$

$$\nabla^2\phi = \frac{2}{c_s^2}\sum_i w_i \left[\phi\left(x + \mathbf{c}_i\right) - \phi(x)\right] \tag{2.18}$$

The same formulas apply to estimate the spatial derivatives of any other quantity. Pressure and viscous forces are

$$\begin{aligned} F_p &= -\tilde{p} c_s^2 \nabla\rho \\ F_\nu &= \nu\left[\nabla\mathbf{u} + (\nabla\mathbf{u})^\top\right]\cdot\nabla\rho \end{aligned} \tag{2.19}$$

respectively, where the fluid kinematic viscosity is $\nu = \tau c_c^L$. The gradient of density is determined based on the gradient of the order parameter [73] that is,

$$\nabla\rho = \frac{\rho_H - \rho_L}{\phi_H - \phi_L}\nabla\phi \tag{2.20}$$

2.15 Forcing term

a generic body force accounts for F_b (e.g., gravity). Macroscopic variables are readily available as [73]

$$\begin{aligned} \tilde{p} &= \sum_i f_i \\ \mathbf{u} &= \sum_i f_i \mathbf{c}_i + \frac{F}{2\rho} \\ \phi &= \sum_i g_i \end{aligned} \tag{2.21}$$

The fluid density q is computed by a linear interpolation,[73] that is,

$$\rho = \rho_L + \frac{\phi - \phi_L}{\phi_H - \phi_L} (\rho_H - \rho_L) \tag{2.22}$$

if the collision matrix is set to $\Lambda = \omega \mathbf{I}$ where I is the unit tensor and $\omega = \frac{1}{\tau + 1/2}$ is the relaxation frequency. The term F_i accounts for external body forces F. The LBE can be divided into two steps, which are collision and streaming. Which are written as

2.16 Collision step

The collision is simply an algebraic local operation process. First, one calculates the density and the macroscopic velocity u to find the equilibrium distributions

$$\begin{aligned} |f_i^\star(x,t)\rangle = |f_i(x,t)\rangle + \Lambda \left[|f_i^{\mathrm{eq}}(x,t)\rangle - |f_i(x,t)\rangle \right] \\ + (\mathbf{I} - \Lambda/2) \, |F_i(x,t)\rangle \end{aligned} \tag{2.23}$$

2.17 Streaming process

After collision process, we stream the resulting distribution $f_i^\star$ to neighbouring nodes. The neighbouring nodes as in Equation 2.24. When these two process are completed, one time step has been elapsed, and the operations are repeated for further process.

$$|f_i\left(x + c_i, t + 1\right)\rangle = |f_i^\star(x, t)\rangle \tag{2.24}$$

2.18 CMs-based i collision operator

In order to build a CMs-based i collision operator, the lattice directions are shifted by the local fluid velocity [95] These shifted discrete velocities $\bar{c}_i$ can be defined as

$$\bar{c}_i = \left[\langle \bar{c}_{ix}|, \langle \bar{c}_{iy}|, \langle \bar{c}_{iz}|\right] \tag{2.25}$$

where

$$\begin{aligned} \bar{c}_{ix} &= \langle c_{ix} - u_x| \\ \bar{c}_{iy} &= \langle c_{iy} - u_y| \\ \bar{c}_{iz} &= \langle c_{iz} - u_z| \end{aligned} \tag{2.26}$$

Populations are transformed into central moments by applying the following transformation matrix T [89]. The relaxation matrix in the populations space then is relaxation matrix in the CMs space are discussed in detail in the section Appendices A.1, A.2, A.3, A.4, A.5, and A.6. Within the BGK approximation,[43] post-collision populations can be written as

$$\begin{aligned} f_i^\star &= f_i + \frac{1}{\tau + 1/2}\left(f_i^{eq} - f_i\right) + F_i \\ g_i^\star &= g_i + \frac{1}{\tau_\phi + 1/2}\left(g_i^{eq} - g_i\right) + G_i \end{aligned} \tag{2.27}$$

where the equilibrium states are [73]

$$
\begin{aligned}
f_i^{eq} &= w_i \left[\tilde{p} + \frac{\mathbf{c}_i \cdot \mathbf{u}}{c_s^2} + \frac{(\mathbf{c}_i \cdot \mathbf{u})^2}{2c_s^4} - \frac{\mathbf{u}^2}{2c_s^2} \right] \\
g_i^{eq} &= w_i \phi \left[1 + \frac{\mathbf{c}_i \cdot \mathbf{u}}{c_s^2} + \frac{(\mathbf{c}_i \cdot \mathbf{u})^2}{2c_s^4} - \frac{\mathbf{u}^2}{2c_s^2} \right]
\end{aligned}
\tag{2.28}
$$

2.19 Algorithm

Cycle of LBM algorithm: An overview of one cycle process of the LB algorithm shown as

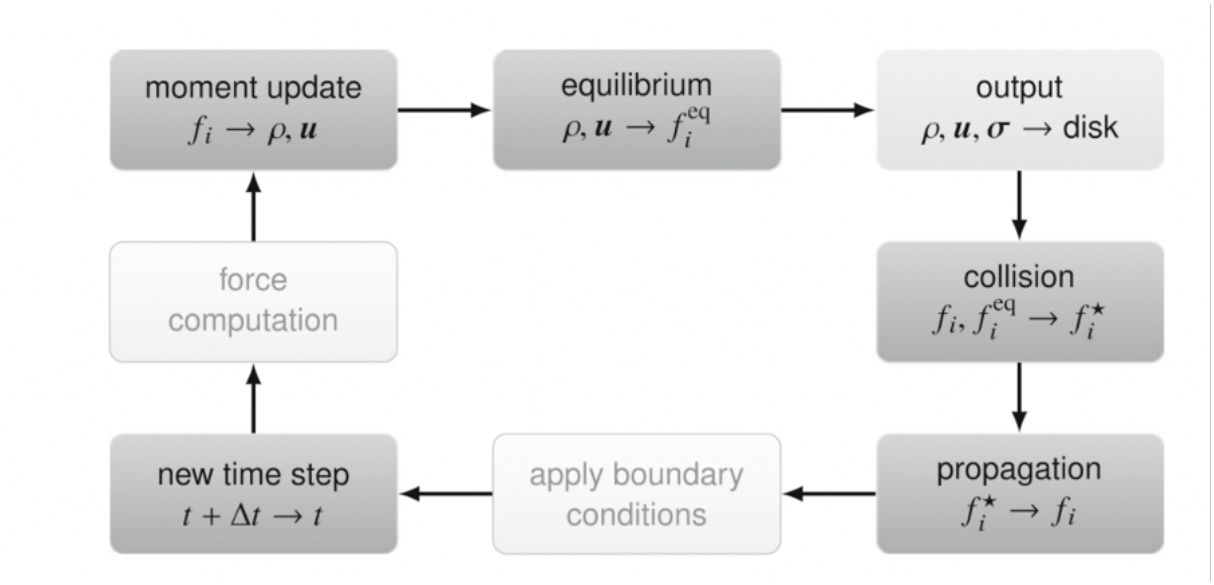

Figure 2.6. An overview of one cycle of the LB algorithm: from the left the dark grey boxes show sub-steps that are necessary for the evolution of the process of the solution. On the right the light grey box indicates the optional output step.
[28]

2.20 Flow chart of LBM algorithm

In this section, LBM Algorithm performed for single mode RTI and multi-mode RTI computation. Computation process discussed detail in Appendix A.10, A.11, A.12, A.13, A.14, A.15, A.16, A.17, A.18, A.19, A.20, A.21. Within the typical time step, the proposed scheme performs the following actions shown in Figure 2.7:

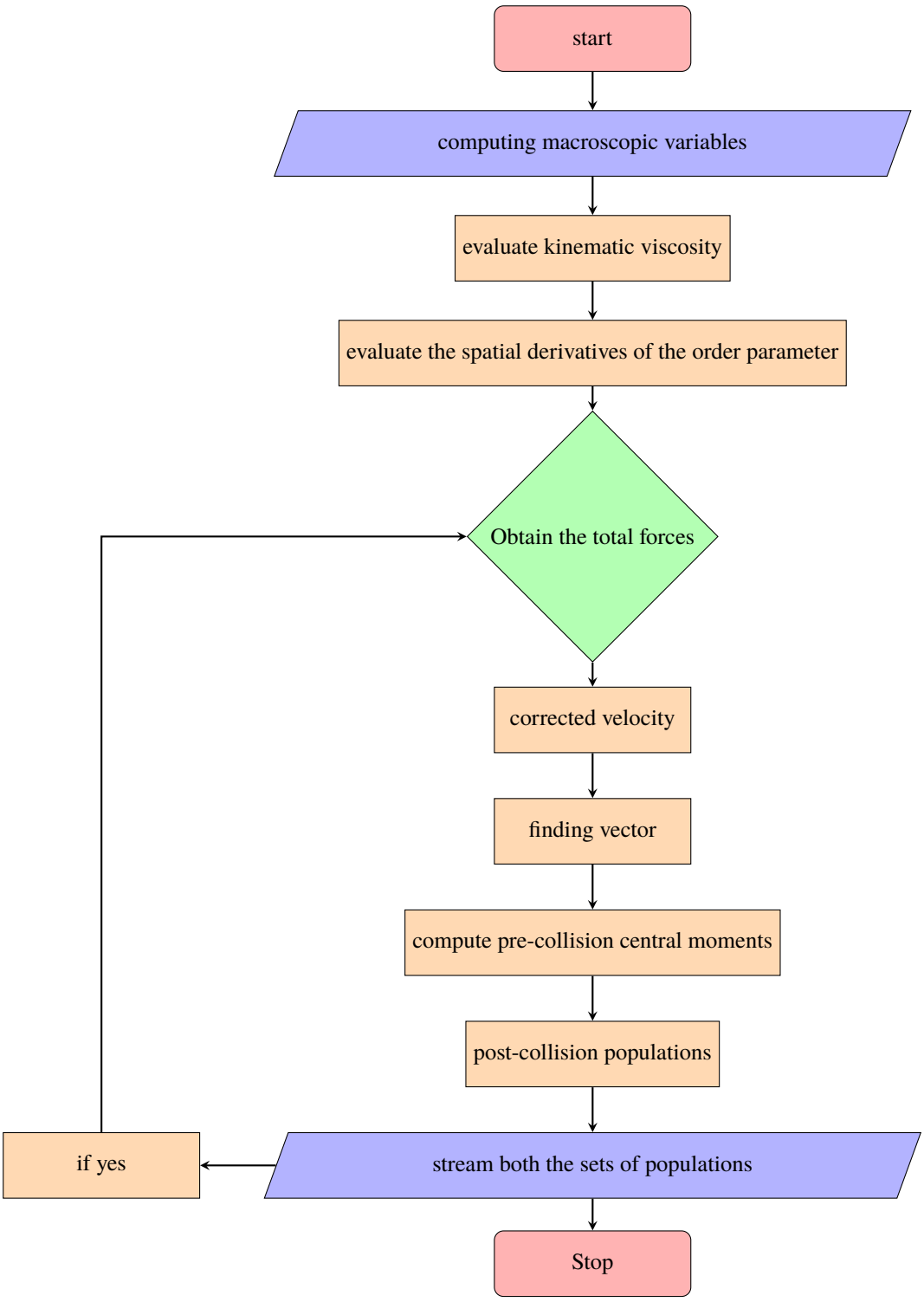

Figure 2.7. Flow chart of computational process by LBM coding

Chapter 3

Single-mode RTI analysis

This chapter is the first of the core results chapters and is taken from the following publication:

A De Rosis and E Enan. A three-dimensional phase-field lattice Boltzmann method for incompressible two components flows, Physics of Fluids 33, 043315 (2021) [2]

This paper presents work undertaken as part of the project. The aim of the project is to investigate the two-dimensional analysis and three dimensions single-mode RTI. My contributions to this paper are as follows: validating the numerical model, setting up and running all of the simulations, post-processing, analysing the result, and writing the introduction and results of the RTI analysis of the paper.

3.1 Context

In this paper, a lattice Boltzmann model (LBM) for the coupled Allen–Cahn–Navier–Stokes equations in three dimensions is presented. Two equations are solved: one for the fluid velocity and one for the order parameter or phase-field variables. Both are written within the general multiple-relaxation-time framework, where all the distribution functions as equilibrium and forcing terms are described by using the full set of Hermite polynomials. The resultant practical implementation is compact. The gradient of the order parameter can be computed by the non-local finite differences or the local central moments. We used central moment-based LBM and finite difference for 2D, and 3D RTI analysis. And analysis is processed for Reynolds numbers such as Re=256, 3000 and 30 000 for various test cases to achieve a very good accuracy and instability by central moments in terms of capturing interface evolution and validated. Specifically, two groups of tests are tackled. The velocity field is superimposed and the order parameter equation is solved for the evolution of the interface of two fluids. Further, these numerical experiments are discussed and the results show the ability of the proposed scheme to capture the correct evolution of the interface.

3.2 Introduction

The flow of two immiscible incompressible fluids at arbitrary density and viscosity contrasts is commonly experienced in many areas of science and engineering. Their study and application are a key part of multiphase and multicomponent flow solvers in modern computational fluid dynamics (CFD). A popular approach to multiphase CFD is represented by the so-called diffusive interface method,[48] where the interface between the two fluids is represented by a transitional layer with finite thickness across the one fluid properties are continuous and vary smoothly. Diffusive interface methods introduce a continuous phase-field variable (also known as order parameter) to identify and distinguish the different phases/components. The evolution of this quantity can be computed by solving the Cahn–Hilliard equation [96] or the Allen–Cahn equation [97] within the traditional CFD based on the solution of the macroscopic Navier–Stokes equations, the phase-field modelling has attracted large attention in recent years leading to finite volume solutions of the C–H and A–C equations coupled to the N–S ones [49][98]

Alternatively to the macroscopic-based formulations,[99]–[102] the lattice Boltzmann method has become a very powerful approach to simulating the flow of viscous fluids [28][103][104]. In short, the LBM idealizes a fluid as collections (also known as distributions or populations) of fictitious particles moving along the links of a fixed Cartesian lattice. These mesoscopic quantities carry with them information about the macroscopic variables (i.e., density and momentum). The widespread adoption of the LBM stems from several advantages. In contrast to Navier–Stokes solvers, which need to treat the non-linear convection term, the LBM does not include such non-linearity. The resultant algorithmic simplicity of the LBM implies easy coding and allows it to be particularly well-suited for massively parallel computing [105] Moreover, the LBM is applicable to simulate multiphase and multicomponent flows due to the possibility to incorporate microscopic interactions [106].

Complex boundaries are easy to deal with using the bounce-back rule and thus the LBM can be applied to simulate flows with complex geometries such as porous media flows [107]. Relevant industrial applications of the LBM cover external aerodynamics, acoustics, and heat transfer. In the last ten years, several companies invested in this technology. The case of Dassault Systemes has bought the popular software XFlow [108], PowerFLOW [109] and OMNIS/LB by Numeca , a commercial branch of Palabos[110]. There are other examples of commercial LBM-based software such as ProLB by CS,[111] ultraFluidX by Altair, and SimScale. Among the rich variety of applications where the LBM has been successfully employed to simulate the multiphase and multicomponent flows which gained impressively

popularity [37][112][113]. Aiming at simulating this class of flows, four different approaches can be identified: the color-gradient model, [30] [34][36][66][68][75][114]–[116], the pseudo-potentialmodel [117]–[120], the free energy model [31] [120][121] and the phase-field approach [12][14][29][33][122][123].

The latter has seen the rise of many recent efforts leading to progressively more sophisticated developments of the theory and numerical implementation. Contributions can be classified into two main groups. The former gathers the works aimed at recovering the Chan–Hillard (C-H) equation. In this regard, Zu and He [61] proposed a scheme with enhanced accuracy and stability with respect to the previous work by Zheng [124] Liang[29][125] developed a multiple-relaxation-time LBM with the introduction of a time derivative in the source term. The latter group develops LBM for the A–C equation. Specifically, a competitive algorithm was proposed by Geier [123] and Fakhari [12] for two and three-dimensional simulations, respectively. In these works, the authors argued that the non-local computation of the gradient of the order parameter can be avoided because the same quantity can be derived by the local estimation of the first-order central moments. Alternative strategies to perform a local calculation of the gradient of the order parameter were proposed by Wang [126] and Liang[127]. Ren[56] proved that the model in Ref. [123] generated artificial terms in the recovered equation. In order to circumvent this problem, they added a time-derivative term. The comparative study by Begmohammadi [128] showed that the artificial terms in the model by Geier [123] do not dramatically affect the accuracy of the solution, which is in turn roughly similar to the one achieved by the methods in Refs.[56] and [126]. Recently, Zu[92] has presented a scheme with exceptionally high accuracy properties.

In this present paper, we propose a three-dimensional (3D) model to solve the coupled Allen–Cahn–Navier–Stokes equations for a system composed of two immiscible incompressible fluids by solving two LBEs through the D3Q19 discretization. We derive a general multiple-relaxation-time framework for both equations respectively. The resultant collision operators are written in terms of central moments and it is demonstrated that the classical raw-moments-based LBM is a sub-case of the central-moments-based one. Recently, central moments have also been adopted by Gruszczynski [73] within the framework of the so-called cascaded LBM [95]. It is also worth noting that an LBM for collision operator in the central moment space with the decoupled interface tracking for simulations of high Reynolds and Weber regimes has been very recently presented by Hosseini [129]. Differently from these works, instead of computing moments of the continuous equilibrium and forcing terms, we adopt the discrete counterparts written with the full set of Hermite polynomials [63][90][130]–[136] and it results in a compact algorithmic procedure. Interestingly, Dinesh Kumar [45] has developed a phase-field LBM for two immiscible fluids. Differently from this work, our approach uses the full set of Hermite polynomials for all the equilibrium and forcing terms.

Moreover, we employ central moments instead of raw ones in the collision operators. In the three-dimensional (3D) interface tracking LB simulations have been recently carried out by Fakhari, [12] who built a double-BGK LBM where the velocity space is discretized by seven and fifteen lattice directions. Here, we show that the adoption of nineteen velocities is instrumental to perform more accurate simulations. The approach presented in this paper is tested against nine well-consolidated benchmark problems exhibiting very good accuracy.

3.3 Two Dimensional Rayleigh–Taylor instability

The Rayleigh–Taylor instability is a very popular benchmark to test the ability of a numerical scheme to tackle a system composed of two immiscible fluids[42][137]. Let us consider a rectangular domain of size W×4W with W=256. Where lattice size is in x axis 256 and Y axis is in 4×W= 1024. A heavy fluid is placed on top of a lighter fluid. The velocity is initially set to zero and the order parameter ϕ is initialized as

$$\begin{gathered}\phi(x,t=0)=\phi_H,\ \text{if}\ y>2W+0.1W\cos\left(2\pi\frac{x}{W}\right)\\ \phi(x,t=0)=\phi_L\end{gathered} \tag{3.1}$$

No-slip walls are enforced at the top and bottom sections, while the domain is periodic in the horizontal direction. The flow is driven by a gravitational force is defined as

$$F=\left[\rho(x,t)-\frac{\rho_H+\rho_L}{2}\right]g \tag{3.2}$$

The gradient of the order parameter can be computed by the non-local finite differences or the local central moments. The latter suffers from grid-scale oscillations. The very good accuracy properties are demonstrated against nine well-consolidated benchmark tests. Specifically, two groups of tests are tackled. In the former, the velocity field is superimposed. Hence, only the equation for the evolution of the order parameter is solved. These numerical experiments demonstrate the ability of the proposed scheme to capture the correct evolution of the interface. In the latter, two immiscible fluids are considered and the two equations are solved. Simulations of the vertical penetration of a wedge-shaped body, two- and three-dimensional Rayleigh–Taylor instability prove that two-fluids systems can be successfully simulated by our approach. Figures 2.6, 3.2 and 3.3 depict the order parameter at salient time instants when $\mathrm{Re}=256$, $\mathrm{Re}=3000$, and $\mathrm{Re}=30000$ respectively.

Table 3.1. 2D Rayleigh–Taylor instability at Re=30 000: vertical position of the spike of the interface normalized by the width of the domain at representative time instants.

t	0	0.5	1.0	1.5	2	2.5	3.0
$y^{\dagger}$	1.900	1.829	1.620	1.365	1.118	0.863	0.575

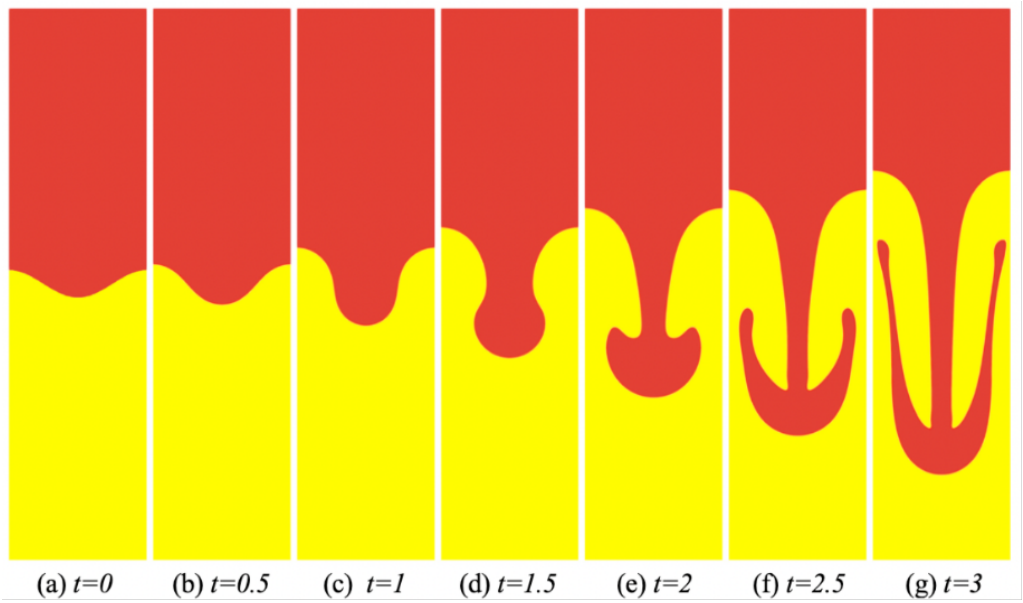

Figure 3.1. Two-dimensional Rayleigh-Taylor instability at time t Re $= 256$: evolution of the interface at various time (a) $t = 0$, (b) $t = 0.5$, (c) $t = 1$, (d) $t = 1.5$, (e) $t = 2$, (f) $t = 2.5$ and $(g)t = 3.0$.

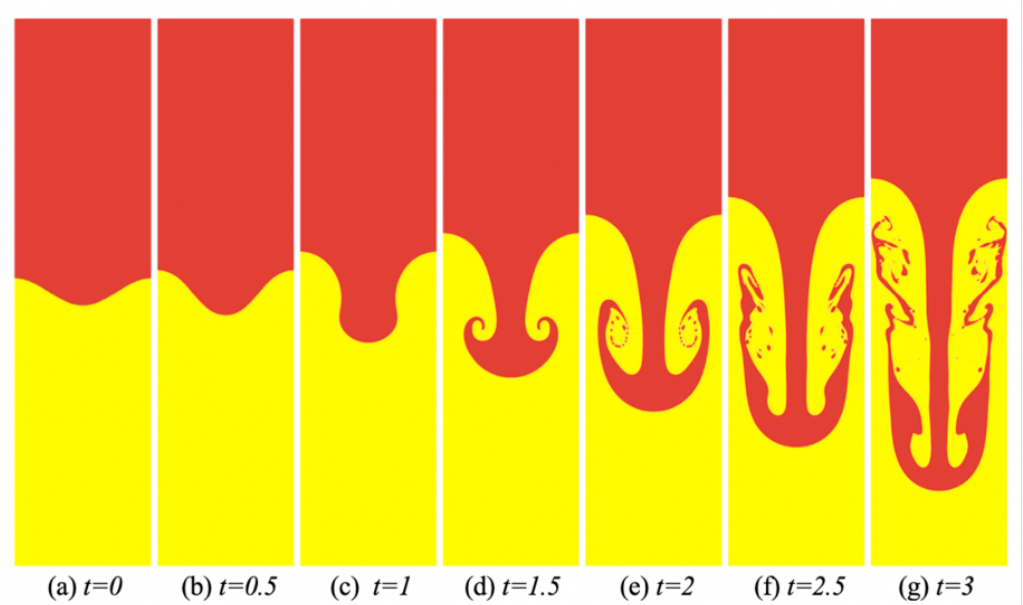

Figure 3.2. Two-dimensional Rayleigh-Taylor instability at Re $= 3000$: evolution of the interface at (a)$t = 0$, (b)$t = 0.5$, (c)$t = 1$, (d)$t = 1.5$, (e)$t = 2$, (f) $t = 2.5$ and (g)$t = 3$.

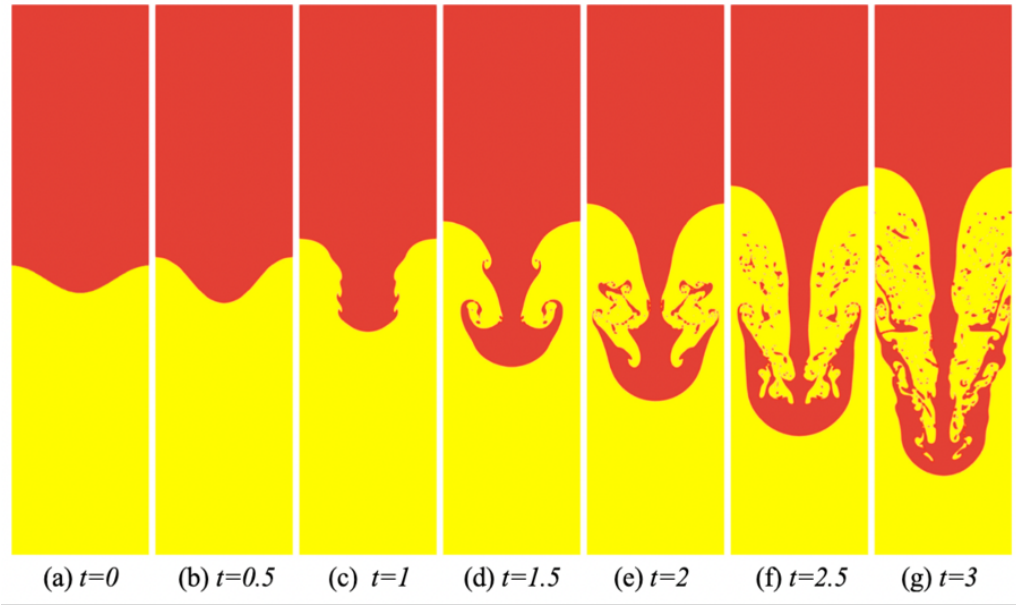

Figure 3.3. Two-dimensional Rayleigh-Taylor instability at Re $= 30000$: evolution of the interface at (a) $t = 0$, (b) $t = 0.5$, (c) $t = 1$, (d) $t = 1.5$, (e) $t = 2$, (f) $t = 2.5$ and $(g)t = 3$.

We validate our scheme against the results presented in Refs. [33][45][50][56] at Re $= 256$ and Re $= 3000$. Figures 3.4 and 3.5 sketches the time evolution of the position of the spike of the interface normalized by the width of the domain W, i.e., $y^{\dagger} = y/W$. One can immediately see that a very good agreement is found between our results and reference ones.

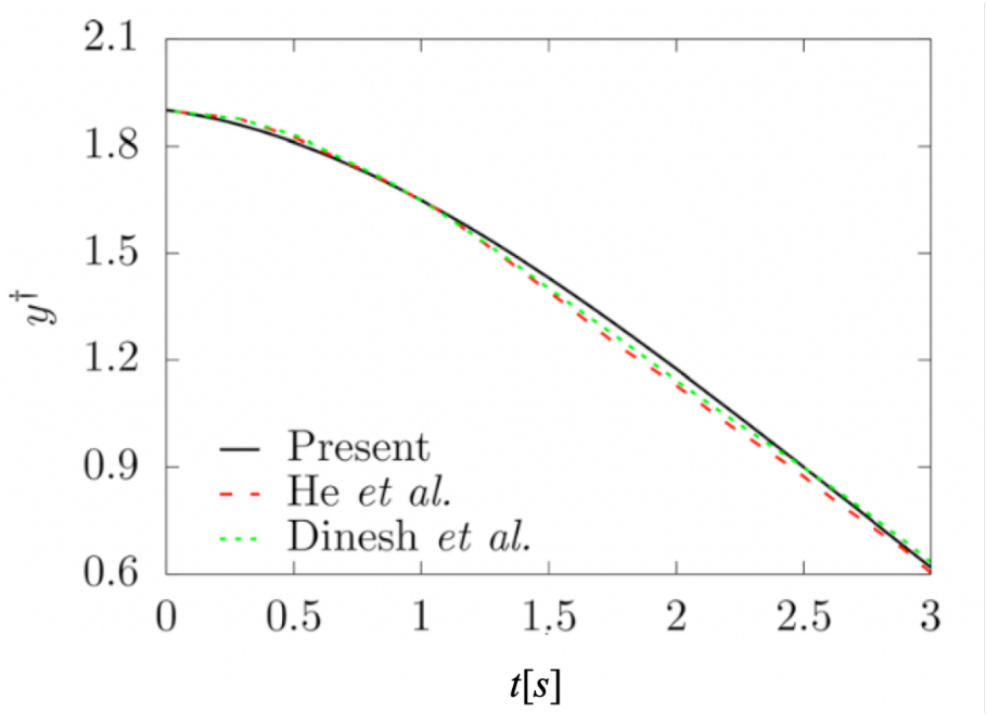

Figure 3.4. 2D Rayleigh-Taylor instability at Re $= 256$
Present findings are compared to those reported by He[50] Dinesh Kumar[45]

From the Figures 3.1, 3.2 we experience the downward penetration of the heavy fluid, accompanied by the roll-up of the primary spike and the subsequent generation of the secondary

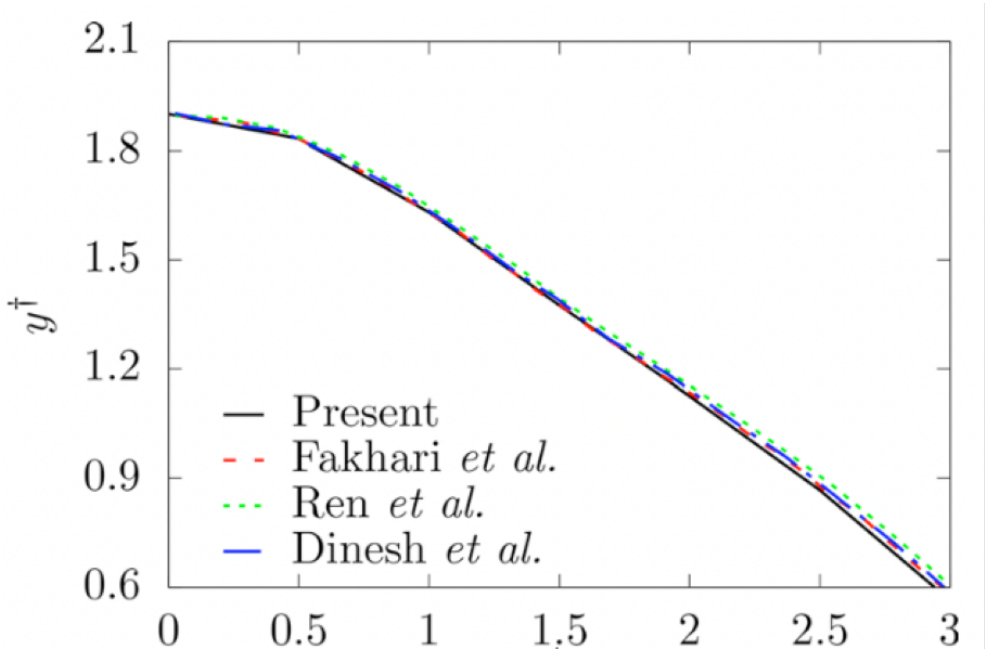

Figure 3.5. 2D Rayleigh-Taylor instability at Re $= 3000$
Present findings are compared to those reported Dinesh Kumar [45] Ren [56] and Fakhari [33]

spike in the upward direction. As Reynolds number grows, the breakup of the secondary spike into multiple droplets becomes more prominent. These features corroborate the observations in [12][45] and [129] where the very same patterns have been observed. An additional simulation is carried out at Re= 30 000 and the order parameter is reported in Figure 3.3. At $t = 1s$, several Kelvin–Helmholtz instabilities arise along the initial perturbation. Moreover, the presence of smaller-scale structures in the domain appears even more evident. For the sake of reference and completeness, the vertical position of the spike of the interface $y^\dagger$ at Re $= 30000$ is reported in Table 3.1 at representative time instants.

3.4 Three dimensional Rayleigh–Taylor instability

We conclude our numerical simulation with the simulation of the 3D Rayleigh–Taylor instability [55]. A three-dimensional domain of size W×4W×W with W=64 is considered. The order parameter ϕ is initialized as

$$\begin{gathered}\phi(x, t=0) = \phi_H, \text{ if } y > 2W + 0.05W[\cos(2\pi x) + \cos(2\pi z)] \\ \phi(x, t=0) = \phi_L, \text{otherwise}\end{gathered} \tag{3.3}$$

Dimensionless governing parameters are Re=256; At=0:5; Ca=960 and Pe=1024. Figure 3.6, the evolution of the interface between the two fluids is sketched at salient time instants.

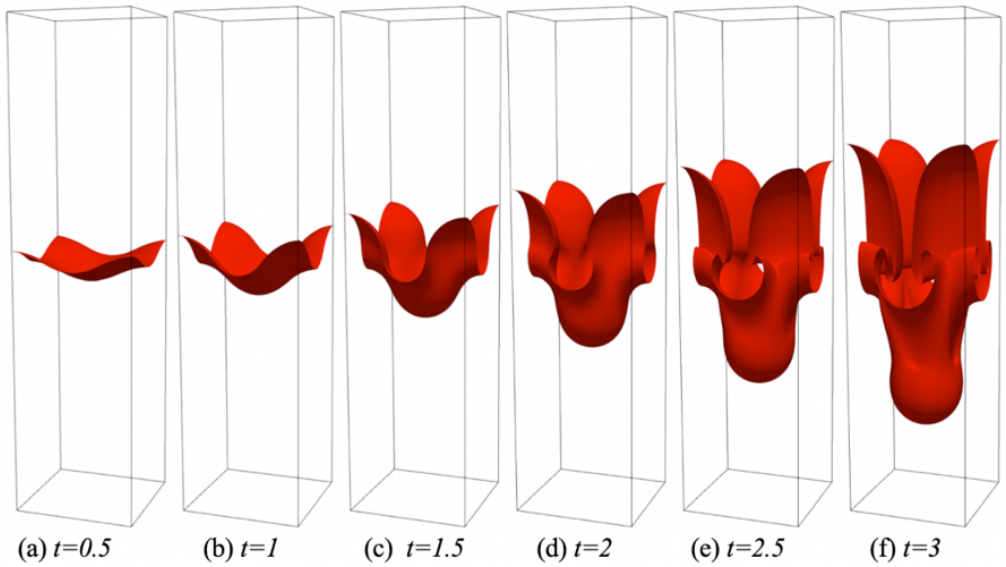

Figure 3.6. 3D Rayleigh-Taylor instability: evolution of the interface at (a) $t = 0.5$, (b) $t = 1$, (c) $t = 1.5$, (d) $t = 2$, (e) $t = 2.5$ and (f) $t = 3$ when Re $= 256$.

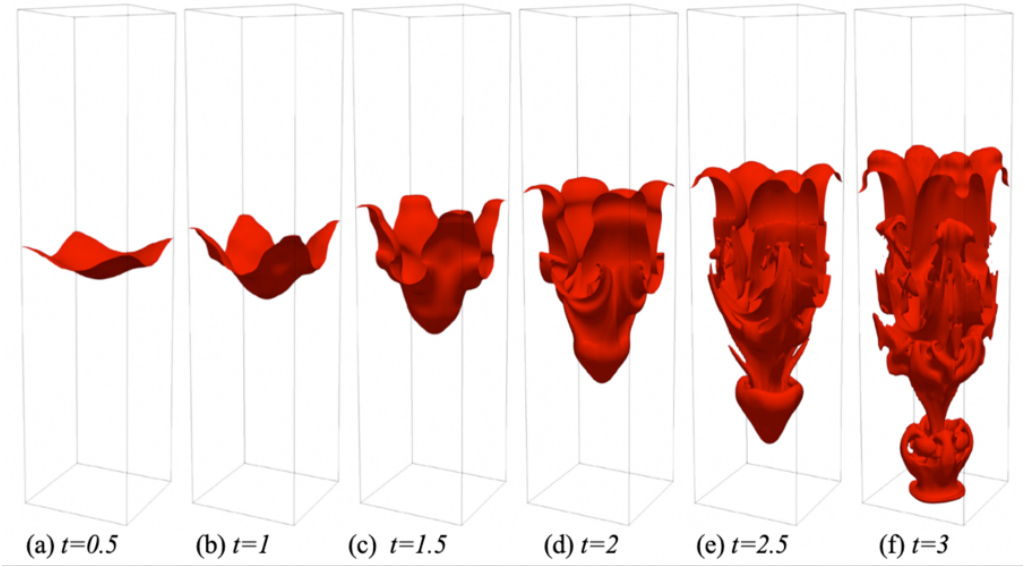

Figure 3.7. 3D Rayleigh-Taylor instability: evolution of the interface at (a) $t = 0.5$, (b) $t = 1$, (c) $t = 1.5$, (d) $t = 2$, (e) $t = 2.5$ and (f) $t = 3$ when Re $= 3000$.

At $t = 2s$, the first roll-up of the heavy fluid appears close to the saddle points due to the presence of a Kelvin–Helmholtz instability mechanism. The roll-up at the edge of the spike starts at a later time. These observations are consistent with consolidated reference data in Ref.[55]. The proposed approach shows a satisfying agreement with data from the literature, even though some discrepancies are also observed as time advances. These could be related to the equilibration of high order moments as well as the increased bulk viscosity of CMs-based algorithms [89][90]. Eventually, we illustrate a turbulent scenario where the Reynolds is set to 3000. Figure 3.7 shows the presence of many small-scale structures arising as a consequence of Kelvin–Helmholtz instabilities. The roll-up of spikes and bubbles is more evident. The heavy fluid falls more rapidly due to the lower viscous friction. The interface impacts the bottom sections at $t \sim 3s$ after having assumed a more conic shape with respect to the previous case.

A more quantitative analysis of the result is reported in Table 3.2. The accuracy of the present approach is assessed by comparing the vertical position of the spike at representative time instants to findings obtained by other models. Various test cases are run for the simulation to achieve the quantitative analysis with central moments, central differences method and multiple relaxation time(MRT). Which three dimensional analysis for color-gradient LBM [89] for collision operator in terms of central moments, three dimensional analysis for D3Q27,[90]color-gradient LBM with collision operator in terms of central moments in the D3Q27 space and three dimensional color-gradient analysis[36] with collision operator in terms of raw moments in the D3Q27 space. The seminal work in Ref. [55], where a three Dimensional numerical analysis done by BGK LB model for multiphase flows. Finally, the 3 Dimensional analysis by phase-field-MRT LB scheme,[138] with collision operator in terms of raw moments in the D3Q19 space. A solution of the coupled Cahn–Hilliard—Navier–Stokes equations numerically analyzed.[139].

Table 3.2. Quantitative analysis of Rayleigh–Taylor instability: time evolution of the position of the spike of the interface at salient time instants. Present results are compared to those from (i) present scheme with finite differences (FD), (ii)present scheme with moments (Mom), (iii) the D3Q19-CGM-CM-LBM [89] (iv) the D3Q27-CGM-CM-LBM, [90] (v) a D3Q27-CGM-MRT LB scheme[36] (vi) a D3Q15-BGK LB model for multiphase flows,[55] (vii) a D3Q19-phase-field-MRT LB scheme, [138] and (viii) a solution of the coupled Navier–Stokes – Cahn–Hilliard equations.[139]

t	FD	Mom	Ref.[89]	Ref.[90]	Ref.[36]	Ref[55]	Ref.[138]	Ref.[139]
0.0	1.898	1.898	1.897	1.897	1.895	1.887	1.888	1.904
0.5	1.858	1.850	1.897	1.897	1.864	1.839	1.860	1.869
1.0	1.741	1.711	1.753	1.753	1.763	1.744	1.755	1.776
1.5	1.553	1.504	1.592	1.591	1.587	1.555	1.569	1.618
2.0	1.304	1.256	1.381	1.378	1.357	1.312	1.325	1.396
2.5	1.001	0.998	1.126	1.121	1.085	1.022	1.037	1.149
3.0	0.648	0.711	0.844	0.791	0.788	0.712	0.740	0.863

For the vertical position of the spike normalized by the width of the domain is reported in Table 3.3 for this case. Interface evolution of two fluids with Reynolds number Re= 30 000 at various times time step $t = 3s$ shown in the table.

Table 3.3. 3D Rayleigh–Taylor instability at Re=30 000 : vertical position of the spike of the interface normalized by the width of the domain at representative time instants.

t	0	0.5	1.0	1.5	2	2.5	3.0
$y^{\dagger}$	1.898	1.848	1.680	1.384	0.964	0.436	0

Chapter 4

Multi-mode RTI Analysis

Numerical Modelling of the multi-mode turbulent Rayleigh-Taylor instability by a central-moments-based lattice Boltzmann method. Enan, Enatri and De Rosis, Alessandro [140]

This chapter presents work undertaken as part of project. Aim of the project to investigate the two dimensional multi-mode mode RTI for two fluids, The projected result submitted for review. which I authored[140]. My contributions to this paper are as follows: Developing the multimode model mathematically and setting-up the numerical simulation and running all of the simulations, post-processing, result analysis, and writing the paper.

4.1 Context

In this paper, we conduct the 2D simulation of the turbulent Rayleigh-Taylor instability at moderate and high Atwood number by the lattice Boltzmann method. We have evaluated several test case for multi-mode immiscible Rayleigh-Taylor instability (RTI) for both the Atwood and Reynolds number. For each test case, a comprehensive range of values of the Reynolds number $100 \leq 30000$ and low Atwood number At = 0.1 and high Atwood number At= 0.5 to 0.83 are considered. First, our approach is to develop a model mathematically from a single-mode RTI to multi-mode RTI. Then, the model is adopted to investigate the multi-mode RTI numerically. Notably, our results have successfully showed capability to capture the linear growth, saturated velocity growth, and chaotic development stages. The work will focus on investigating the late time stage evolution of two dimensional RTI of two or immiscible fluids and to perform a long time simulation resulting of the spike and bubble front acceleration with various Reynolds number to observe flow accuracy and stability. We analyse the effects of the initial conditions in terms of the perturbation spike and bubble growth at the fluid interface and it is found that the instability develops faster at the intermediate stage at high Reynolds number. Literature data for different values of the Reynolds number, shows satisfactory agreement with our present work results.

4.2 Introduction

The RTI gained popularity among engineers, researchers and computational scientists for decays. And a large number of simulation works were reported. RTI is eminently classic and basic interfacial instability. Relevant industrial applications of the LBM cover external aerodynamics, acoustics, and heat transfer [2]. In the last ten years, several companies invested in this technology. Rayleigh–Taylor instability (RTI) occurs when fluids of different densities at the interface are accelerated against the density gradient[55][141]where instability develops[40][41][142] at the later stage and unstable flow becomes turbulent [143]. Previously for many years, researchers and scientists worked on singled mode RTI by LBM method for two fluids simulation to observe the initial perturbation and amplitude of the perturbation of the fluid. Their investigation was on experimentally, theoretically and numerically for single-mode RTI at moderate Atwood number for miscible, inviscid and immiscible two fluids[55][144][145][146]. RTI divided into single-mode and multi-mode depend on the initial perturbation at the interface[51]. It's important to understand the phenomena of single-mode RTI for that we will discuss this further.

Recently 2D single-mode RTI with a low Atwood number was numerically investigated at various Reynolds numbers by Hu [147] and reported that the bubble velocities for a medium range of Reynolds numbers were decelerated and accelerated repeatedly after the reacceleration stage, they named this stage as the deceleration-acceleration stage. However, they discussed the bubble velocity effect by the vorticity near the bubble tip and the evolution of bubble vorticity which continues with the Kelvin-Helmholtz (KH) vortices formed on the spike and bubble interface at a higher Reynolds number. The growth of single-mode RTI at a low Atwood number(A= 0.04) has been investigated by Wei [148] using direct Numerical simulation (DNS) with an underlining of the effects of initial conditions and Reynolds number. Their result shows that the bubble acceleration becomes stationary at long times and sufficiently high Reynolds numbers, indicating quadratic growth. RTI experience at the stage of acceleration and deceleration of interface with the chaotic-mixing development at higher and lower Reynolds numbers with the result of initial perturbation like wavelength, amplitude and diffusion thickness.

However, recently a detailed study on the growth of compressible single-mode RTI at different Reynolds numbers and Atwood numbers were reported by Bian[149]. And They conducted the simulation to an analysis of the effects of Reynolds numbers and Atwood numbers. The analysis was based on Raleigh Taylor's Instability(RTI) of late-time growth, and vorticity dynamics. Which shows a clear correlation between the vortices inside the bubble and reacceleration due to the symmetrical axis of bubble and spike [148]. Their result shows that

for a sufficiently high Reynolds number, the bubble late-time acceleration is persistent. In terms of flow modelling, RTI presents as a notably challenging test case for algorithms to capture the flow physics features such as turbulent mixing, diffusion, body force treatment, interface capturing, and transition to turbulence[150]. RTI is mainly characterized by the Atwood number [150] and density ratio is measured in terms of the Atwood number[69]. High density ratios and high Reynolds numbers in numerical modelling remains challenging and intractable [33][58].

Many years scientists and researchers is dealing with issues in RTI such as the classical linear stability theory issues. This issued was attributed by Rayleigh[40][41]. They analyzed the effect of the initial condition in terms of perturbation wavelength and amplitude[51]. Lattice Boltzmann's method is a powerful new method for simulating complex fluid systems which attracted many researchers in computational physics. According to kinetic theory, the LBM method solves the macroscopic properties for multiphase and multicomponent flows [151]

The growth of the RTI which is affected by the Reynolds number can be divided into four stages [42] and the growth rate depends on the Atwood number or density ratio, viscosity, surface tension and compressibility. In the first stage, the exponential growth of the amplitude with the time [41]. Accordingly linear stability theory, the amplitude perturbation is much smaller than the wavelength. In the second stage, the heavy fluid falls into the lighter fluid in the form of spikes and the lighter fluid rises into the heavy fluid in the form of bubbles. In the third stage, the Kelvin-Helmholtz instability occurs due to a higher Reynolds number and a velocity difference across the interface between two immiscible and incompressible fluids and a roll-up of vortices forms a mushroom-type shape of the spikes. The heavy fluid falls more rapidly due to the lower viscous friction [2] because the non-linearity becomes significantly stronger. In the fourth stage, the evolution of chaotic mixing/chaotic growth stage or turbulent. At the higher Reynolds number, the secondary spike breaks up into multiple droplets more eminent which asserted by[2][33][129].

From our recent work, two and three-dimensional lattice Boltzmann simulations of single mode RTI have confirmed that the simulation was unstable at higher Reynolds number with initial perturbations, non-linearity growth, spike and bubbles phenomena and chaotic mixing of the two miscible fluids [2][42]. The evolution of nonlinear of the 2D or3D RTI simulation for the multi-mode in the late stages at moderate or higher Atwood number well investigated by attempting several test cases.

As reviewed above, there have been some numerical works investigated in the late-time single-mode, multi-mode RTI that provides a good understanding of this complex instability phenomenon. However, most of these studies only focus on the lower Atwood number. The present work of us will provide the detail of the higher Atwood number used for the numerical analysis. This insight will minimize the gap in the previous work from the literature review and provide a better understanding of the RTI fluid system. However, a majority of these works only focus on cases with small or moderate Reynolds numbers in which the time duration of the RTI instability is relatively short.

Recently, a single-mode and dual-mode(multimode) RTI investigated by Ding[152] for molecular dynamics. They developed the model for the microscopic instabilities and they observed the growth behaviour and evolution pattern of microscopic RTI could exhibit notable differences from the macroscopic counterpart. Single mode Rayleigh Taylor instability with lower density ratio such as 3(dimensionless number) with moderate Atwood number simulated for two-phase flow by Huang [153]. They have been reported that the numerical solution maintains symmetry despite the complicated interface evolution structure.

Lately, Multi-mode, single-mode RTI for 2D and 3D incompressible immiscible flow of direct numerical simulation is reported by Hamzehloo[154] and their results are verified with the single mode and multi-mode RTI at various Reynolds numbers with medium Atwood number. They have found that high Reynolds number and surface tension could possibly prevent the formation of Kelvin-Helmholtz instabilities. As reviewed above, there have been some works on the multi-mode immiscible RTI, that can provide a good insight into the understanding of this complex instability phenomenon of RTI by the lattice Boltzmann method. In addition, the quantitative description of the late-time growth of the multi-mode mode RTI is still very lacking. To fill this gap, we invoked an improved mesoscopic lattice Boltzmann algorithm to systematically explore the interface behaviour as late-time dynamics of the multi-mode RTI in a rectangular duct with the influences of moderate Atwood numbers and a wide range of Reynolds numbers are investigated in detail.

In this current work, we invoke the numerical analysis for two immiscible fluids to analyse multi-mode RTI via the phase-field lattice Boltzmann method. A numerical simulation is carried out for various test cases to observe the late-time dynamics of the multiphase flow. Substantially observe the results of the effects on the flow simulation by using the wide range of Reynolds numbers. The initial conditions in terms of the perturbation wavelength and amplitude on the interfacial behaviour, the evolution of the bubble amplitude, and the spike are discussed in detail in a later section.

4.3 Effect of lower and higher Atwood number

To study the effect of the Atwood number on the two-dimensional multi-mode RTI, we first perform numerical simulations at various Atwood numbers such as At = 0.1, 0.5 and 0.7 with the constant Reynolds number Re= 3000 which shown in the Figures 4.1, 4.2, 4.3 and secondly, we perform the simulation for the lower to higher Atwood number with a lower to higher Reynolds number. We use the mesh number horizontally y axis, Height (H)= 2000 and in x axis, width (W)= 1000, Higher lattice points written as 2000×1000, $\Delta t = 0.004$, Pe = 50, surface tension = 0.01. In this work, the viscosity ratio between the two fluid phases is O(10^3). And the density ratios are considered 3 to 10.76 for Atwood number 0.5 to 0.9 by calculating $\rho H/\rho L$. The perturbation of the interface between the heavier and lighter fluids is applied as an initial condition h = $0.5 \times ny + nx \times 0.002 \times h$.

For the flow to reach the late-time stage we used a longer vertical domain for higher Atwood numbers. The snapshots are showing the performance of the Atwood number At= 0.1 with Reynolds number Re = 3000 in the Figure 4.1. And for higher Atwood number At = 0.5, At = 0.7 with Reynolds number Re= 3000 in the Figures 4.2, 4.3 shows interface behavior of the fluids from initial stage to chaotic mixing stage. Where the positions of the bubble front, spike tip, and saddle point are observed in the simulation.

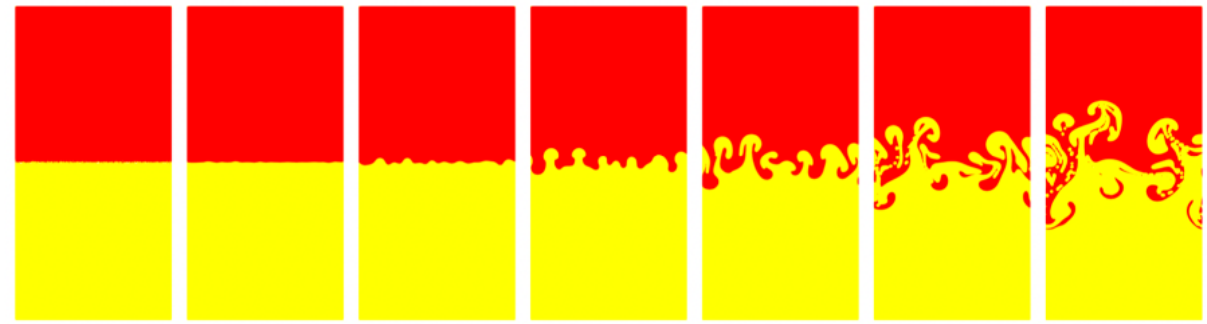

Figure 4.1. Evolution of interface with time instance at Re= 3000 and At= 0.1

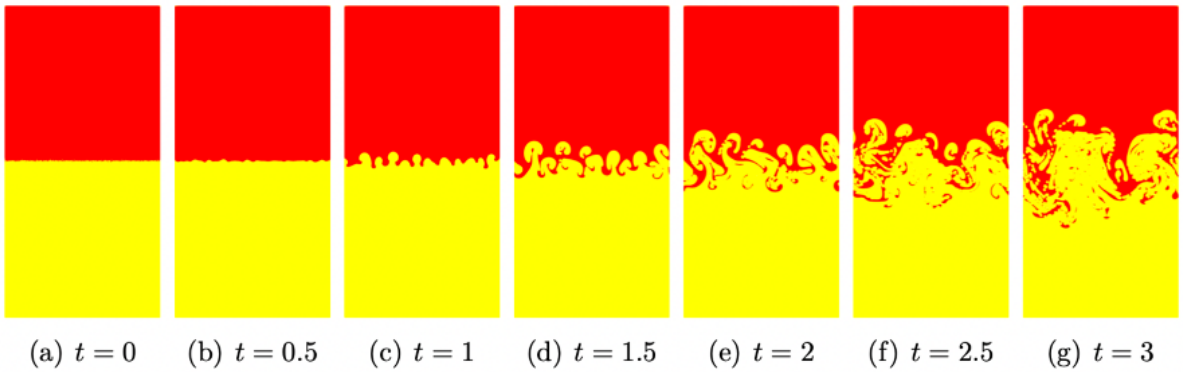

Figure 4.2. Evolution of interface with time instance at Re= 3000 and At= 0.5

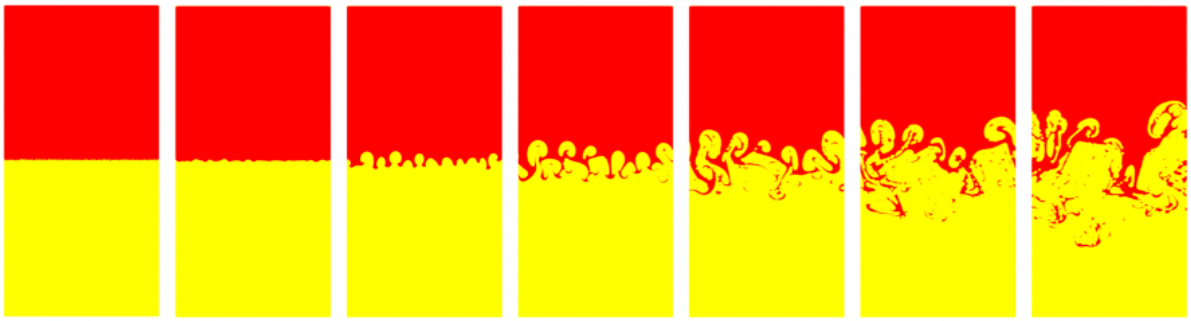

Figure 4.3. Evolution of interface with time instance at Re= 3000 and At= 0.7

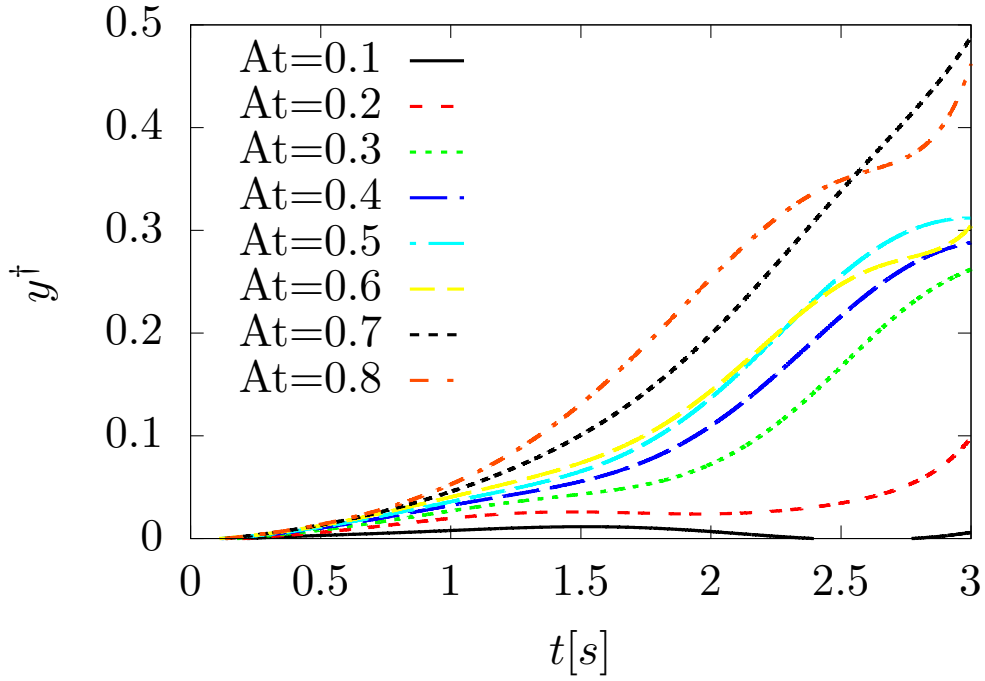

Figure 4.4. Evolution of interface with at various Atwood number of Re=3000 with time instance for 2D multi-mode RT instabilities

Figure 4.4 shows the various test results of the Atwood number with Reynolds number Re= 3000 which describe the fluid growth or perturbation of the interface with time $t = 3s$. Initially, at time $t = 1s$, the fluid slowly increased the length and later stage it lost the consistency of motion and shows the chaotic mixing with the small bubbles at time t = 3s. Basically, the entire process flows lose control due to heavy fluid falling more rapidly on lighter fluid due to the lower viscous friction. And the density ratios are considered 3 to 10.76 (dimensionless number) for Atwood number 0.5 to 0.9 which is calculated by $\rho H/\rho L$. It can be found that for all different Atwood numbers, a heavy fluid and light fluid penetrate into each other at the early stage and form spikes and bubbles. The spike rolls up along its tip and vortices are visible in the system.

The size of the vortex decreased or increased with the Atwood number. The portion of the spike roll-ups further at the tail end and extended to form a mushroom-like structure which is due to the nonlinear effect at the interface. Further, as time goes on, the interactions between fluids gradually develop the KH instability, which provides the circular motion of the interface at multiple positions and a complex large-scale interfacial structure formed. At higher Atwood number, the penetration lengths of the spike and bubble front increase and decrease respectively with various Reynolds number and shows instability. From the various test case simulation of higher Reynolds number such as Re = 30 000, 10 000, 5000 and 3000 with At = 0.6, 0.7, 0.8, 0.81, 0.82, 0.83. It has been observed that flow simulation was stable and the numerical computation time was taking longer time. Simulation were unstable with the higher Atwood number of 0.84, 0.85,0.86, 0.87, 0.88 and 0.89.

At the moderate or lower Atwood number (At = 0.1), Figures 4.1 to 4.3 the bubble and the spike position do not change much at the interface, almost remain the same due to interface growth at the upper and bottom part equally at the initial stage(t=0s). Bubble and spike positions are determined by the lowest and highest point of the interface. However, as the Atwood number increase, the interface changes or grows faster where the spike tip and bubbles position lost the initial state. Figure 4.3 which shows spikes amplitude increases with time and shows a greater value at a higher Atwood number, indicating in this case the growth of the spike at the higher Atwood number which reported by [2][147][149] and [155][156] in their single-mode RTI numerical simulations. Besides, the bubble amplitude is found to follow a similar pattern in that amplitude increases with the Atwood number. The amplitude increase range is reduced at higher Atwood numbers. From the Figure 4.4 we observe that the two-dimensional RTI simulation results show a strong dependency on the Atwood number. Where fluid flow shows instability with higher Atwood numbers with At= 02, 0.3, 0.4 , 0.5, 0.6, 0.7, 0.8.

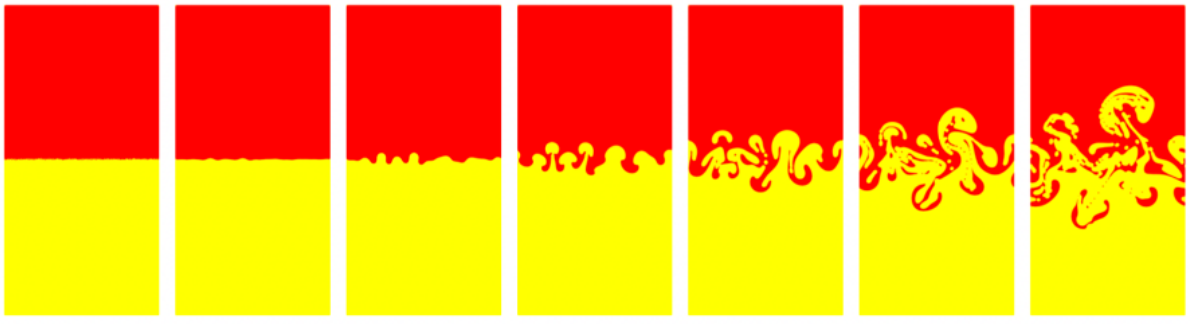

Figure 4.5. Evolution of interface with time instance at Re= 5000 and At= 0.1

Figures 4.5, 4.6 and 4.7 shows the interfacial behavior with higher Reynolds number Re= 5000 at Atwood numbers 0.1, 0.5 and 0.7. Figure 4.8 shows the fluid flow loses control when the Reynolds number increases. And fluid flow shows non-linearity behaviour with Rayleigh

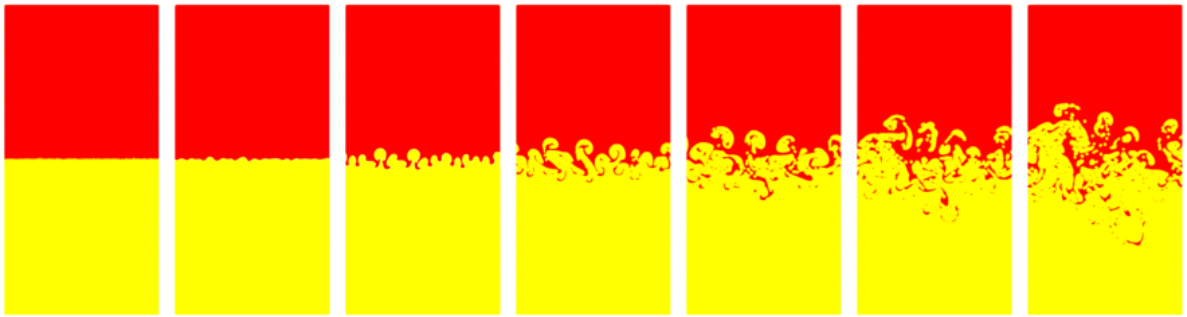

Figure 4.6. Evolution of interface with time instance at Re= 5000 and At= 0.5

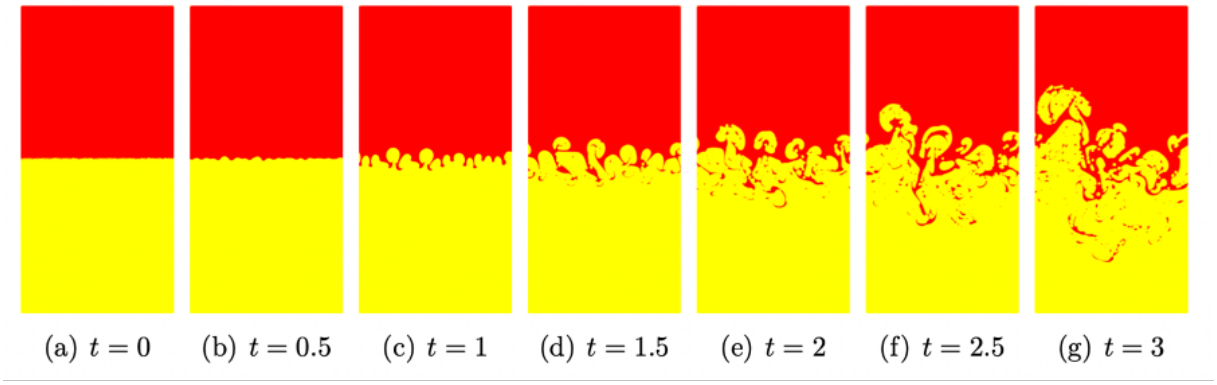

Figure 4.7. Evolution of interface with time instance at Re= 5000 and At= 0.7

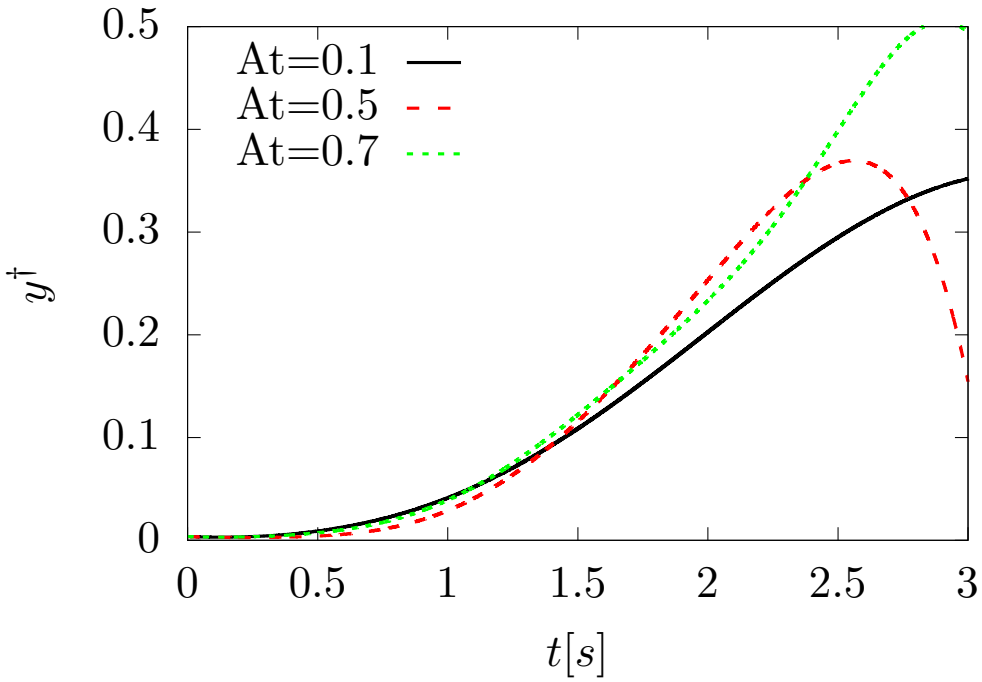

Figure 4.8. Evolution of interface with at various Atwood numbers of Re=5000 with time instance for 2D multi-mode RT instabilities

Taylor instability with the Atwood number At= 0.1 where Figure 4.4 shows the linear behaviour of the fluid flow with the Reynolds number Re=3000.

With the higher Atwood number At= 0.5 and 0.7, Figures 4.4 and 4.8, the fluid flow shows the similar non-linearity behaviour with RTI at Re= 5000. Flow loses the stability after the time step $t = 0.5s$ and shows the non-linearity behaviour at time step $t = 3s$. Figure 4.4 shows the same non-linearity behaviour as time increases.

4.4 Effect of higher Reynolds number

In the section on the effect of the higher Reynolds number, we have investigated a number of test cases on a wide range of Reynolds numbers at multi-mode fluid conditions. To check RTI in the two-phase fluid, first, we ran the simulation on various test cases on Reynolds number and Atwood numbers with time step $t = 3s$. Such as Reynolds numbers Re=100, 500, 1000, 3000, 5000, 10 000 and 30 000. Which Atwood numbers used as At= 0.1, 0.2, 0.3, 0.4, 0.5, 0.6 and 0.7. The main focus of this investigation is to observe the interface flow behaviour of two fluids cases on Reynolds number and Atwood number. For that we have simulated test cases and observe the time evolution of the multi-mode Rayleigh Taylor instability with Reynolds numbers Re= 10 000 and 30 000. And Atwood number used At = 0.1 for time step $t = 3s$. The snapshots of interfacial patterns shown in Figures 4.9, 4.10, 4.11, 4.12, 4.13 and 4.14. Snapshots are produced only for Reynolds numbers Re= 10 000 and 30 000 with Atwood numbers are 0.1, 0.5 and 0.7. For better understanding the numerical analysis, we not only simulated the Re= 10 000 with Atwood numbers At= 0.1, 0.5, 0.7. We run the simulation for Atwood numbers At= 0.2, 0.3, 0.4, 0.6, 0.7 with Reynolds number Re= 10 000 where snapshots are not shown. However the overall results are shown for all Atwood numbers in Figure4.16. To observe the differences of interfacial behavior of two fluids with higher Reynolds number with the lower to higher Atwood number. Where the results are from Figure 4.16 shows the distinct behaviour throughout the process which leads to flow instability by the rapid growth of the fluid motion and then chaotic mixing of the two fluids at time increases.

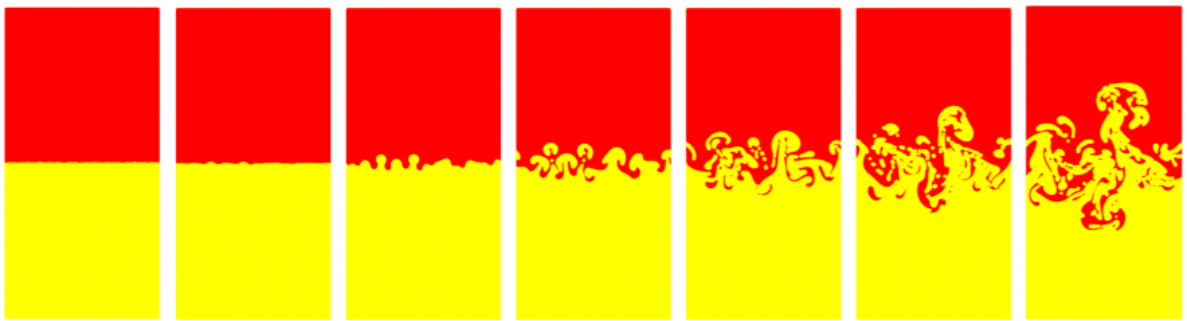

(a) $t = 0$ (b) $t = 0.5$ (c) $t = 1$ (d) $t = 1.5$ (e) $t = 2$ (f) $t = 2.5$ (g) $t = 3$

Figure 4.9. Evolution of interface with time instance at Re= 10000 and At= 0.1

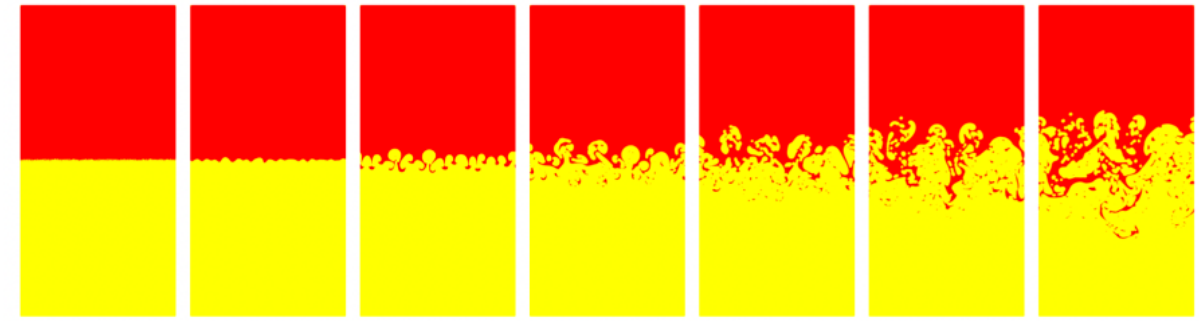

(a) $t = 0$ (b) $t = 0.5$ (c) $t = 1$ (d) $t = 1.5$ (e) $t = 2$ (f) $t = 2.5$ (g) $t = 3$

Figure 4.10. Evolution of interface with time instance at Re= 10000 and At= 0.5

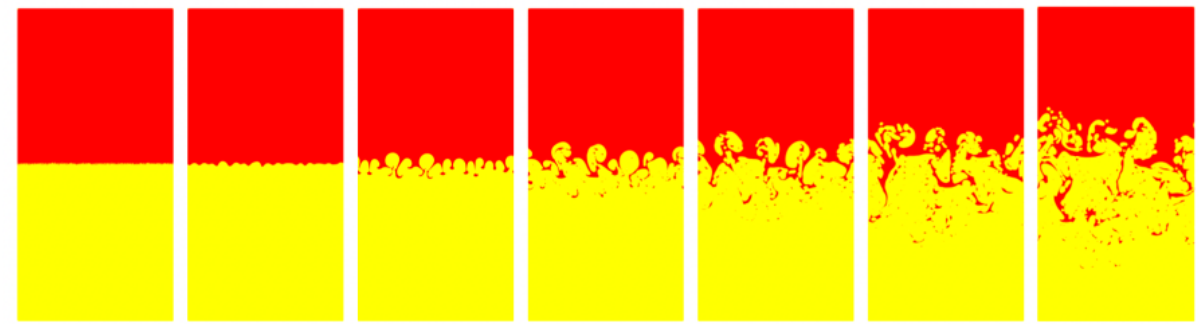

(a) $t = 0$ (b) $t = 0.5$ (c) $t = 1$ (d) $t = 1.5$ (e) $t = 2$ (f) $t = 2.5$ (g) $t = 3$

Figure 4.11. Evolution of interface with time instance at Re= 10000 and At= 0.7

From the observation of simulation results, the flow shows the distinct behaviour. Which the interfacial dynamic of fluids shows the similar results at the initial stage of the interface which heavy fluid falls down and light fluids rise up under the influences of gravitational force. Later stage the flow penetrate into each other and develops spikes and small bubbles. Moreover, the spike and bubble dynamic display chaotic mixing behaviour with Rayleigh Taylor Instability(RTI). As time progress, nonlinear coupling of the modes reflects at bubble and spikes interface by the interaction among the modes which becomes more intensive at high Reynolds number. Which forms a large-scale interface or chaotic structure known as the mixing layer becomes fully turbulent develops turbulence and shows instability in the flow. In addition, there is the occurrence of small scales of bubbles and vortices generated at the mixing layer.

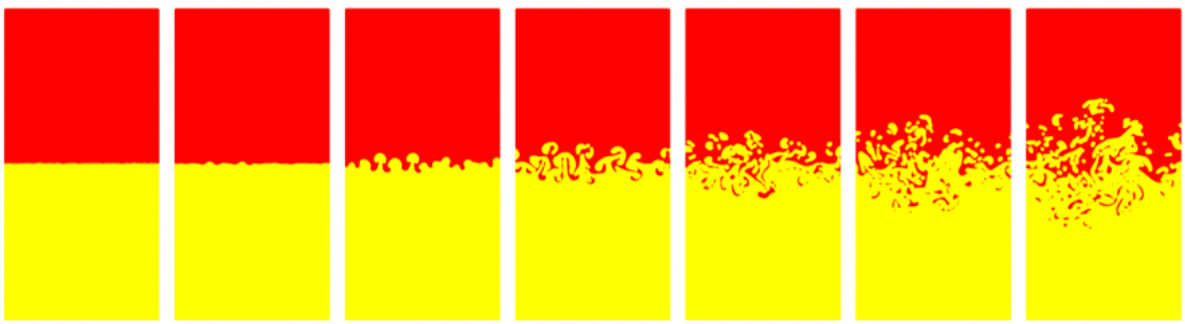

(a) $t = 0$ (b) $t = 0.5$ (c) $t = 1$ (d) $t = 1.5$ (e) $t = 2$ (f) $t = 2.5$ (g) $t = 3$

Figure 4.12. Evolution of interface with time instance at Re= 30 000 and At= 0.1

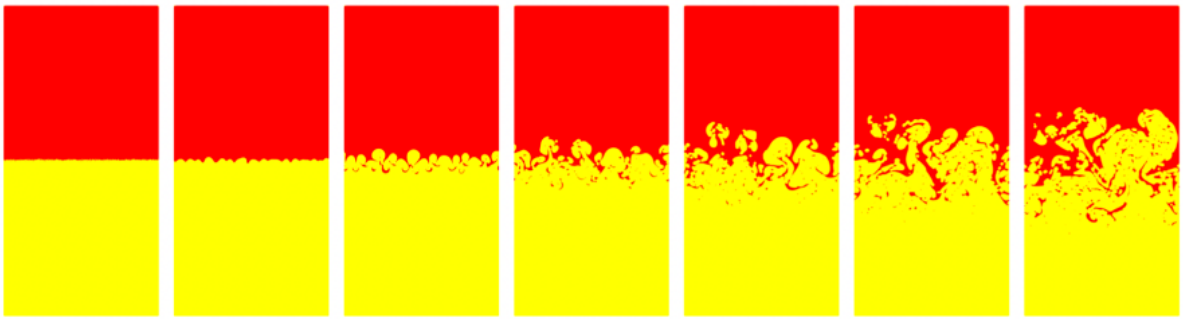

(a) $t = 0$ (b) $t = 0.5$ (c) $t = 1$ (d) $t = 1.5$ (e) $t = 2$ (f) $t = 2.5$ (g) $t = 3$

Figure 4.13. Evolution of interface with time instance at Re= 30 000 and At= 0.5

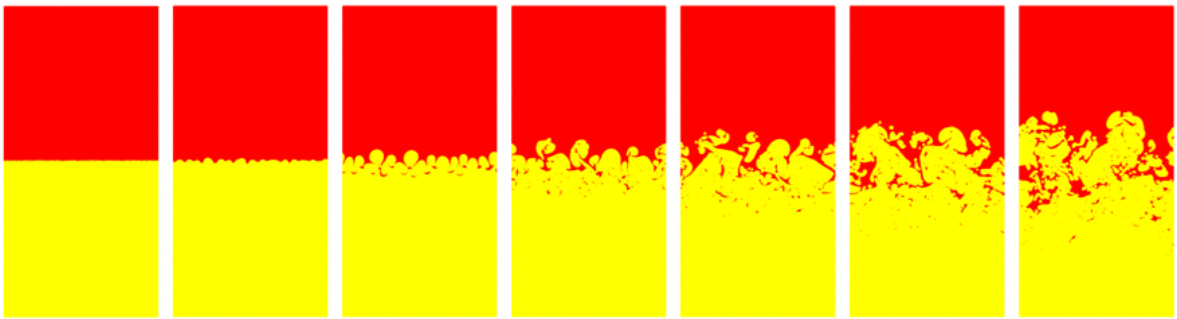

(a) $t = 0$ (b) $t = 0.5$ (c) $t = 1$ (d) $t = 1.5$ (e) $t = 2$ (f) $t = 2.5$ (g) $t = 3$

Figure 4.14. Evolution of interface with time instance at Re= 30 000 and At= 0.7

Furthermore, the simulation executed for two fluids flow to observe the interface behavior with lower Reynolds number 100, 500, 1000 which Snapshots are not shown. To observe the difference between lower to higher Reynolds number, we analysis the the interface behavior of the two fluids with Reynolds number such as Re= 100, 500, 1000 , 3000, 5000, 10 000 and 30 000 which shown in the Figure Figure 4.15. Figure 4.15, shows the flow consistency at lower time step $t = 0.5s$. And flow shows instability when time reaches at time $t = 3s$.

From the observation of simulation, it has been studied that simulation/computational time takes more at higher time steps ($t = 15s$ where figure is not produced) and simulation undergoes instability. However, the simulation shows stability with the lower time step like $t = 3s$ with lower to higher Atwood number. The fluid height changes with each time interval where we observe the fluid flow deformation which means the fluid flow loses control drastically showing the turbulence at the end of the time of the simulation process.

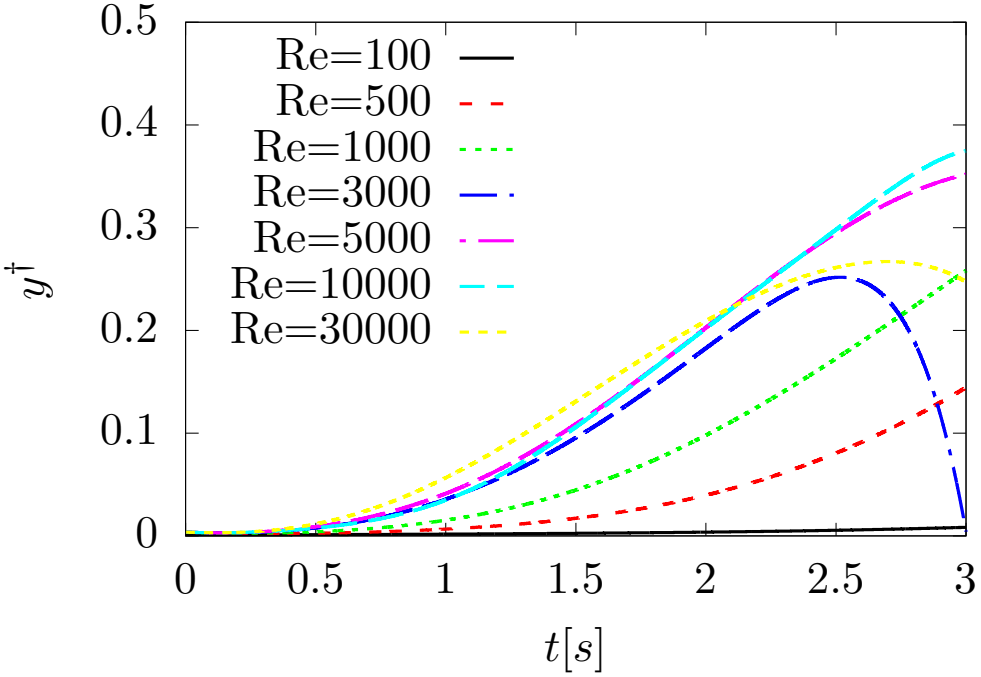

Figure 4.15. Evolution of interface with At=0.1 at time instance for 2D multi mode RT instabilities with various Reynolds number

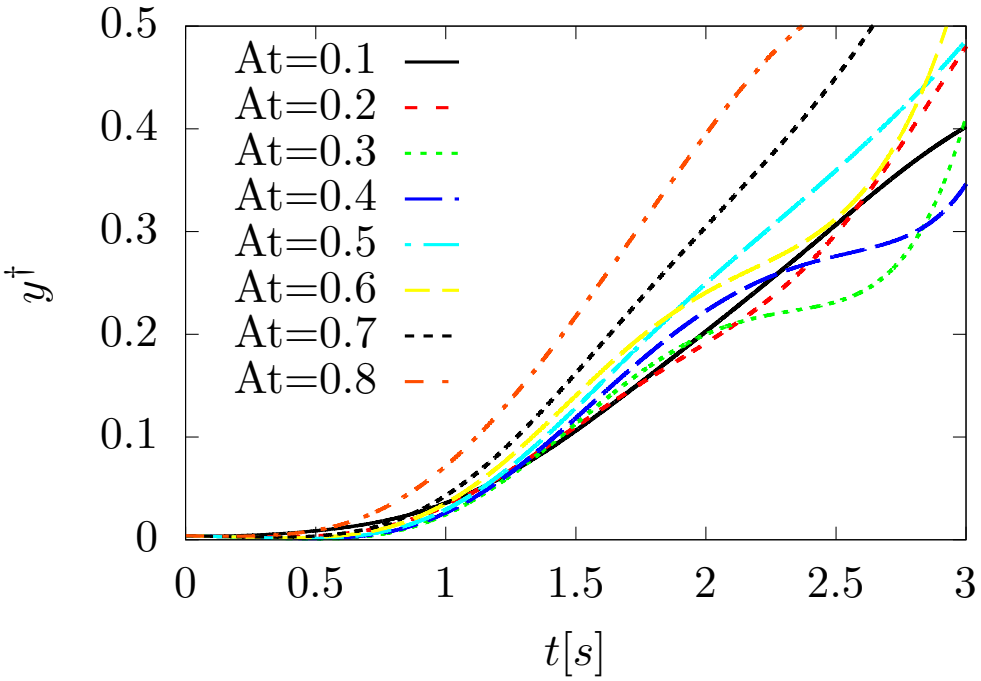

Figure 4.16. Evolution of interface with at various Atwood numbers of Re=10 000 with time instance for 2D multi mode RT instabilities

4.5 Grid Independence analysis for single-mode and multi-mode RTI

To ensure that the numerical results are grid independent, the grid resolution test is carried by simulating a test case with Re = 3000; At= 0.1 on three different sets of grids such are 1024×4048, 512×2048, 256×1024 and 128×512 for single-mode and multi-mode RTI studied.

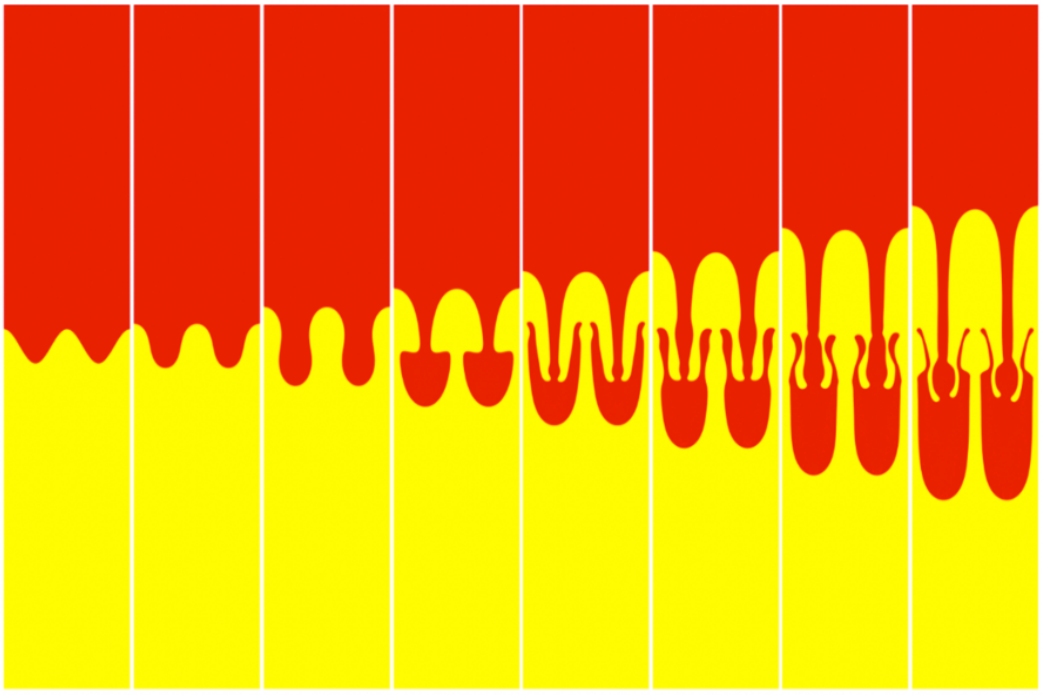

Figure 4.17. Snapshot of grid size 1024 ×4096: Multi-mode RTI interface position at Re=3000; At= 0.1 with various time instance

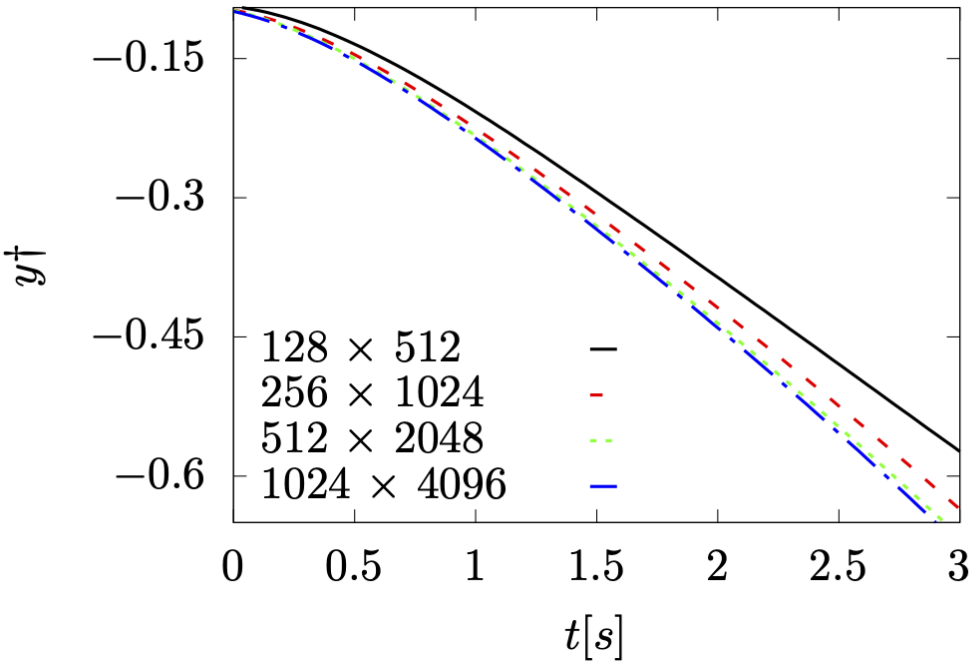

Figure 4.18. Grid convergence analysis result of Multi-mode RTI: interface position vs time of Re=3000 with At=0.1 while X = 2 ×double(x) / (double(nx-1))

Single-mode and multi-mode RTI in a domain size 1×4 and $[0, \pi d/2] \times [0, \pi d/2]$ considered for grid independence test cases.The interface is initially located at $y_0 = \pi d/2$ an initial perturbation is applied to the velocity field. The amplitude, Am = 0.005 is applied.

In the interface evolution process at time step $t = 3s$ with At= 0.1, showing the positions of the spike or bubble tip in Figures 4.17 and 4.19 with size of 1024 ×4096. Figure 4.18 suggests that the higher number of grid provides better accuracy in terms of capturing the exact position of fluid evolution than the intermediate grid size. And Figure 4.20 shows the instability at lower grid numbers at 512 ×2048, 256 ×1024.

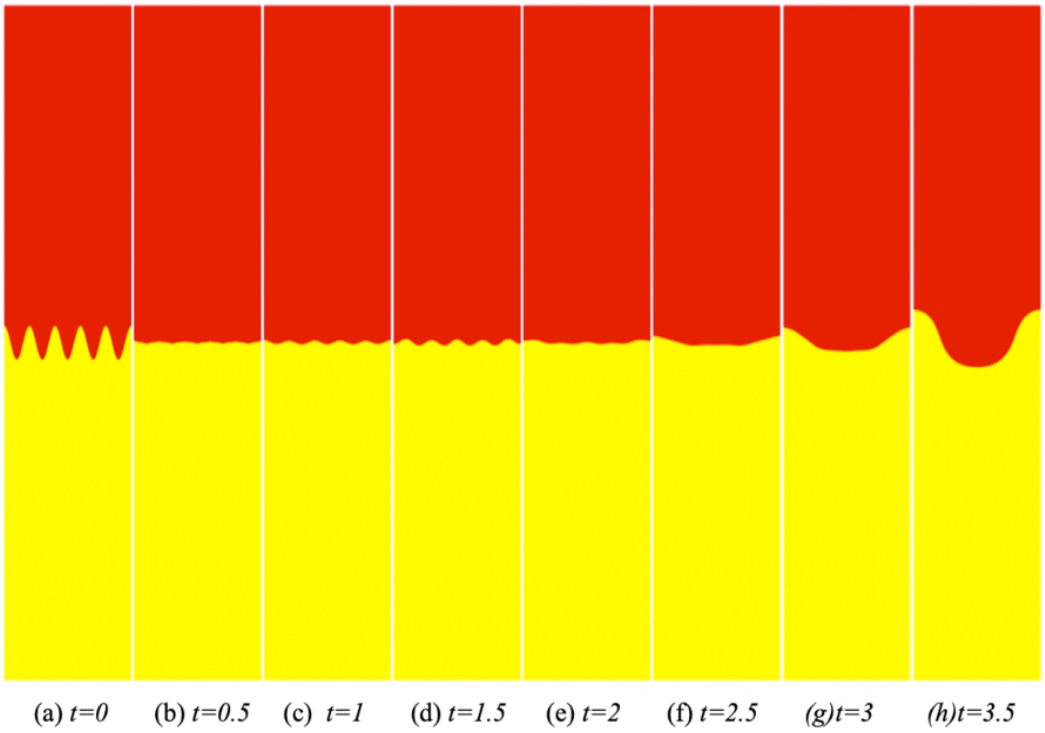

Figure 4.19. Snapshot of grid size 1024 ×4096 while distance of grid at x= 5(x) / (double(nx-1)) : interface position at time with Re= 3000; At=0.1

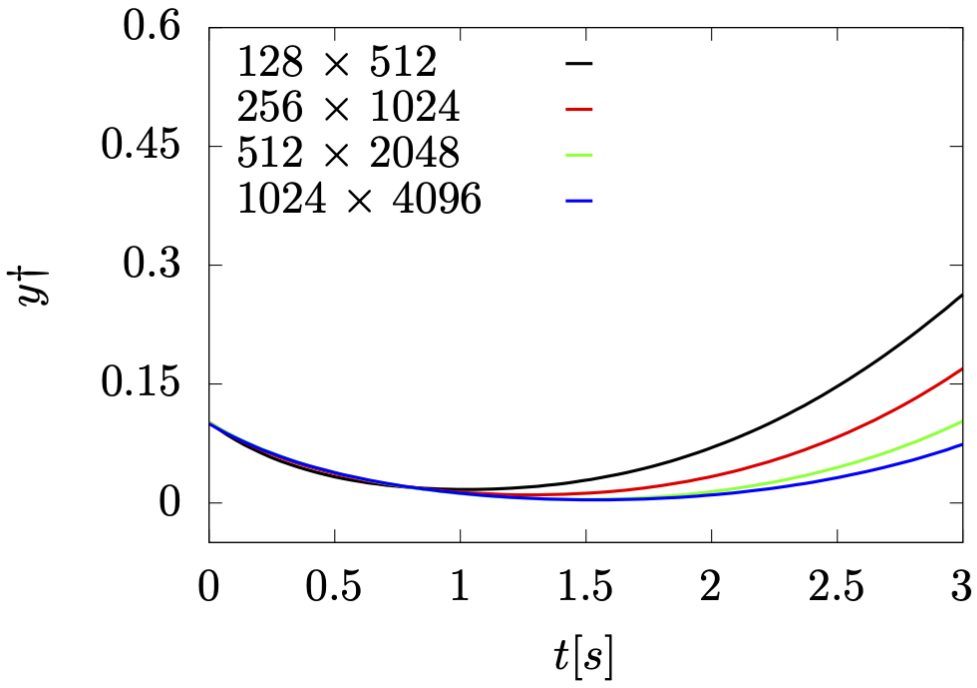

Figure 4.20. Grid Independence analysis with various grid size: interface position vs time of Re= 3000 with At= 0.1 while X = 5 ×double(x) / (double(nx-1))

Consequently to achieve the grid convergence solution, to use effective method as local time step method on uniform mesh to create an acceleration in the solution in wide range of Reynolds number[53]. Therefore, from the single mode snapshot Figure 4.21 it has been investigated that there is a bright white random noise appears at the spike perturbation at the lower grid number 128 ×512, whereas the bright random white noise when increase the number of grid at 256 ×1024 reduces. And the bright white random noise disappears at the spike and proved smoothness in the flow, while using the higher grid numbers 512 ×2048.

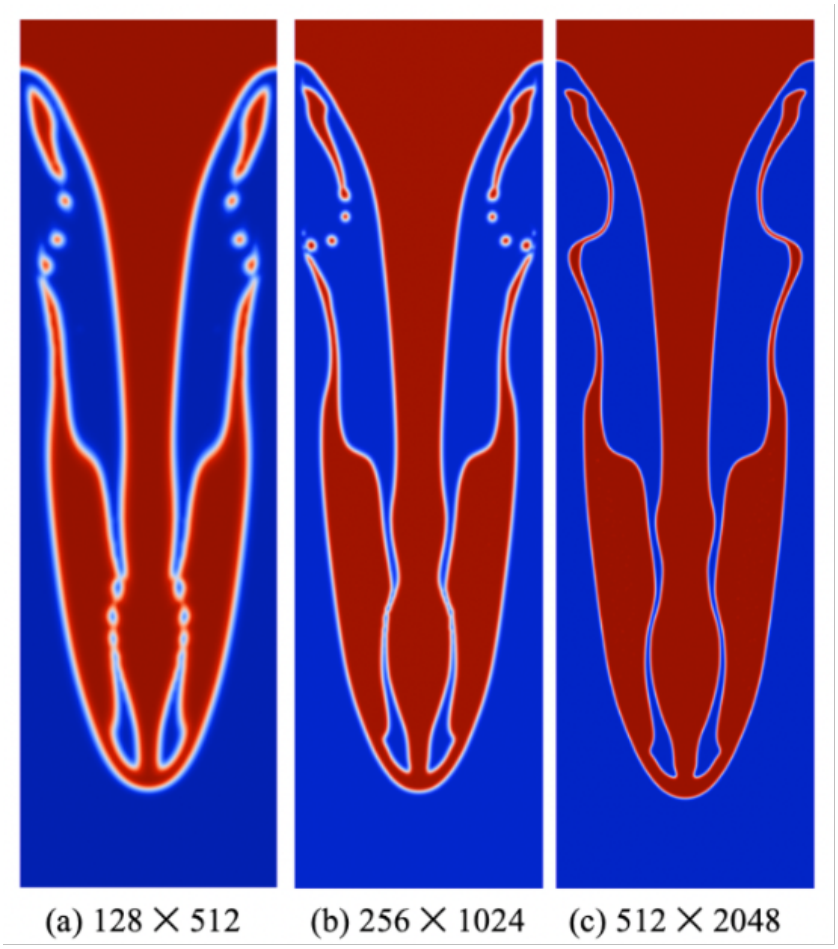

Figure 4.21. Grid independence analysis at various grid size: (a) 128 ×512, (b) 256 ×1024 (c) 512 ×2048 at Re=3000; At=0.1 for single mode RTI

Table 4.1. Normalized Error at various grid size with Re= 3000

t	Error at Ny 512	Error at Ny 1024
0	0	0
0.5	3.66	1
1	1	0.33
1.5	0.55	0.11
2	17	5
2.5	4.09	1.36
3	2.28	0.84
3.5	1.028	0.5

That means higher number of grid number provides better resolution. It's worth noting that the error increases with the coarse grid than the fine grid that shown in Table 4.1. It is worth to look into the computational cost and memory consumption in terms of D2Q9-CM-LBM rather than D3Q19-CM-LBM. Using of higher number of grid to achieve the higher grid resolution, require more computation time. Figure 4.21 shows the flow convergence with time instance $t = 3s$ sat Re= 3000; At= 0.1. The grid numbers were considered for the simulation such as 128 ×512, 256 ×1024 and 512 ×2048.

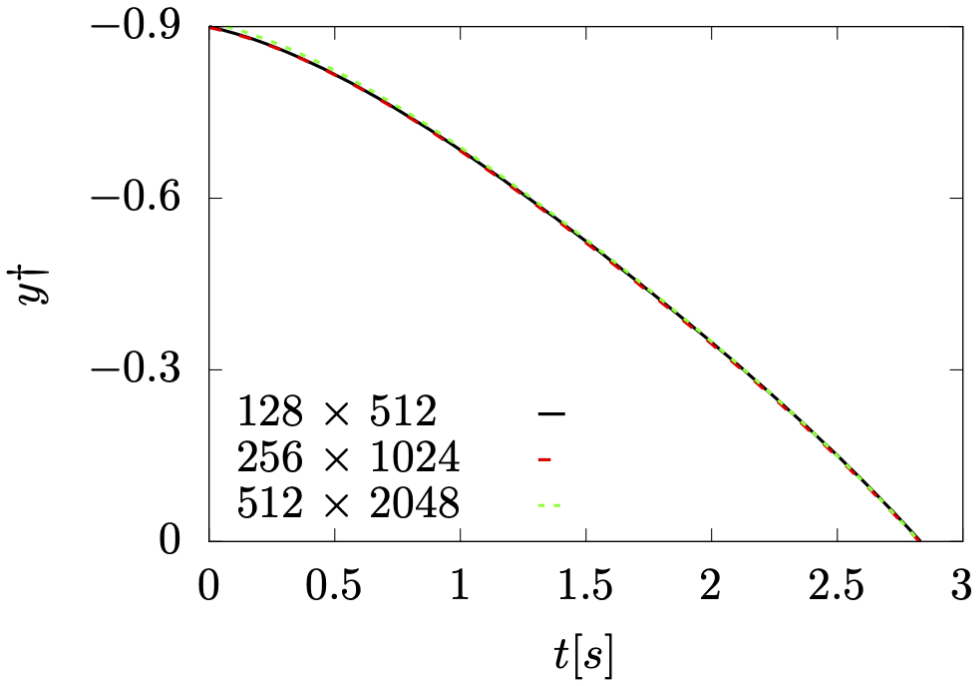

Figure 4.22. Grid independent analysis for Re=3000 with At= 0.1 in single-mode RTI: The fluid interface position vs time

Table 4.2 shows the computation time of various grid size at Re= 3000 for single-mode and multi-mode, At = 0.1. Memory usage involved by the D3Q19-CM-LBM and D3Q9-CM-LBM within a generic LBM run. The most complete discretization involves an additional cost of 30% for D2Q19 and D3Q19-CM-LBM[89]. From the Table 4.2 shows the computation time for multi-mode is 7508707 ms for lower grid size 128 ×256. And 2.48744e+06 ms for grid size 256 ×512 respectively. The computation time for single mode is 7508707 ms for lower grid size 128 ×256. And 2.48744e+06 ms for 256 ×512 respectively. It suggests that the computational time increases while size of grid size are increases. Similarly, computation time is lower in single-mode grid size 128 ×256 is 723951 ms. And for higher grid size 256 ×512 in single-mode computation time is 5.8842e+06 ms respectively. It suggests that the computational time increases while size of grid size are increases. The fine grid 1024×4096 takes more computation time than 512 ×2048 for both single-mode and multi-mode.

And with the grid size 512 ×2048 computational time used 4.41832e+07 ms for single-mode and 4.38496e+07 ms for multi-mode. the advantage of our method is more clear when grid numbers are increase, there is more flow accuracy and stability.

Table 4.2. Computation time for various lattice points for 2D multi-mode and single-mode RTI

Lattice size	At	Re	Am	Computation time
128×256 multi-mode	0.1	3000	0.005	750807 ms
256×1024 multi-mode	0.1	3000	0.005	2.48744e+06 ms
512×2048 multi-mode	0.1	3000	0.005	4.38496e+07 ms
128×256 single-mode	0.1	3000	0.005	723951ms ms
256×1024 single-mode	0.1	3000	0.005	5.8842e+06 ms
512×2048 single-mode	0.1	3000	0.005	4.41832e+07 ms

Chapter 5

Conclusions and Future work

This chapter will summarise the main conclusions from Chapters 3 and 4 as well as provide recommendations for future directions of research.

5.1 Single-mode RTI (Chapter 3)

A 3D lattice Boltzmann method to compute the evolution of a system composed of two fluids by means of the D3Q19 discretization has been reported. The two collision processes are written within a general multiple-relaxation-time framework. The proposed approach shows very good accuracy properties, which are evaluated against two different tests. The performance is particularly satisfying if compared to the adoption of the D3Q7 LBM. The gradient of the order parameter can be computed by finite difference or first-order central moments. The latter enforces the locality of the algorithm, thus reducing the involved run time. However, this tends to slightly deteriorate the accuracy of the method. Given all these observations, we can conclude that the proposed approach represents a potential candidate to perform reliable computations of multiphase and multicomponent flows.

5.2 Multi-mode RTI (Chapter 4)

A proposed numerical model for 2D single and multi-mode immiscible RTI with a wide range of Reynolds numbers using the central-moment-based lattice Boltzmann method has been investigated. Phase tracking for multiphase fluids is the main concern for investigation. For this several test cases are investigated for higher density and viscosity fluid with lower to

higher Atwood number to observe the interface evolution with time instance. In the process of evolution, from top to bottom of the fluid we observe several stages known as Linear growth, saturated velocity growth, and chaotic development stages. A comprehensive range of values of the Atwood number (from 0.1 to 0.9) and Reynolds number (from 100 to 30 000) is considered. Linear growth, saturated velocity growth, and chaotic development stages are captured by the algorithm successfully. For different Atwood numbers, we observe a different kind of dynamic behaviour of the two fluids at the interface from top to bottom which is shown in the figure. In the observation of higher Reynolds number simulation, the modes collide with each other increasing the interaction with time instances and increasing the large scales of deformation or turbulence. Later, the large scale of deformation creates a break up at the interface and exhibits the turbulence and chaotic mixing of the two fluids. The whole process takes place of instability where fluid flow loses control and exhibits the formation of small bubbles which mix up rapidly and accelerated to the top of the fluid.

5.3 Summary of findings

This thesis has described work towards numerical modelling of 2D and 3D RTI analysis of multiphase and multicomponent fluid flows by lattice Boltzmann method. Where the individual test cases are investigated for Rayleigh-Taylor instability of two different densities fluids and validated with existing model work. Specifically, the main aims were:

- to investigate the interface evolution process of two fluids by phase tracking method. Interface evolution process observed at various stages which are linear stage, intermediate stage and chaotic mixing stage with time instance.

To highlight the main findings of the results are to check accuracy, stability and grid independence analysis by Rayleigh-Taylor which are:

- 2D Single-mode RTI with wide range of Reynolds number
- 3D Single-mode RTI with a wide range of Reynolds number
- 2D Single-mode RTI with a wide range of Atwood number

- 2D Multi-mode RTI with a wide range of Reynolds number
- 2D multi-mode RTI with a wide range of Atwood number
- 2D single-mode and multi-mode RTI with various grid sizes with fixed Reynolds number and Atwood number
- 2D single-mode and multi-mode RTI for grid independence test with various grid size
- Computation time analysis for single-mode and multi-mode
- Normalized error for various grid size

5.4 Limitations of the present work

First, most of the work on the phase-field LBM is limited to two-phase flows, and the phase-field-based LBM schemes for multiphase (more than three phases) flows are still in progress [125][157][158] Secondly, almost all phase-field-based LB models are only suitable for isothermal multiphase flows, and it is desirable to develop the phase-field-based LB models for non-isothermal multiphase flows [159]–[161] and finally, more advanced phase-field-based LB models for multiphase flows with surfactants and multiphase electrohydrodynamic flows are also needed [162][163].

2D and 3D Single-mode RTI simulated for lower Reynolds number with fixed Atwood number (lower Atwood number) which provides accurate results in terms of stability and grid convergence however outcomes for multi-mode RTI are not the same compared to single-mode RTI analysis. Here in this multi-mode RTI analysis to investigate whether central-moments-LBM can be used or able to tackle consequences in terms of stability and convergence numerically. There are some limitations for multi-mode RTI such as are:

- For example Atwood and Reynolds numbers should be below a certain threshold. In multi-mode RTI, with higher lattice points with higher Reynolds, number simulation CPU times require longer time where simulation shows instability and its not possible to get an accurate result in the local computer where it requires a high-performance computer.

- For example, Atwood and Reynolds numbers should be below a certain threshold. In multi-mode RTI, with higher lattice points with higher Reynolds, number simulation CPU times require longer time where simulation shows instability and its not possible to get an accurate result in the local computer where we require a high-performance computer

- While considering lower lattice/grid points such as 128, 256 and 512 and for 2D simulation requires less CPU time with a lower time range of simulation ($t = 3s$)

- Consume more CPU time while using a higher Reynolds number at a longer time range simulation (for example: ($t = 15s$). And the occurrence of lower resolution in the simulation with instability and inaccuracy at the coarse mesh (Grid points 128)

- By increasing the grid points 256, 512 and 1024 the grid resolution of the fine grid provides better resolution with stability and accuracy in the simulation

There are some limitations for single-mode RTI such are:

- Consumes more CPU time($t = 15s$) for higher Reynolds number with higher Atwood number. There is a chance to crash the commercial computer

5.5 Suggestions for future work

In conclusion, it's necessary to highlight the focal point in the investigation of our present work. Particularly, 2D and 3D numerical analyses were executed for single-mode and multi-mode RTI by lattice Boltzmann method (LBM) for multiphase and multicomponent (incompressible) fluid flow. Mostly, concentrated to investigate the central-moment-based lattice Boltzmann method for multiphase and multicomponent fluid flow at high density and viscosity ratio with a wide range of Reynolds number and Atwood number for single-mode and multi-mode Rayleigh-Taylor instability. To Examine the flow accuracy, stability and grid independence. In consequence, the multiphase and multicomponent fluid flow emphasizes looking into other unsolved issues in the research field. Hence, the present work could be extended to our future work in various new methods. Especially for the 3D numerical analysis for multi-mode RTI.

Rayleigh-Taylor with higher grid number and Reynolds number by lattice Boltzmann to check the accuracy, instability and grid independency (resolution). Apart from that, the advanced simplified LBM method could be used for multiphase and multicomponent fluid flow issues in heat transfer (energy) applications. On the other hand, we can further study and analyse the 2D and 3D numerical analysis for multiphase fluid by considering advanced methods such are:

- by implementing TRT (Two relaxation time) collision operator in LBM
- by using Palabos (Parallel lattice Boltzmann solver)
- by considering parallel computing such are GPU and open MPI (Message Passing Interface) in LBM drag to deal with the issue of storage memory
- by considering three-phase fluid flow (Complex flow) by LBM

References

[1] P.-H. Chiu and Y.-T. Lin, "A conservative phase field method for solving incompressible two-phase flows," Journal of Computational Physics, vol. 230, no. 1, pp. 185–204, 2011.

[2] A. De Rosis and E. Enan, "A three-dimensional phase-fieldLattice Boltzmann method for incompressible two-components flows," Physics of Fluids, vol. 33, no. 4, p. 043 315, 2021.

[3] P. G. Drazin, Introduction to hydrodynamic stability. Cambridge university press, 2002, vol. 32.

[4] M. Espinoza, M. Andersson, J. Yuan, and B. Sundén, "Compress effects on porosity, gas-phase tortuosity, and gas permeability in a simulated pem gas diffusion layer," International Journal of Energy Research, vol. 39, no. 11, pp. 1528–1536, 2015.

[5] B. Indraratna, N. M. Phan, T. T. Nguyen, and J. Huang, "Simulating subgrade soil fluidization using lbm-dem coupling," International Journal of Geomechanics, vol. 21, no. 5, p. 04 021 039, 2021.

[6] L. Axner, A. G. Hoekstra, A. Jeays, P. Lawford, R. Hose, and P. Sloot, "Simulations of time harmonic blood flow in the mesenteric artery: Comparing finite element and Lattice Boltzmann methods," Biomedical engineering online, vol. 8, no. 1, pp. 1–8, 2009.

[7] Y. Han and P. A. Cundall, "Lbm–dem modeling of fluid-solid interaction in porous media," International Journal for Numerical and Analytical Methods in Geomechanics, vol. 37, no. 10, pp. 1391–1407, 2013.

[8] H. Gan, X. Shan, T. Eriksson, B. Lok, and Y. Lam, "Reduction of droplet volume by controlling actuating waveforms in inkjet printing for micro-pattern formation," Journal of micromechanics and microengineering, vol. 19, no. 5, p. 055 010, 2009.

[9] W. Li, R. D. Vigil, I. A. Beresnev, P. Iassonov, and R. Ewing, "Vibration-induced mobilization of trapped oil ganglia in porous media: Experimental validation of a capillary-physics mechanism," Journal of Colloid and Interface Science, vol. 289, no. 1, pp. 193–199, 2005.

[10] S.-Y. Teh, R. Lin, L.-H. Hung, and A. P. Lee, "Droplet microfluidics," Lab on a Chip, vol. 8, no. 2, pp. 198–220, 2008.

[11] J. Wang, P. Brisk, and W. H. Grover, "Random design of microfluidics," Lab on a Chip, vol. 16, no. 21, pp. 4212–4219, 2016.

[12] A. Fakhari, M. Geier, and D. Bolster, "A simple phase-field model for interface tracking in three dimensions," Computers & Mathematics with Applications, vol. 78, no. 4, pp. 1154–1165, 2019.

[13] S. L. Anna, "Droplets and bubbles in microfluidic devices," Annual Review of Fluid Mechanics, vol. 48, pp. 285–309, 2016.

[14] H. Wang, X. Yuan, H. Liang, Z. Chai, and B. Shi, "A brief review of the phase-field-based Lattice Boltzmann method for multiphase flows," Capillarity, vol. 2, no. 3, pp. 33–52, 2019.

[15] C. E. Brennen and C. E. Brennen, "Fundamentals of multiphase flow," 2005.

[16] V. Cristini and Y.-C. Tan, "Theory and numerical simulation of droplet dynamics in complex flows—a review," Lab on a Chip, vol. 4, no. 4, pp. 257–264, 2004.

[17] A. Leshansky, S. Afkhami, M.-C. Jullien, and P. Tabeling, "Obstructed breakup of slender drops in a microfluidic T junction," Physical review letters, vol. 108, no. 26, p. 264 502, 2012.

[18] "Https://commons.wikimedia.org/wiki/file:golden$_g ate_b ridge_a t_s unset_1 .jpg$,"

[19] "Https://commons.wikimedia.org/wiki/file:golden$_g ate_b ridge_a t_s unset_1 .jpg$,"

[20] "Https://www.eso.org/public/images/potw1334a/,"

[21] "Https://commons.wikimedia.org/w/index.php curid=406688,"

[22] D. Link, S. L. Anna, D. Weitz, and H. Stone, "Geometrically mediated breakup of drops in microfluidic devices," Physical review letters, vol. 92, no. 5, p. 054 503, 2004.

[23] M.-C. Jullien, M.-J. Tsang Mui Ching, C. Cohen, L. Menetrier, and P. Tabeling, "Droplet breakup in microfluidic t-junctions at small capillary numbers," Physics of Fluids, vol. 21, no. 7, p. 072 001, 2009.

[24] B. Kintses, L. D. van Vliet, S. R. Devenish, and F. Hollfelder, "Microfluidic droplets: New integrated workflows for biological experiments," Current opinion in chemical biology, vol. 14, no. 5, pp. 548–555, 2010.

[25] M. Wörner, "Numerical modeling of multiphase flows in microfluidics and micro process engineering: A review of methods and applications," Microfluidics and nanofluidics, vol. 12, no. 6, pp. 841–886, 2012.

[26] M. Kataja, A. Koponen, V. M. Luukkainen, M. Manninen, U. Ojaniemi, J. Poranen, J. Salmela, P. Selenius, J. Halttunen, M. Honkanen, *et al.*, "Multiphase flows in process industry: Promoni," 2005.

[27] J. Hardy, Y. Pomeau, and O. De Pazzis, "Time evolution of a two-dimensional model system. i. invariant states and time correlation functions," Journal of Mathematical Physics, vol. 14, no. 12, pp. 1746–1759, 1973.

[28] T. Krüger, H. Kusumaatmaja, A. Kuzmin, O. Shardt, G. Silva, and E. M. Viggen, "The Lattice Boltzmann method," Springer International Publishing, vol. 10, no. 978-3, pp. 4–15, 2017.

[29] H. Liang, B. Shi, Z. Guo, and Z. Chai, "Phase-field-based multiple-relaxation-time lattice boltzmann model for incompressible multiphase flows," Physical Review E, vol. 89, no. 5, p. 053 320, 2014.

[30] A. K. Gunstensen and D. H. Rothman, "Microscopic modeling of immiscible fluids in three dimensions by a Lattice Boltzmann method," EPL (Europhysics Letters), vol. 18, no. 2, p. 157, 1992.

[31] M. R. Swift, E. Orlandini, W. Osborn, and J. Yeomans, "Lattice Boltzmann simulations of liquid-gas and binary fluid systems," Physical Review E, vol. 54, no. 5, p. 5041, 1996.

[32] X. Shan and H. Chen, "Simulation of nonideal gases and liquid-gas phase transitions by the Lattice Boltzmann equation," Physical Review E, vol. 49, no. 4, p. 2941, 1994.

[33] A. Fakhari, T. Mitchell, C. Leonardi, and D. Bolster, "Improved locality of the phase-field Lattice-Boltzmann model for immiscible fluids at high density ratios," Physical Review E, vol. 96, no. 5, p. 053 301, 2017.

[34] D. H. Rothman and J. M. Keller, "Immiscible cellular-automation fluids," Journal of Statistical Physics, vol. 52, no. 3, pp. 1119–1127, 1988.

[35] A. K. Gunstensen, D. H. Rothman, S. Zaleski, and G. Zanetti, "Lattice Boltzmann model of immiscible fluids," Physical Review A, vol. 43, no. 8, p. 4320, 1991.

[36] S. Saito, Y. Abe, and K. Koyama, "Lattice Boltzmann modeling and simulation of liquid jet breakup," Physical Review E, vol. 96, no. 1, p. 013 317, 2017.

[37] D. Grunau, S. Chen, and K. Eggert, "A Lattice Boltzmann model for multiphase fluid flows," Physics of Fluids A: Fluid Dynamics, vol. 5, no. 10, pp. 2557–2562, 1993.

[38] M. Abramowitz and I. A. Stegun, *Handbook of mathematical functions with formulas, graphs, and mathematical tables*. US Government printing office, 1964, vol. 55.

[39] S. Leclaire, A. Parmigiani, B. Chopard, and J. Latt, "Three-dimensional Lattice Boltzmann method benchmarks between Color-gradient and Pseudo-potential immiscible multi-component models," International Journal of Modern Physics C, vol. 28, no. 07, p. 1 750 085, 2017.

[40] R. Lord, "Investigation of the character of the equilibrium of an incompressible heavy fluid of variable density," Scientific papers, pp. 200–207, 1900.

[41] G. I. Taylor, "The instability of liquid surfaces when accelerated in a direction perpendicular to their planes. i," Proceedings of the Royal Society of London. Series A. Mathematical and Physical Sciences, vol. 201, no. 1065, pp. 192–196, 1950.

[42] D. H. Sharp, "Overview of Rayleigh-Taylor instability," 1983.

[43] E. G. P. Bhatnagar and M. Krook, "A model for collision processes in gases. i. small amplitude processes in charged and neutral one-component systems," Phys. Rev, vol. 378, no. 94, p. 511, 1954.

[44] Y.-H. Qian, D. d'Humières, and P. Lallemand, "Lattice BGK models for Navier-Stokes equation," EPL (Europhysics Letters), vol. 17, no. 6, p. 479, 1992.

[45] E. Dinesh Kumar, S. Sannasiraj, and V. Sundar, "Phase field Lattice Boltzmann model for air-water two phase flows," Physics of Fluids, vol. 31, no. 7, p. 072 103, 2019.

[46] G. Tryggvason, B. Bunner, A. Esmaeeli, D. Juric, N. Al-Rawahi, W. Tauber, J. Han, S. Nas, and Y.-J. Jan, "A front-tracking method for the computations of multiphase flow," Journal of computational physics, vol. 169, no. 2, pp. 708–759, 2001.

[47] M. Sussman, P. Smereka, and S. Osher, "A level set approach for computing solutions to incompressible two-phase flow," Journal of Computational physics, vol. 114, no. 1, pp. 146–159, 1994.

[48] D. M. Anderson, G. B. McFadden, and A. A. Wheeler, "Diffuse-interface methods in fluid mechanics," Annual review of fluid mechanics, vol. 30, no. 1, pp. 139–165, 1998.

[49] D. Jacqmin, "Calculation of two-phase navier-stokes flows using phase-field modeling," Journal of computational physics, vol. 155, no. 1, pp. 96–127, 1999.

[50] X. He, S. Chen, and R. Zhang, "A Lattice Boltzmann scheme for incompressible multiphase flow and its application in simulation of Rayleigh-Taylor instability," Journal of computational physics, vol. 152, no. 2, pp. 642–663, 1999.

[51] H. Liang, X. Hu, X. Huang, and J. Xu, "Direct numerical simulations of multi-mode immiscible Rayleigh-Taylor instability with high Reynolds numbers," Physics of Fluids, vol. 31, no. 11, p. 112 104, 2019.

[52] P. Nathen, D. Gaudlitz, M. J. Krause, and N. A. Adams, "On the stability and accuracy of the bgk, mrt and rlb Boltzmann schemes for the simulation of turbulent flows," Commun Comput Phys, vol. 23, no. 3, pp. 1–31, 2018.

[53] T. Imamura, K. Suzuki, T. Nakamura, and M. Yoshida, "Acceleration of steady-state Lattice Boltzmann simulations on non-uniform mesh using local time step method," Journal of Computational Physics, vol. 202, no. 2, pp. 645–663, 2005.

[54] K. A. Yuana, B. Jalaali, E. P. Budiana, A. Widyaparaga, *et al.*, "Lattice Boltzmann simulation of the Rayleigh-Taylor instability (RTI) during the mixing of the immiscible fluids," European Journal of Mechanics-B/Fluids, vol. 85, pp. 276–288, 2021.

[55] X. He, R. Zhang, S. Chen, and G. D. Doolen, "On the three-dimensional Rayleigh-Taylor instability," Physics of Fluids, vol. 11, no. 5, pp. 1143–1152, 1999.

[56] F. Ren, B. Song, M. C. Sukop, and H. Hu, "Improved Lattice boltzmann modeling of binary flow based on the conservative Allen-Cahn equation," Physical Review E, vol. 94, no. 2, p. 023 311, 2016.

[57] B. Jalaali, M. R. E. Nasution, K. A. Yuana, O. Dinaryanto, *et al.*, "Investigating the effects of viscosity and density ratio on the numerical analysis of Rayleigh-Taylor instability in two-phase flow using Lattice Boltzmann method: From early stage to equilibrium state," Applied Mathematics and Computation, vol. 411, p. 126 490, 2021.

[58] A. Prosperetti and G. Tryggvason, Computational methods for multiphase flow. Cambridge university press, 2009.

[59] Z.-S. Mao and A. Dukler, "The motion of taylor bubbles in vertical tubes. i. a numerical simulation for the shape and rise velocity of taylor bubbles in stagnant and flowing liquid," *Journal of computational physics*, vol. 91, no. 1, pp. 132–160, 1990.

[60] R. Collins, "A simple model of the plane gas bubble in a finite liquid," *Journal of Fluid Mechanics*, vol. 22, no. 4, pp. 763–771, 1965.

[61] Y. Zu and S. He, "Phase-field-based Lattice Boltzmann model for incompressible binary fluid systems with density and viscosity contrasts," Physical Review E, vol. 87, no. 4, p. 043 301, 2013.

[62] T. Inamuro, T. Ogata, S. Tajima, and N. Konishi, "A Lattice Boltzmann method for incompressible two-phase flows with large density differences," Journal of Computational physics, vol. 198, no. 2, pp. 628–644, 2004.

[63] A. De Rosis and A. Tafuni, "A phase-field Lattice Boltzmann method for the solution of water-entry and water-exit problems," Computer-Aided Civil and Infrastructure Engineering, 2020.

[64] H. Haohao, S. Yanping, Y. Jianyang, C. Fu, and L. Tian, "Numerical analysis of water exit for a sphere with constant velocity using the Lattice Boltzmann method," Applied Ocean Research, vol. 84, pp. 163–178, 2019.

[65] J. Shentu, T. Zhao, D. Li, and X. Zhao, "Numerical simulations for water entry of Hydrophobic objects," Ocean Engineering, vol. 190, p. 106 485, 2019.

[66] T. Reis and T. N. Phillips, "Lattice Boltzmann model for simulating immiscible two-phase flows," Journal of Physics A: Mathematical and Theoretical, vol. 40, no. 14, p. 4033, 2007.

[67] H. Liu, A. J. Valocchi, and Q. Kang, "Three-dimensional Lattice Boltzmann model for immiscible two-phase flow simulations," Physical Review E, vol. 85, no. 4, p. 046 309, 2012.

[68] M. Latva-Kokko and D. H. Rothman, "Diffusion properties of gradient-based Lattice Boltzmann models of immiscible fluids," Physical Review E, vol. 71, no. 5, p. 056 702, 2005.

[69] D. Chiappini, G. Bella, S. Succi, F. Toschi, and S. Ubertini, "Improved Lattice Boltzmann without parasitic currents for rayleigh-taylor instability," Communications in Computational Physics, vol. 7, no. 3, p. 423, 2010.

[70] A. Banari, C. F. Janßen, and S. T. Grilli, "An efficient Lattice Boltzmann multiphase model for 3d flows with large density ratios at high Reynolds numbers," Computers and Mathematics with Applications, vol. 68, no. 12, pp. 1819–1843, 2014.

[71] L. Fei and K. H. Luo, "Consistent forcing scheme in the cascaded Lattice Boltzmann method," Physical Review E, vol. 96, no. 5, p. 053 307, 2017.

[72] D. d'Humières and B. Shizgal, "Rarefied gas dynamics: Theory and simulations," The American Institute of Aeronautics and Astronautics, pp. 450–458, 1992.

[73] G. Gruszczyński, T. Mitchell, C. Leonardi, T. Barber, *et al.*, "A cascaded phase-field Lattice Boltzmann model for the simulation of incompressible, immiscible fluids with high density contrast," Computers & Mathematics with Applications, vol. 79, no. 4, pp. 1049–1071, 2020.

[74] Y. Ba, H. Liu, Q. Li, Q. Kang, and J. Sun, "Multiple-relaxation-time Color-gradient Lattice Boltzmann model for simulating two-phase flows with high density ratio," Physical Review E, vol. 94, no. 2, p. 023 310, 2016.

[75] S. Saito, A. De Rosis, A. Festuccia, A. Kaneko, Y. Abe, and K. Koyama, "Color-gradient Lattice Boltzmann model with nonorthogonal central moments: Hydrodynamic melt-jet breakup simulations," Physical Review E, vol. 98, no. 1, p. 013 305, 2018.

[76] A. De Rosis, "Nonorthogonal central-moments-based Lattice Boltzmann scheme in three dimensions," Physical Review E, vol. 95, no. 1, p. 013 310, 2017.

[77] S. Leclaire, A. Parmigiani, O. Malaspinas, B. Chopard, and J. Latt, "Generalized three-dimensional Lattice Boltzmann Color-gradient method for immiscible two-phase pore-scale imbibition and drainage in porous media," Physical Review E, vol. 95, no. 3, p. 033 306, 2017.

[78] S. Leclaire, N. Pellerin, M. Reggio, and J.-Y. Trépanier, "A multiphase Lattice Boltzmann method for simulating immiscible liquid-liquid interface dynamics," Applied Mathematical Modelling, vol. 40, no. 13-14, pp. 6376–6394, 2016.

[79] L. Li, X. Jia, Y. Liu, and M. Su, "Simulation of double droplets impact on liquid film by a simplified Lattice Boltzmann model," Applied Thermal Engineering, vol. 98, pp. 656–669, 2016.

[80] Z. Chen, C. Shu, and D. Tan, "Highly accurate simplified Lattice Boltzmann method," Physics of Fluids, vol. 30, no. 10, p. 103 605, 2018.

[81] Z. Chen and C. Shu, "On numerical diffusion of simplified Lattice Boltzmann method," International Journal for Numerical Methods in Fluids, vol. 92, no. 9, pp. 1198–1211, 2020.

[82] L. Yang, C. Shu, Z. Chen, Y. Wang, and G. Hou, "A simplified Lattice Boltzmann flux solver for multiphase flows with large density ratio," International Journal for Numerical Methods in Fluids, vol. 93, no. 6, pp. 1895–1912, 2021.

[83] Y. Peng, C. Shu, and Y. Chew, "Simplified thermal Lattice Boltzmann model for incompressible thermal flows," Physical Review E, vol. 68, no. 2, p. 026 701, 2003.

[84] Z. Chen, C. Shu, and D. Tan, "Immersed boundary-simplified Lattice Boltzmann method for incompressible viscous flows," Physics of Fluids, vol. 30, no. 5, p. 053 601, 2018.

[85] S. Dash, "A flexible forcing immersed boundary-simplified Lattice Boltzmann method for two and three-dimensional fluid-solid interaction problems," Computers & Fluids, vol. 184, pp. 165–177, 2019.

[86] A. Komrakova, O. Shardt, D. Eskin, and J. Derksen, "Lattice Boltzmann simulations of drop deformation and breakup in shear flow," International Journal of Multiphase Flow, vol. 59, pp. 24–43, 2014.

[87] H. Xi and C. Duncan, "Lattice Boltzmann simulations of three-dimensional single droplet deformation and breakup under simple shear flow," Physical Review E, vol. 59, no. 3, p. 3022, 1999.

[88] A. De Rosis, "Non-orthogonal central moments relaxing to a discrete equilibrium: A d2q9 Lattice Boltzmann model," EPL (Europhysics Letters), vol. 116, no. 4, p. 44 003, 2017.

[89] A. De Rosis and C. Coreixas, "Multiphysics flow simulations using d3q19 Lattice Boltzmann methods based on central moments," Physics of Fluids, vol. 32, no. 11, p. 117 101, 2020.

[90] A. De Rosis, R. Huang, and C. Coreixas, "Universal formulation of central-moments-based Lattice Boltzmann method with external forcing for the simulation of multiphysics phenomena," Physics of Fluids, vol. 31, no. 11, p. 117 102, 2019.

[91] J. H. Ferziger, M. Perić, and R. L. Street, Computational methods for fluid dynamics. Springer, 2002, vol. 3.

[92] Y. Zu, A. Li, and H. Wei, "Phase-field Lattice Boltzmann model for interface tracking of a binary fluid system based on the allen-cahn equation," Physical Review E, vol. 102, no. 5, p. 053 307, 2020.

[93] P. L. Bhatnagar, E. P. Gross, and M. Krook, "A model for collision processes in gases. i. small amplitude processes in charged and neutral one-component systems," Physical review, vol. 94, no. 3, p. 511, 1954.

[94] X. Shan, "Analysis and reduction of the spurious current in a class of multiphase Lattice Boltzmann models," Physical Review E, vol. 73, no. 4, p. 047 701, 2006.

[95] M. Geier, A. Greiner, and J. G. Korvink, "Cascaded digital Lattice Boltzmann automata for high Reynolds number flow," Physical Review E, vol. 73, no. 6, p. 066 705, 2006.

[96] J. W. Cahn and J. E. Hilliard, "Free energy of a nonuniform system. i. interfacial free energy," The Journal of Chemical Physics, vol. 28, no. 2, pp. 258–267, 1958. DOI: 10.1063/1.1744102. eprint: https://doi.org/10.1063/1.1744102. [Online]. Available: https://doi.org/10.1063/1.1744102.

[97] S. M. Allen and J. W. Cahn, "Mechanisms of phase transformations within the miscibility gap of fe-rich Fe-Al alloys," Acta Metallurgica, vol. 24, no. 5, pp. 425–437, 1976.

[98] V. E. Badalassi, H. D. Ceniceros, and S. Banerjee, "Computation of multiphase systems with phase field models," Journal of computational physics, vol. 190, no. 2, pp. 371–397, 2003.

[99] A. Belhocine, "Numerical study of heat transfer in fully developed laminar flow inside a circular tube," The International Journal of Advanced Manufacturing Technology, vol. 85, no. 9, pp. 2681–2692, 2016.

[100] A. Belhocine and W. Z. Wan Omar, "An analytical method for solving exact solutions of the convective heat transfer in fully developed laminar flow through a circular tube," Heat Transfer—Asian Research, vol. 46, no. 8, pp. 1342–1353, 2017.

[101] A. Belhocine and O. I. Abdullah, "Numerical simulation of thermally developing turbulent flow through a cylindrical tube," The International Journal of Advanced Manufacturing Technology, vol. 102, pp. 2001–2012, 2019.

[102] A. Belhocine and W. Z. W. Omar, "Analytical solution and numerical simulation of the generalized levèque equation to predict the thermal boundary layer," Mathematics and Computers in Simulation, vol. 180, pp. 43–60, 2021.

[103] R. Benzi, S. Succi, and M. Vergassola, "The Lattice Boltzmann equation: Theory and applications," Physics Reports, vol. 222, no. 3, pp. 145–197, 1992.

[104] S. Succi, *The Lattice Boltzmann equation: for complex states of flowing matter*. Oxford University Press, 2018.

[105] K. Kutscher, M. Geier, and M. Krafczyk, "Massively parallel Lattice Boltzmann simulations of turbulent flow over and inside porous media," in *Fundamentals of High Lift for Future Civil Aircraft*, Springer, 2021, pp. 513–527.

[106] J. Chin, "Lattice Boltzmann simulation of the flow of binary immiscible fluids with different viscosities using the Shan-Chen microscopic interaction model," Philosophical Transactions of the Royal Society of London. Series A: Mathematical, Physical and Engineering Sciences, vol. 360, no. 1792, pp. 547–558, 2002.

[107] E. S. Boek and M. Venturoli, "Lattice-Boltzmann studies of fluid flow in porous media with realistic rock geometries," Computers & Mathematics with Applications, vol. 59, no. 7, pp. 2305–2314, 2010.

[108] D. M. Holman, R. M. Brionnaud, and Z. Abiza, "Solution to industry benchmark problems with the Lattice-Boltzmann code xflow," in *Proceeding in the European Congress on Computational Methods in Applied Sciences and Engineering (ECCOMAS)*, 2012.

[109] E. Fares, "Unsteady flow simulation of the ahmed reference body using a Lattice Boltzmann approach," Computers & fluids, vol. 35, no. 8-9, pp. 940–950, 2006.

[110] J. Latt, O. Malaspinas, D. Kontaxakis, A. Parmigiani, D. Lagrava, F. Brogi, M. B. Belgacem, Y. Thorimbert, S. Leclaire, S. Li, *et al.*, "Palabos: Parallel Lattice Boltzmann solver," Computers & Mathematics with Applications, vol. 81, pp. 334–350, 2021.

[111] Y. Feng, J. Miranda-Fuentes, S. Guo, J. Jacob, and P. Sagaut, "Prolb: A Lattice Boltzmann solver of large-eddy simulation for atmospheric boundary layer flows," Journal of Advances in Modeling Earth Systems, vol. 13, no. 3, e2020MS002107, 2021.

[112] L. Chen, Q. Kang, Y. Mu, Y.-L. He, and W.-Q. Tao, "A critical review of the pseudopotential multiphase Lattice Boltzmann model: Methods and applications," International journal of heat and mass transfer, vol. 76, pp. 210–236, 2014.

[113] H. Huang, M. Sukop, and X. Lu, "Multiphase Lattice Boltzmann methods: Theory and application," 2015.

[114] S. Leclaire, M. Reggio, and J.-Y. Trépanier, "Numerical evaluation of two recoloring operators for an immiscible two-phase flow Lattice Boltzmann model," Applied Mathematical Modelling, vol. 36, no. 5, pp. 2237–2252, 2012.

[115] S. Bakhshian, H. S. Rabbani, S. A. Hosseini, and N. Shokri, "New insights into complex interactions between heterogeneity and wettability influencing two-phase flow in porous media," Geophysical Research Letters, vol. 47, no. 14, e2020GL088187, 2020.

[116] S. Bakhshian, M. Murakami, S. A. Hosseini, and Q. Kang, "Scaling of imbibition front dynamics in heterogeneous porous media," Geophysical Research Letters, vol. 47, no. 14, e2020GL087914, 2020.

[117] X. Shan and H. Chen, "Lattice Boltzmann model for simulating flows with multiple phases and components," Physical review E, vol. 47, no. 3, p. 1815, 1993.

[118] M. Sbragaglia, R. Benzi, L. Biferale, S. Succi, K. Sugiyama, and F. Toschi, "Generalized Lattice Boltzmann method with multirange pseudopotential," Physical Review E, vol. 75, no. 2, p. 026 702, 2007.

[119] G. Falcucci, S. Ubertini, and S. Succi, "Lattice Boltzmann simulations of phase-separating flows at large density ratios: The case of doubly-attractive Pseudo-potentials," Soft Matter, vol. 6, no. 18, pp. 4357–4365, 2010.

[120] R. Huang, H. Wu, and N. A. Adams, "Eliminating cubic terms in the pseudopotential Lattice Boltzmann model for multiphase flow," Physical Review E, vol. 97, no. 5, p. 053 308, 2018.

[121] T. Inamuro, N. Konishi, and F. Ogino, "A galilean invariant model of the Lattice Boltzmann method for multiphase fluid flows using free-energy approach," Computer physics communications, vol. 129, no. 1-3, pp. 32–45, 2000.

[122] H. Liu, A. J. Valocchi, Y. Zhang, and Q. Kang, "Lattice Boltzmann phase-field modeling of thermocapillary flows in a confined microchannel," Journal of Computational Physics, vol. 256, pp. 334–356, 2014.

[123] M. Geier, A. Fakhari, and T. Lee, "Conservative phase-field lattice boltzmann model for interface tracking equation," Physical Review E, vol. 91, no. 6, p. 063 309, 2015.

[124] H. Zheng, C. Shu, and Y. Chew, "Lattice Boltzmann interface capturing method for incompressible flows," Physical Review E, vol. 72, no. 5, p. 056 705, 2005.

[125] H. Liang, B. Shi, and Z. Chai, "Lattice Boltzmann modeling of three-phase incompressible flows," Physical Review E, vol. 93, no. 1, p. 013 308, 2016.

[126] H. Wang, Z. Chai, B. Shi, and H. Liang, "Comparative study of the Lattice Boltzmann models for allen-cahn and cahn-hilliard equations," Physical Review E, vol. 94, no. 3, p. 033 304, 2016.

[127] H. Liang, J. Xu, J. Chen, H. Wang, Z. Chai, and B. Shi, "Phase-field-based Lattice Boltzmann modeling of large-density-ratio two-phase flows," Physical Review E, vol. 97, no. 3, p. 033 309, 2018.

[128] A. Begmohammadi, R. Haghani-Hassan-Abadi, A. Fakhari, and D. Bolster, "Study of phase-field Lattice Boltzmann models based on the conservative Allen-Cahn equation," Physical Review E, vol. 102, no. 2, p. 023 305, 2020.

[129] S. A. Hosseini, H. Safari, and D. Thevenin, "Lattice Boltzmann solver for multiphase flows: Application to high weber and reynolds numbers," Entropy, vol. 23, no. 2, p. 166, 2021.

[130] O. Malaspinas, "Increasing stability and accuracy of the Lattice Boltzmann scheme: Recursivity and regularization," arXiv preprint arXiv:1505.06900, 2015.

[131] C. Coreixas, G. Wissocq, G. Puigt, J.-F. Boussuge, and P. Sagaut, "Recursive regularization step for high-order Lattice Boltzmann methods," Physical Review E, vol. 96, no. 3, p. 033 306, 2017.

[132] A. De Rosis and K. H. Luo, "Role of higher-order hermite polynomials in the central-moments-based Lattice Boltzmann framework," Physical Review E, vol. 99, no. 1, p. 013 301, 2019.

[133] A. De Rosis, "A central moments-based Lattice Boltzmann scheme for shallow water equations," Computer Methods in Applied Mechanics and Engineering, vol. 319, pp. 379–392, 2017.

[134] ——, "Preconditioned Lattice Boltzmann method for steady flows: A noncascaded central-moments-based approach," Physical Review E, vol. 96, no. 6, p. 063 308, 2017.

[135] A. De Rosis, E. Lévêque, and R. Chahine, "Advanced Lattice Boltzmann scheme for high-Reynolds-number magneto-hydrodynamic flows," Journal of Turbulence, vol. 19, no. 6, pp. 446–462, 2018.

[136] M. B. Asadi, A. De Rosis, and S. Zendehboudi, "Central-moments-based Lattice Boltzmann for associating fluids: A new integrated approach," The Journal of Physical Chemistry B, vol. 124, no. 14, pp. 2900–2913, 2020.

[137] D. L. Youngs, "Numerical simulation of turbulent mixing by Rayleigh-Taylor instability," Physica D: Nonlinear Phenomena, vol. 12, no. 1-3, pp. 32–44, 1984.

[138] N. Wang, H. Liu, and C. Zhang, "Three-dimensional phase-field Lattice Boltzmann model for incompressible multiphase flows," Journal of Computational Science, vol. 17, pp. 340–356, 2016.

[139] H. G. Lee and J. Kim, "Numerical simulation of the three-dimensional Rayleigh-Taylor instability," Computers & Mathematics with Applications, vol. 66, no. 8, pp. 1466–1474, 2013.

[140] E. Enan and A. De Rosis, "Numerical modelling of the multi-mode turbulent rayleigh-taylor instability by a central-moments-based lattice boltzmann method," 2022, Ready to be submitted.

[141] S. I. Abarzhi, A. Gorobets, and K. R. Sreenivasan, "Rayleigh-Taylor turbulent mixing of immiscible, miscible and stratified fluids," Physics of Fluids, vol. 17, no. 8, p. 081 705, 2005.

[142] S. Chandrasekhar, Hydrodynamic and hydromagnetic stability. Courier Corporation, 2013.

[143] M. Chertkov, I. Kolokolov, and V. Lebedev, "Effects of surface tension on immiscible Rayleigh-Taylor turbulence," Physical Review E, vol. 71, no. 5, p. 055 301, 2005.

[144] J. Waddell, C. Niederhaus, and J. W. Jacobs, "Experimental study of Rayleigh-Taylor instability: Low Atwood number liquid systems with single-mode initial perturbations," Physics of Fluids, vol. 13, no. 5, pp. 1263–1273, 2001.

[145] V. Goncharov, "Analytical model of nonlinear, single-mode, classical Rayleigh-Taylor instability at arbitrary Atwood numbers," Physical review letters, vol. 88, no. 13, p. 134 502, 2002.

[146] G. Tryggvason, "Numerical simulations of the Rayleigh-Taylor instability," Journal of Computational Physics, vol. 75, no. 2, pp. 253–282, 1988.

[147] Z.-X. Hu, Y.-S. Zhang, B. Tian, Z. He, and L. Li, "Effect of viscosity on two-dimensional single-mode Rayleigh-Taylor instability during and after the reacceleration stage," Physics of Fluids, vol. 31, no. 10, p. 104 108, 2019.

[148] T. Wei and D. Livescu, "Late-time quadratic growth in single-mode Rayleigh-Taylor instability," Physical Review E, vol. 86, no. 4, p. 046 405, 2012.

[149] X. Bian, H. Aluie, D. Zhao, H. Zhang, and D. Livescu, "Revisiting the late-time growth of single-mode Rayleigh-Taylor instability and the role of vorticity," Physica D: Nonlinear Phenomena, vol. 403, p. 132 250, 2020.

[150] I. Yilmaz, "Analysis of Rayleigh-Taylor instability at high Atwood numbers using fully implicit, non-dissipative, energy-conserving large eddy simulation algorithm," Physics of Fluids, vol. 32, no. 5, p. 054 101, 2020.

[151] Z. Guo and C. Shu, *Lattice Boltzmann method and its application in engineering*. World Scientific, 2013, vol. 3.

[152] J. Ding, P. Sun, S. Huang, and X. Luo, "Single-and dual-mode Rayleigh-Taylor instability at microscopic scale," Physics of Fluids, vol. 33, no. 4, p. 042 102, 2021.

[153] Z. Huang, G. Lin, and A. M. Ardekani, "Consistent, essentially conservative and balanced-force phase-field method to model incompressible two-phase flows," Journal of Computational Physics, vol. 406, p. 109 192, 2020.

[154] A. Hamzehloo, P. Bartholomew, and S. Laizet, "Direct numerical simulations of incompressible Rayleigh-Taylor instabilities at low and medium Atwood numbers," Physics of Fluids, vol. 33, no. 5, p. 054 114, 2021.

[155] P. Ramaprabhu, G. Dimonte, P. Woodward, C. Fryer, G. Rockefeller, K. Muthuraman, P.-H. Lin, and J. Jayaraj, "The late-time dynamics of the single-mode Rayleigh-Taylor instability," Physics of Fluids, vol. 24, no. 7, p. 074 107, 2012.

[156] T. Luo, J. Wang, C. Xie, M. Wan, and S. Chen, "Effects of compressibility and atwood number on the single-mode Rayleigh-Taylor instability," Physics of Fluids, vol. 32, no. 1, p. 012 110, 2020.

[157] R. H. H. Abadi, A. Fakhari, and M. H. Rahimian, "Numerical simulation of three-component multiphase flows at high density and viscosity ratios using Lattice Boltzmann methods," Physical Review E, vol. 97, no. 3, p. 033 312, 2018.

[158] L. Zheng and S. Zheng, "Phase-field-theory-based Lattice Boltzmann equation method for n immiscible incompressible fluids," Physical Review E, vol. 99, no. 6, p. 063 310, 2019.

[159] H. Liu, A. J. Valocchi, Y. Zhang, and Q. Kang, "Phase-field-based Lattice Boltzmann finite-difference model for simulating thermocapillary flows," Physical Review E, vol. 87, no. 1, p. 013 010, 2013.

[160] L. Zheng, S. Zheng, and Q. Zhai, "Continuous surface force based Lattice Boltzmann equation method for simulating thermocapillary flow," Physics Letters A, vol. 380, no. 4, pp. 596–603, 2016.

[161] Y. Hu, D. Li, X. Niu, and S. Shu, "A diffuse interface Lattice Boltzmann model for thermocapillary flows with large density ratio and thermophysical parameters contrasts," International Journal of Heat and Mass Transfer, vol. 138, pp. 809–824, 2019.

[162] X. Liu, Z. Chai, and B. Shi, "A phase-field-based Lattice Boltzmann modeling of two-phase electro-hydrodynamic flows," Physics of Fluids, vol. 31, no. 9, p. 092 103, 2019.

[163] H. Liu, Y. Ba, L. Wu, Z. Li, G. Xi, and Y. Zhang, "A hybrid Lattice Boltzmann and finite difference method for droplet dynamics with insoluble surfactants," Journal of Fluid Mechanics, vol. 837, pp. 381–412, 2018.

[164] M. E. McCracken and J. Abraham, "Multiple-relaxation-time Lattice-Boltzmann model for multiphase flow," Physical Review E, vol. 71, no. 3, p. 036 701, 2005.

[165] R. Adhikari and S. Succi, "Duality in matrix Lattice Boltzmann models," Physical Review E, vol. 78, no. 6, p. 066 701, 2008.

[166] C. Coreixas, G. Wissocq, B. Chopard, and J. Latt, "Impact of collision models on the physical properties and the stability of Lattice Boltzmann methods," Philosophical Transactions of the Royal Society A, vol. 378, no. 2175, p. 20 190 397, 2020.

[167] C. Coreixas, B. Chopard, and J. Latt, "Comprehensive comparison of collision models in the Lattice Boltzmann framework: Theoretical investigations," Physical Review E, vol. 100, no. 3, p. 033 305, 2019.

[168] I. Karlin and P. Asinari, "Factorization symmetry in the Lattice Boltzmann method," Physica A: Statistical Mechanics and its Applications, vol. 389, no. 8, pp. 1530–1548, 2010.

[169] Z. Guo, C. Zheng, and B. Shi, "Discrete lattice effects on the forcing term in the Lattice Boltzmann method," Physical review E, vol. 65, no. 4, p. 046 308, 2002.

Appendix A

Appendix

LBM with GMRT

General multiple-relaxation-time LBM for the evolution of the velocity field, it is of interest to underline that Equation 2.10 is the well known second order truncated expression of the equilibrium state. LBE with the forcing term as [2][71][164]

$$\begin{aligned} |f_i\left(x+c_i, t+1\right)\rangle = & |f_i(x,t)\rangle + \Lambda\left[|f_i^{\mathrm{eq}}(x,t)\rangle - |f_i(x,t)\rangle\right] \\ & + \left(\mathbf{I} - \Lambda/2\right)|F_i(x,t)\rangle\,. \end{aligned} \tag{A.1}$$

Let us collect pre-collision, equilibrium and post-collision CMs as

$$\Lambda = \mathrm{T}^{-1}\mathrm{K}\mathrm{T},$$

where $\mathbf{K} = \mathrm{diag}[1,1,1,1,1,\omega,\omega,\omega,\omega,\omega,1,\ldots,1]$ is the 19 ×19 relaxation matrix in the CMs space.

Where T is written as followa [2]

$$\mathbf{T} = \begin{bmatrix} \left\langle |c_i|^0 \right| \\ \left\langle \bar{c}_{ix} \right| \\ \left\langle \bar{c}_{iy} \right| \\ \left\langle \bar{c}_{iz} \right| \\ \left\langle \bar{c}_{ix}^2 + \bar{c}_{iy}^2 + \bar{c}_{iz}^2 \right| \\ \left\langle \bar{c}_{ix}^2 - \bar{c}_{iy}^2 \right| \\ \left\langle \bar{c}_{iy}^2 - \bar{c}_{iz}^2 \right| \\ \left\langle \bar{c}_{ix}\bar{c}_{iy} \right| \\ \left\langle \bar{c}_{ix}\bar{c}_{iz} \right| \\ \left\langle \bar{c}_{iy}\bar{c}_{iz} \right| \\ \left\langle \bar{c}_{ix}^2\bar{c}_{iy} \right| \\ \left\langle \bar{c}_{ix}\bar{c}_{iy}^2 \right| \\ \left\langle \bar{c}_{ix}^2\bar{c}_{iz} \right| \\ \left\langle \bar{c}_{ix}\bar{c}_{iz}^2 \right| \\ \left\langle \bar{c}_{iy}^2\bar{c}_{iz} \right| \\ \left\langle \bar{c}_{iy}\bar{c}_{iz}^2 \right| \\ \left\langle \bar{c}_{ix}^2\bar{c}_{iy}^2 \right| \\ \left\langle \bar{c}_{ix}^2\bar{c}_{iz}^2 \right| \\ \left\langle \bar{c}_{iy}^2\bar{c}_{iy}^2 \right| \end{bmatrix} \tag{A.2}$$

Pre collision, equilibrium and post collision CMs[2] calculated by

$$\begin{aligned} |k_i\rangle &= [k_0, \dots, k_i, \dots, k_{18}]^\top \\ |k_i^{\text{eq}}\rangle &= [k_0^{\text{eq}}, \dots, k_i^{\text{eq}}, \dots, k_{18}^{\text{eq}}]^\top \\ |k_i^{\star}\rangle &= [k_0^{\star}, \dots, k_i^{\star}, \dots, k_{18}^{\star}]^\top \end{aligned} \tag{A.3}$$

By applying the transporting matrix T to form the function as,

$$\begin{aligned} |k_i\rangle &= \mathbf{T}\,|f_i\rangle \\ |k_i^{\text{eq}}\rangle &= \mathbf{T}\,|f_i^{\text{eq}}\rangle \end{aligned} \tag{A.4}$$

As a consequence, equilibrium CMs for D2Q19 read as follows:

$$\begin{aligned} k_0^{eq} &= \tilde{p} \\ tok_{18}^{eq} &= \tilde{p}\left[c_s^4 + c_s^2\left(u_y^2 + u_z^2\right) + u_y^2 u_z^2\right] - c_s^2\left(u_y^2 + u_z^2\right) - u_y^2 u_z^2 \end{aligned} \tag{A.5}$$

$$\begin{aligned} |k_i^\star\rangle &= (\mathbf{I} - \mathbf{K})\mathbf{T}\,|f_i\rangle + \mathbf{KT}\,|f_i^{\mathrm{eq}}\rangle\,, \\ &= (\mathbf{I} - \mathbf{K})\,|k_i\rangle + \mathbf{K}\,|k_i^{\mathrm{eq}}\rangle \end{aligned} \tag{A.6}$$

The collision process takes place as

$$\begin{aligned} k_0^\star &= \rho, \\ k_4^\star &= 3\rho c_s^2, \\ k_5^\star &= (1-\omega)k_5, \\ k_6^\star &= (1-\omega)k_6 \\ k_7^\star &= (1-\omega)k_7, \\ k_8^\star &= (1-\omega)k_8, \\ k_9^\star &= (1-\omega)k_9, \\ k_{16}^\star &= \rho c_s^4, \\ k_{17}^\star &= \rho c_s^4, \\ k_{18}^\star &= \rho c_s^4, \end{aligned} \tag{A.7}$$

3D GMRT-LBM for f_i

Before deriving the general multiple-relaxation-time LBM for the evolution of the velocity field, it is of interest to underline that equation 2.28 is the well-known second-order truncated expression of the equilibrium state. However, several authors demonstrated that the full potential of any LB discretization (in terms of physical and numerical properties) can only be achieved by using the complete allowable set of Hermite polynomials.[130][131] [165] [166] Following Coreixas et al.[167] and De Rosis and Coreixas,[89] we propose to rewrite Equation 2.27 as:

$$
\begin{aligned}
f^{eq}_{(0,0,0)} =& \frac{1}{3}\left[\tilde{p} - \left(u_x^2+u_y^2+u_z^2\right) + 3\left(u_x^2u_y^2+u_x^2u_z^2+u_y^2u_z^2\right)\right] \\
f^{eq}_{(\psi,0,0)} =& \frac{1}{18}\left[\tilde{p} + 3\psi u_x + 3\left(u_x^2-u_y^2-u_z^2\right)\right. \\
& \left. -9\psi\left(u_xu_y^2+u_xu_z^2\right) - 9\left(u_x^2u_y^2+u_x^2u_z^2\right)\right] \\
f^{eq}_{(0,\lambda,0)} =& \frac{1}{18}\left[\tilde{p} + 3\lambda u_y + 3\left(-u_x^2+u_y^2-u_z^2\right)\right. \\
& \left. -9\lambda\left(u_x^2u_y+u_yu_z^2\right) - 9\left(u_x^2u_y^2+u_y^2u_z^2\right)\right] \\
f^{eq}_{(0,0,\chi)} =& \frac{1}{18}\left[\tilde{p} + 3\chi u_z + 3\left(-u_x^2-u_y^2+u_z^2\right)\right. \\
& \left. -9\chi\left(u_x^2u_z+u_y^2u_z\right) - 9\left(u_x^2u_z^2+u_y^2u_z^2\right)\right] \\
f^{eq}_{(\psi,\lambda,0)} =& \frac{1}{36}\left[\tilde{p} + 3\left(\psi u_x+\lambda u_y\right) + 3\left(u_x^2+u_y^2\right) + 9\psi\lambda u_xu_y\right. \\
& \left. +9\left(\lambda u_x^2u_y+\psi u_xu_y^2\right) + 9u_x^2u_y^2\right] \\
f^{eq}_{(\psi,0,\chi)} =& \frac{1}{36}\left[\tilde{p} + 3\left(\psi u_x+\chi u_z\right) + 3\left(u_x^2+u_z^2\right) + 9\psi\chi u_xu_z\right. \\
& \left. +9\left(\chi u_x^2u_z+\psi u_xu_z^2\right) + 9u_x^2u_z^2\right] \\
& \left. +9\left(\chi u_y^2u_z+\lambda u_yu_z^2\right) + 9u_y^2u_z^2\right]
\end{aligned}
\tag{A.8}
$$

where $(\psi,\lambda,\chi) \in \{\pm 1\}^3$ and the tensor product notation has been adopted for the sake of compactness.[71][168][164]. After this premise, let us express the LBE with the forcing term as

$$
\begin{aligned}
|f_i^\star(x,t)\rangle =& |f_i(x,t)\rangle + \Lambda\left[|f_i^{\mathrm{eq}}(x,t)\rangle - |f_i(x,t)\rangle\right] \\
& + \left(\mathbf{I}-\Lambda/2\right)|F_i(x,t)\rangle
\end{aligned}
\tag{A.9}
$$

Above the Equation A.9 collapses into the aforementioned BGK LBM if the collision matrix is set to $= \omega \mathbf{I}$, where I is the unit tensor and $\omega = \frac{1}{\tau+1/2}$ is the relaxation frequency. The term F_i accounts for external body forces F and its prefactor is responsible for the discrete effects originating from the change of variables that aims at obtaining a numerical scheme explicit in time [2][169].

Algorithm of computation

Within the typical time step, the proposed scheme performs the following actions:

(a) Compute the macroscopic variables

$$\begin{aligned} \tilde{p} &= \sum_i f_i \\ \mathbf{u} &= \sum_i f_i \mathbf{c}_i + \frac{F}{2\rho} \\ \phi &= \sum_i g_i \end{aligned} \tag{A.10}$$

(b) Evaluate the spatial derivatives of the order parameter, velocity and density

$$\begin{aligned} \nabla\phi &= \frac{1}{c_s^2} \sum_i w_i \mathbf{c}_i \phi\left(x + \mathbf{c}_i\right) \\ \nabla\mathbf{u} &= \frac{1}{c_s^2} \sum_i w_i \mathbf{c}_i \mathbf{u}\left(x + \mathbf{c}_i\right) \\ \nabla\rho &= \frac{\rho_H - \rho_L}{\phi_H - \phi_L} \nabla\phi \end{aligned} \tag{A.11}$$

(c) Interpolate the relaxation time τ and and get the kinematic viscosity $\nu = \tau c_s^2$

$$\tau = \tau_L + \frac{\phi - \phi_L}{\phi_H - \phi_L}(\tau_H - \tau_L) \tag{A.12}$$

(d) Obtain the forces

$$\begin{aligned} F_s &= \mu_\phi \nabla\phi \\ F_p &= -\tilde{p} c_s^2 \nabla\rho, \\ F_\nu &= \nu\left[\nabla\mathbf{u} + (\nabla\mathbf{u})^\top\right] \cdot \nabla\rho. \end{aligned} \tag{A.13}$$

F_b accounts for any external body forces (e.g., gravity). (e) Correct the fluid velocity

$$\mathbf{u} = \sum_i f_i \mathbf{c}_i + \frac{F}{2\rho} \tag{A.14}$$

(f) Determine the vector F_ϕ

$$F_\phi = c_s^2 \frac{1 - 4(\phi - \phi_0)^2}{\xi} \cdot \frac{\nabla\phi}{|\nabla\phi|} \tag{A.15}$$

(g) Compute the only non-zero pre-collision central moments

$$\begin{aligned} k_5 &= f_1 + f_2 - f_3 - f_4 + f_{11} + f_{12} + f_{13} \\ &+ f_{14} - f_{15} - f_{16} - f_{17} - f_{18} + \left(u_x^2 - u_y^2\right)(\tilde{p} - 2), \\ k_6 &= f_3 + f_4 - f_5 - f_6 + f_7 + f_8 + f_9 \\ &+ f_{10} - f_{11} - f_{12} - f_{13} - f_{14} + \left(u_y^2 - u_z^2\right)(\tilde{p} - 2), \\ k_7 &= f_7 + f_8 - f_9 - f_{10} + u_x u_y (\tilde{p} - 2), \\ k_8 &= f_{11} + f_{12} - f_{13} - f_{14}, + u_x u_z (\tilde{p} - 2), \\ k_9 &= f_{15} + f_{16} - f_{17} - f_{18} + u_y u_z (\tilde{p} - 2), \\ k_{1,\phi} &= g_1 - g_2 + g_7 - g_8 + g_9 - g_{10} + g_{11} - g_{12} + g_{13} - g_{14} - \phi u_x, \\ k_{2,\phi} &= g_3 - g_4 + g_7 - g_8 - g_9 + g_{10} + g_{15} - g_{16} + g_{17} - g_{18} - \phi u_y, \\ k_{3,\phi} &= g_5 - g_6 + g_{11} - g_{12} - g_{13} + g_{14} + g_{15} - g_{16} - g_{17} + g_{18} - \phi u_z. \end{aligned} \tag{A.16}$$

(h) Calculate the post-collision central moments

$$
\begin{aligned}
k_0^\star &= \tilde{p}, \\
k_1^\star &= \frac{F_x}{2} - u_x(\tilde{p}-1), \\
k_2^\star &= \frac{F_y}{2} - u_y(\tilde{p}-1), \\
k_3^\star &= \frac{F_z}{2} - u_z(\tilde{p}-1), \\
k_4^\star &= \tilde{p}\left(1+u_x^2+u_y^2+u_z^2\right) - u_x^2 - u_y^2 - u_z^2, \\
k_5^\star &= (1-\omega)k_5 + \left(u_x^2-u_y^2\right)(\tilde{p}-1), \\
k_6^\star &= (1-\omega)k_6 + \left(u_y^2-u_z^2\right)(\tilde{p}-1), \\
k_7^\star &= (1-\omega)k_7 + u_x u_y(\tilde{p}-1), \\
k_8^\star &= (1-\omega)k_8 + u_x u_z(\tilde{p}-1), \\
k_9^\star &= (1-\omega)k_9 + u_y u_z(\tilde{p}-1), \\
k_{10}^\star &= \frac{F_y c_s^2}{2} - u_y\left(3u_x^2+1\right)(\tilde{p}-1)c_s^2, \\
k_{11}^\star &= \frac{F_x c_s^2}{2} - u_x\left(3u_y^2+1\right)(\tilde{p}-1)c_s^2, \\
k_{12}^\star &= \frac{F_z c_s^2}{2} - u_z\left(3u_x^2+1\right)(\tilde{p}-1)c_s^2, \\
k_{13}^\star &= \frac{F_x c_s^2}{2} - u_x\left(3u_z^2+1\right)(\tilde{p}-1)c_s^2,
\end{aligned}
\tag{A.17}
$$

$$
\begin{aligned}
k_{14}^\star &= \frac{F_y c_s^2}{2} - u_z\left(3u_y^2+1\right)(\tilde{p}-1)c_s^2, \\
k_{15}^\star &= \frac{F_z c_s^2}{2} - u_y\left(3u_z^2+1\right)(\tilde{p}-1)c_s^2, \\
k_{16}^\star &= \tilde{p}\left[c_s^4 + c_s^2\left(u_x^2+u_y^2\right) + u_x^2u_y^2\right] - c_s^2\left(u_x^2+u_y^2\right) - u_x^2u_y^2, \\
k_{17}^\star &= \tilde{p}\left[c_s^4 + c_s^2\left(u_x^2+u_z^2\right) + u_x^2u_z^2\right] - c_s^2\left(u_x^2+u_z^2\right) - u_x^2u_z^2, \\
k_{18}^\star &= \tilde{p}\left[c_s^4 + c_s^2\left(u_y^2+u_z^2\right) + u_y^2u_z^2\right] - c_s^2\left(u_y^2+u_z^2\right) - u_y^2u_z^2 \\
&\text{and } \left|k_{i,\phi}^\star\right\rangle
\end{aligned}
\tag{A.18}
$$

$$
\begin{aligned}
k^{\star}_{0,\phi} &= \phi \\
k^{\star}_{1,\phi} &= \left(1-\omega_{\phi}\right) k_{1,\phi} + \left(1-\omega_{\phi}/2\right) F_{x,\phi} \\
k^{\star}_{2,\phi} &= \left(1-\omega_{\phi}\right) k_{2,\phi} + \left(1-\omega_{\phi}/2\right) F_{y,\phi} \\
k^{\star}_{3,\phi} &= \left(1-\omega_{\phi}\right) k_{3,\phi} + \left(1-\omega_{\phi}/2\right) F_{z,\phi} \\
k^{\star}_{4,\phi} &= \phi \\
k^{\star}_{10,\phi} &= F_{y,\phi} c_s^2/2 \\
k^{\star}_{11,\phi} &= F_{x\phi} c_s^2/2 \\
k^{\star}_{12,\phi} &= F_{z,\phi} c_s^2/2 \\
k^{\star}_{13,\phi} &= F_{x,\phi} c_s^2/2 \\
k^{\star}_{14,\phi} &= F_{z\phi} c_s^2/2 \\
k^{\star}_{15,\phi} &= F_{y,\phi} c_s^2/2 \\
k^{\star}_{16,\phi} &= \phi c_s^4 \\
k^{\star}_{17,\phi} &= \phi c_s^4 \\
k^{\star}_{18,\phi} &= \phi c_s^4.
\end{aligned}
\tag{A.19}
$$

(i) Reconstruct post-collision populations for the flow and phase fields by the two-steps strategy

$$
\begin{aligned}
\left|f_i^{\star}\right\rangle &= \mathbf{M}^{-1}\mathbf{N}^{-1}\left|k_i^{\star}\right\rangle \\
\left|g_i^{\star}\right\rangle &= \mathbf{M}^{-1}\mathbf{N}^{-1}\left|g_{i,\phi}^{\star}\right\rangle
\end{aligned}
\tag{A.20}
$$

(j) Advance in time by streaming both the sets of populations as

$$
\begin{aligned}
\left|f_i\left(x+\mathbf{c}_i, t+1\right)\right\rangle &= \left|f_i^{\star}(x,t)\right\rangle \\
\left|g_i\left(x+\mathbf{c}_i, t+1\right)\right\rangle &= \left|g_i^{\star}(x,t)\right\rangle
\end{aligned}
\tag{A.21}
$$